12-2013

Alluvial Geochronology and Watershed Analysis of the Golo River, Northeastern Corsica, France

Emilee M. Skyles
Utah State University

ALLUVIAL GEOCHRONOLOGY AND WATERSHED ANALYSIS OF THE GOLO RIVER, NORTHEASTERN CORSICA, FRANCE

by

Emilee M. Skyles

A thesis submitted in partial fulfillment
of the requirements for the degree

of

MASTER OF SCIENCE

in

Geology

Approved:

_____	_____
Dr. Tammy Rittenour Major Professor	Dr. Joel Pederson Committee Member
_____	_____
Dr. Patrick Belmont Committee Member	Mark R. McLellan Vice President for Research and Dean of the School of Graduate Studies

UTAH STATE UNIVERSITY
Logan, Utah

2013

ABSTRACT

Alluvial Geochronology and Watershed Analysis of the Golo River, Northeastern Corsica, France

by

Emilee M. Skyles, Master of Science
Utah State University, 2013

Major Professor: Dr. Tammy M. Rittenour
Department: Geology

The Golo River in northeastern Corsica, France, is a short, steep, mixed bedrock-alluvial river (~95 km, 2706 m relief) in the Western Mediterranean with formerly glaciated headwaters. The small size and location of the Golo River make this system ideal for observing the response of this watershed to fluctuations in sea-level, climate, and tectonics.

Four aggradational packages of Golo River allluvial sediment are preserved on the Marana Plain: two fill terraces and two inset fill-cut terraces. Optically stimulated luminescence (OSL) dating of these alluvial terraces suggests the younger aggradational deposits are marine isotope stage (OIS) 3 and Holocene in age, with OIS 2 deposits assumed to be preserved in an entrenched channel under the Holocene surface deposits as a result of sea-level influence. The oldest Golo River terrace may be associated with OIS 6-OIS 8; however a quartz OSL age for this deposit remains unresolved. These aggradational terrace deposits are interpreted to have formed due to increased

sediment production during glacial conditions despite lower sea-level and in turn directly related to the coastal geometric configuration.

Analysis of the hypsometry and slope histograms from the entire Golo watershed suggests a mature, fluvially dominated system. Perturbations are evidenced by knickzones and convexities seen in longitudinal profiles and slope-area plots. For example, knickzones at and above the Alpine contact advocate movement of the Alpine Fault and migrating knickpoints near the boundary of the Mte Cinto caldera margin have enhanced convexities in profiles in Golo River tributaries, such as the Asco and Tartagine Rivers. Near the headwaters of the Golo and Asco Rivers, convexities are concordant with mapped glacial deposits, suggesting the influence of glacial scour.

The longitudinal profile of the lower canyon reach of the Golo River (lower 42 km) has a broad convexity in tandem with many stair-stepping knickpoints. Similarly, all tributaries in this reach have increased profile steepness and have waterfalls above the confluence with the Golo River. These data suggest that the Golo River is incising faster than its tributaries and that a large tectonically driven change in base-level may be driving incision.

(160 pages)

PUBLIC ABSTRACT

Alluvial Geochronology and Watershed Analysis of the Golo River, Northeastern Corsica, France

The Golo River in Corsica, France, is a short, steep river (~95 km, 2706 m relief) in the Western Mediterranean with formerly glaciated headwaters. The small size and location of the Golo River make this system ideal for observing the influence of climate and sea-level change on river dynamics over the 100,000 years. A rapidly advancing dating technique, optically stimulated luminescence, was utilized to determine the timing of these river deposits on the coastal plain in order to frame them in the context of previous glacial and interglacial episodes. Climate fluctuations in the headwaters supplied the vast majority of sediment into the system during glacial time periods, which was then transported and deposited near the mouth of the Golo River on the coastal Marana Plain. Sea-level also played a vital role in defining a geometric configuration that ultimately governed whether large amounts of sediment stored onshore or offshore. Analysis of the Golo River longitudinal profile and watershed reveals changes in steepness and gradient that are related to changes in rock type, fault movement and tectonically-driven base-level fall.

Emilee Skyles

ACKNOWLEDGMENTS

I would like to express my deepest gratitude to my advisor, Dr. Tammy Rittenour, for enduring the endless rounds of edits and all her efforts to get me to the finish line. She was a bounty of knowledge and inspiration in the field and I am most thankful for the chance to expand my understanding of landscape processes and geochronology under her guidance. I would also like to thank my committee members, Dr. Joel Pederson and Dr. Patrick Belmont, for their contributions and encouragement throughout this process.

A big thank you to the primary funding agency for this project, ExxonMobil, and USU Geology Department for supporting me through teaching and research assistantships.

I am also most grateful for those that joined me in field excursions and provided key information in various forms and facets. Fieldwork was greatly enhanced by the accompaniment of Dr. Mike Blum, whose topic knowledge and interest was a vital asset, Dr. Gweneal Jouet and Dr. Guiditta Fellin, whose help with language barriers and broadened perspectives on the project were indispensable. Also, Michelle Summa-Nelson in the Utah State Luminescence Lab was an immense help with sample preparation and analysis, without whom I would still be lost in macros and spreadsheets. I would also like to extend my appreciation to Dr. Ray Kenny, Dr. Karl Wegmann, Dr. Bob Carson, and the KECK Consortium for setting my pursuit of this dream in motion.

No one can truly prepare you for what goes into being a graduate student. It was inspiring to be surrounded by so many knowledgeable and diverse scholars and peers at Utah State University. Thank you to my family and friends for the unending encouragement and support. And last but certainly not least, to my partner in crime, Dana Osorno, who supported me steadfastly through the late nights and long times apart.

Emilee Skyles

CONTENTS

Page

LIST OF TABLES

LIST OF FIGURES

Figure Page

CHAPTER 1

INTRODUCTION AND BACKGROUND

Topics in fluvial geomorphology and landscape evolution have rapidly advanced over the last few decades as quantitative analyses have provided new ways to understand the influence of climate, sea-level, and tectonics on river dynamics. In keeping with this, the focus of this study is to map and date deposits of the Golo River coastal plain and examine the response of river profiles with respect to climate, sea-level, bedrock and tectonic controls. While tectonism is suggested to be a minor influence on terrace development on the coastal plain over the 100 kyr time-scale investigated, climate and sea-level change are expected to have a greater effect due to late Pleistocene glaciation of the headwaters and direct interaction with glacio-eustatic changes in the Tyrrhenian Sea at the mouth of the Golo River.

Study Area

Geography

Corsica is a small island territory (8732 km^2) of France in the western Mediterranean Sea and is bordered by the Tyrrhenian Sea to the east and Ligurian Sea to the west (Figure 1.1A). The Golo River drains the larger part of northern Corsica, flowing east-northeast into the Tyrrhenian Sea. The Golo River is a short steep (~90 km, 0.022m/km), formerly glaciated system with a drainage area of ~1000 km^2. Its catchment includes Mt. Cinto (2706 m asl), the highest peak on the island, and four major tributaries: the Lagani, Tartagine, Asco, and

Casaluna (Figure 1.1B). The spring source of the Golo River (2000m asl) is located to the south of the peaks of Paglia Orba (2525 m asl) and Capu Tafunatu (2335 m asl).

The Golo River generally has high stream power and sediment transport capacity due to its steep gradients and experiences high-magnitude floods throughout the year (Mather, 2009). The Golo River is a mixed bedrock-alluvial river with two distinct bedrock reaches (Hercynian and Alpine) and two alluvial reaches (Francardo basin and Marana Plain). Well-preserved discontinuous strath terraces are most common in the schist terrain of the lower bedrock canyon, ranging from 5-45 m above the channel. Previous workers correlated these bedrock strath terraces to the alluvial terraces on the coastal plain based on their relative position above the river (e.g. Lahondère et al., 1994). Age control on their formation is limited as recent optically stimulated luminescence (OSL) ages suggest that some of the alluvium overlying these strath surfaces are resultant of younger flood deposits as opposed to initial strath planation (e.g. Sømme et al., 2011).

Geology

Corsica has a complex geologic history and geologic rock units can be subdivided into four primary provences (Figure 1.2). The Hercynian complex on the western two-thirds of Corsica predominantly consists of Carboniferous Hercynian calc-alkaline granites and Permian rhyolites emplaced during the

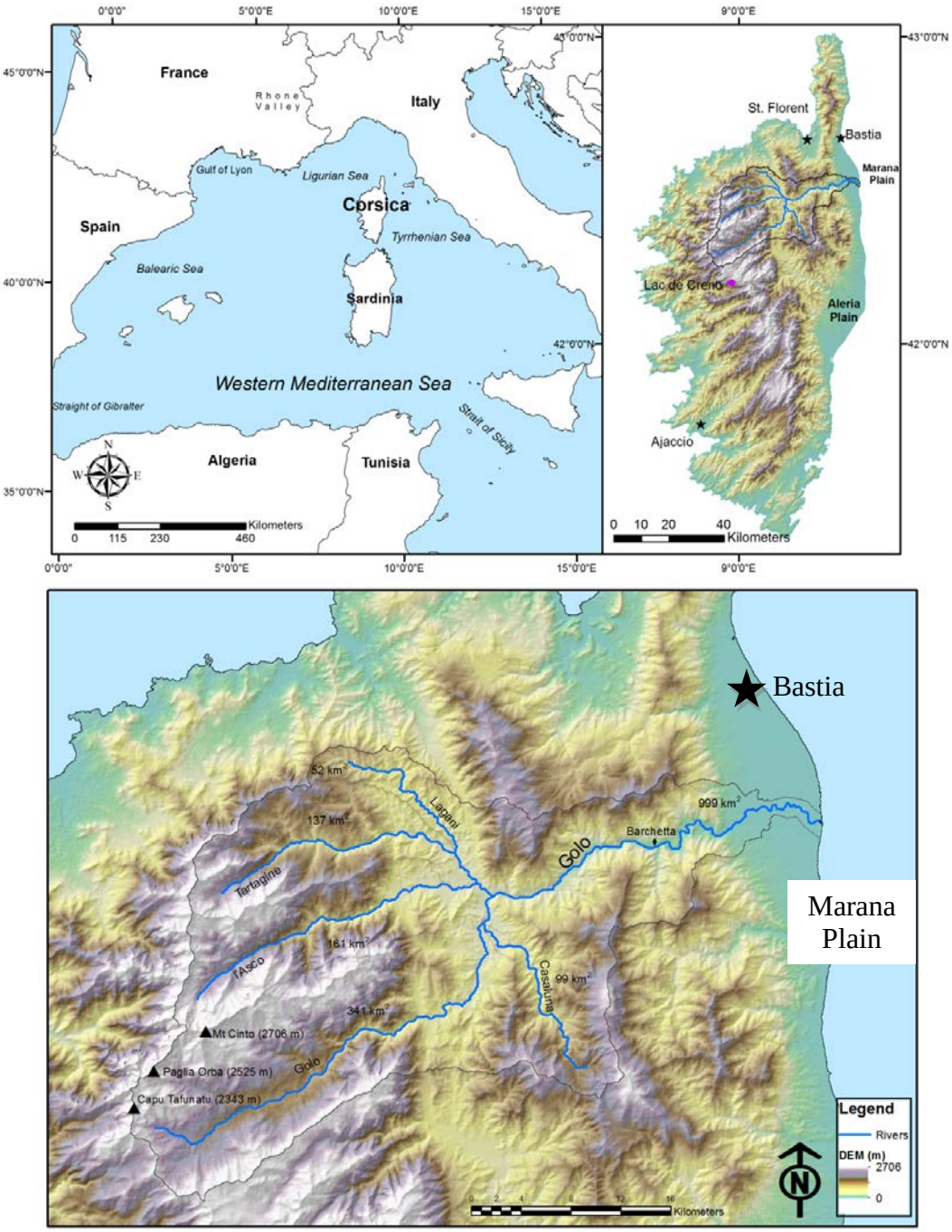

Figure 1.1 Location maps A) General location map of the western Mediterranean and digital elevation model of Corsica with the Golo River watershed outlined in black and locations referenced within the text. B) Enlarged view of Golo watershed with individual tributaries and prominent peaks labeled.

Late Paleozoic Hercynian Orogeny between Laurasia and Gondwana to form Pangea (Tommasini et al., 1995). The northeastern portion of Corsica (Alpine Corsica) is dominated by Late Cretaceous to Eocene oceanic and crustal thrust sheets of high pressure/low temperature metamorphic units that were metamorphosed during the Tertiary Alpine Orogeny between the African and Eurasian plate (Durand-Delga, 1984). Later, another phase of compressional tectonics in the Late Eocene formed the Alps, Apennines, Pyrenees and other regional mountain ranges (Malavieille et al., 1998; Michard and Martinotti, 2002). In the Early Oligocene, there was a transition to large-scale extension and the collapse of the over thickened orogenic wedge accompanied by reactivation of the Alpine contacts (Jolivet et al., 1991; Brunet et al., 2000). Continental rifting and counterclockwise rotation of the Corsica-Sardinia block away from mainland France continued as the Ligurian Basin (to the northwest) opened during Late Oligocene to Middle Miocene (Larroque et al., 2009). Starting in the early Miocene, continued convergence of the African and Eurasian plates resulted in the uplift of the Hercynian basement and thrusting of the Alpine units (Mazzoli and Helman, 1994; Fellin et al., 2005b).

Post-Miocene tectonic adjustment and reactivation of multiple extensional and compressional faulting is evidenced by apatite-fission track dating (AFT), and to a lesser degree, alluvial deposits (Conchon, 1977; Zarki-Jakni et al., 2004; Fellin et al., 2005a, 2005b). AFT ages at the Hercynian-Alpine contact indicate extensional faulting in central Corsica at the beginning of the Miocene (~23 Ma)

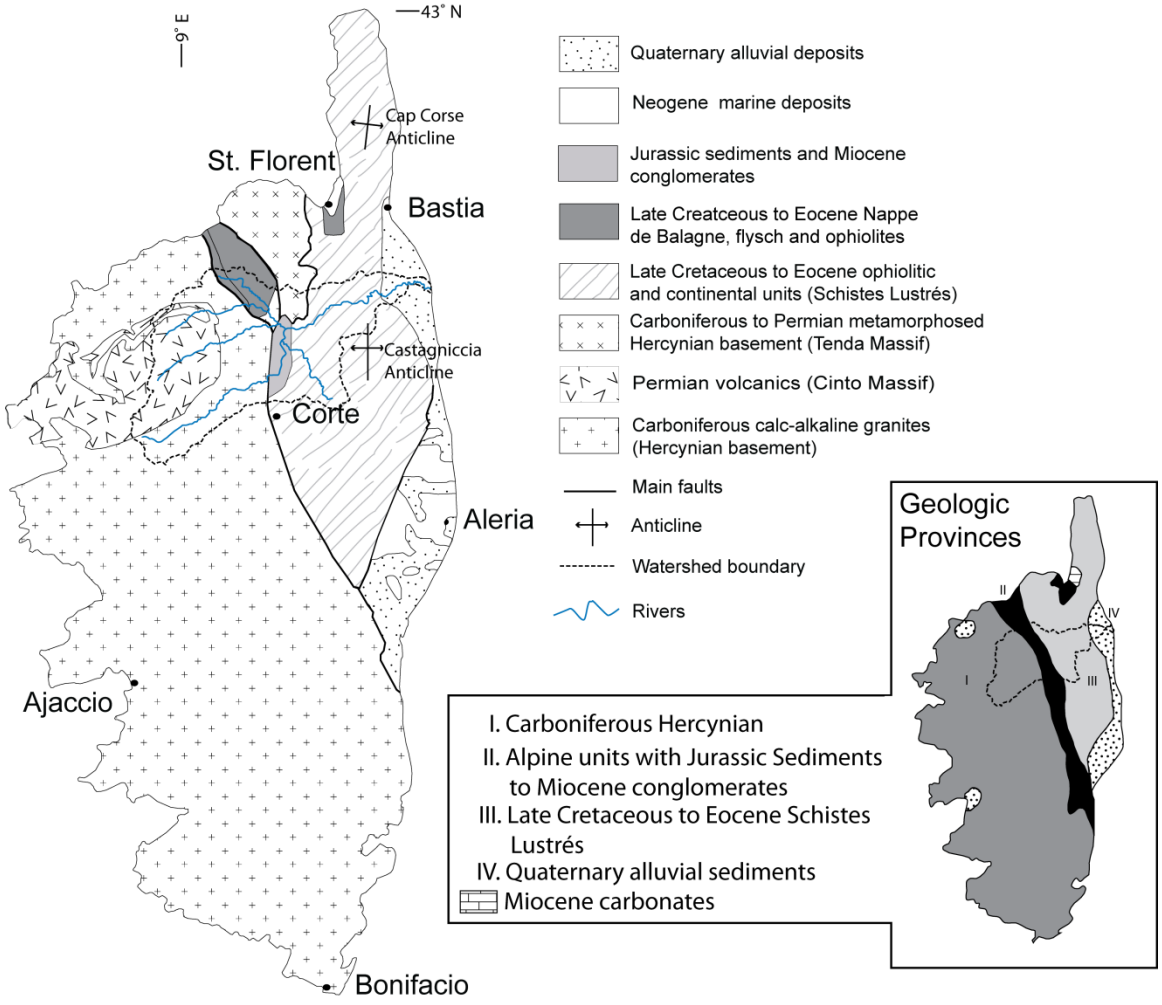

Figure 1.2 Geologic maps A) Corsica with Golo River watershed outlined (Modified from Fellin et al., 2005a, 2005b). B) Generalized map of the major geologic provenances described within the text (modified from Reille et al., 1997).

followed by basin subsidence from 20-10 Ma (Zarki-Jakni et al., 2004; Fellin et al., 2005b). Sediments with clasts from the Hercynian calc-alkaline granites were deposited in small Miocene basins, such as the St. Florent and Francardo basins (Figure 1.1B), implying that the ancestral Golo River once entered the Ligurian Sea through St. Florent Bay on the northern part of the island (Fellin et al., 2005a, 2005b). Compressional faulting during the Tortonian (11.5-7.2 Ma) inverted these basins and likely deflected the Golo River into its current path as a result of the uplift of the Tenda Massif (Fellin et al., 2005b; Cavazza et al., 2001, Cavazza et al., 2007). AFT ages also point to the growth of the Cap Corse-Castagniccia anticline at this time (Fellin et al., 2005b) (Figure 1.2). As a result of anticline growth and topographic reorganization, clasts from the Alpine units were deposited on the Aleria Plain south of the Marana Plain (Figure 1.1) during the Messinian to Late Pliocene (7.2-2.6 Ma) and are also correlated to the reactivation of extension along the mountain front fault (Conchon, 1977, Jolivet et al., 1998; Mauffret et al., 1999). Finally, a pop-up structure on the Marana Plain suggests left-oblique compressional-transpressional reactivation during the Pliocene to Quaternary (2.6-0.1 Ma) (Fellin et al., 2005b) with eastward tilted alluvial deposits suggestive of a response to flexural uplift in the Alpine units (Conchon, 1977). Alternating cycles of compression and extension are mostly concordant with the convergence vector of the African- European plates (Fellin et al., 2005b).

As a result of this tectonic history, present day Corsica can be subdivided into four primary provinces: 1) calc-alkaline Hercynian granites and rhyolites 2) Jurassic terrestrial sediments, and Miocene conglomerates and continental sediments and 3) Cretaceous to Eocene Alpine metamorphic rocks 4) Quaternary sediments primarily on the coastal plain (Reille et al., 1997) (Figure 1.2B).

Climate

Climate in Corsica is characterized as sub-tropical Mediterranean with dry, warm summers and temperate, wet winters. Corsica's Mediterranean climate is influenced by the interaction between sea-surface temperature, circulation and atmospheric conditions. The Mediterranean Sea is a semi-closed basin that is currently connected to the Atlantic Ocean through the Strait of Gibraltar, and can be divided into the eastern and western Mediterranean at the Strait of Sicily (Figure 1.1A) (Rohling et al., 2009). Present day sea-surface temperatures at 10m depth in the Western Mediterranean Sea and the northeastern coast of Corsica range from 21-24º C in the summer, 13-15º C in the winter and 17-19º C mean annual temperature (Hayes et al., 2005).

Regional climate is also influenced by atmospheric circulation patterns such as the decadal North Atlantic Oscillation (NAO) (Hurrell, 1995). Operating primarily as a result of pressure differences between the Azores high and the Icelandic low-pressure cell, the NAO's positive and negative phases influence the jet stream and storm tracks (Hurrell, 1995). Positive NAO conditions push the jet

stream farther north and lead to dry conditions in the Mediterranean whereas negative NAO conditions lead to wet episodes in the Mediterranean (Hurrell, 1995).

The western Mediterranean is subject to both continental and polar air masses moving over Europe that become channelized through the Rhone Valley (Krumrie, 2009). This is responsible for the dry air that forms the Mistral winds, which cause strong evaporation and reduced sea-surface temperature in the Gulf of Lyon (Rohling et al., 2009).

In Corsica, mean annual precipitation increases from 600 mm per year near sea level along the western coast to ~1100 mm per year at 2000 m asl near the highest peaks (Bruno et al., 2001). Bastia, in northeastern Corsica, receives 786 mm of precipitation per year with November as the wettest month and July as the driest month (Figure 1.3) (france.meteofrance.com). During winter, snow falls on the high peaks. While glaciers were present during the Pleistocene, no perennial snow fields currently exist in the high mountains. Vegetation ranges from low maquis shrubs into *Pinus nigra* ssp. *laricio* forests before transitioning into sparse alpine vegetation on the highest peaks (Reille et al., 1997).

A gaging station at Barchetta (le Golo à Volpajola) has recorded daily flow values since 1961 and the Golo River has been dam-controlled at Calacuccia since 1968 (Figure 1.4A). This gaging station is located ~18 km upstream from the mouth of the river at 80 m asl and measures stream flow for the contributing

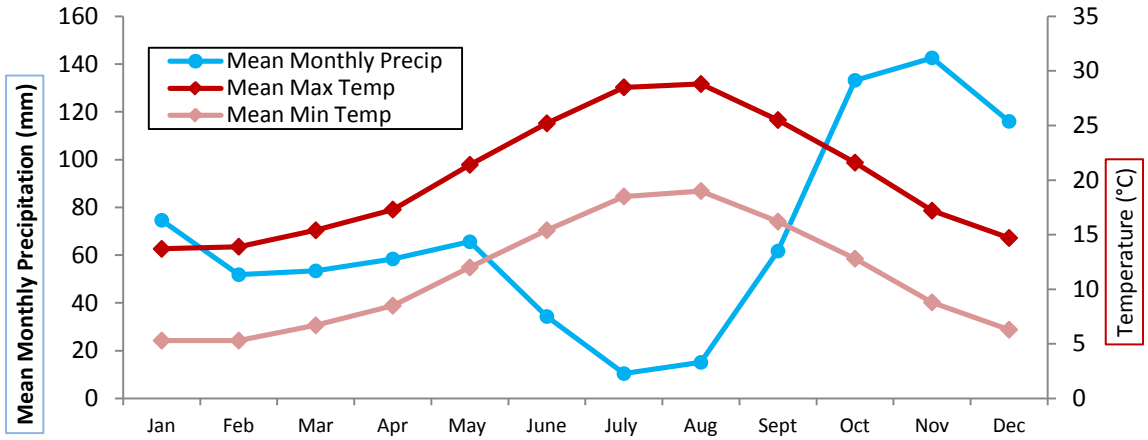

Figure 1.3 Nine-year record (2001-2009) of temperature and precipitation for Bastia, northeastern Corsica. High temperatures and low precipitation mark the summer months while increased precipitation and cooler temperatures mark the transition into winter (france.meteofrance.com).

926 km^2 upstream. The hydrograph for the Golo shows a bimodal distribution with high flow seasons in the spring, due to snowmelt runoff, and in the fall, due to high intensity precipitation events (Figure 1.4B). The fall and winter months show the most variability and deviation from the mean (Figure 1.4C). The low flow season for the Golo River is predominantly in the summer months (July and August) when temperatures are high and precipitation is low. There is some correlation between the period of highest precipitation in November and increased stream flow; however, the record also shows a strong spring runoff signature in March-April (Figure1.4). Two events high-flow events in October of 1976 and 1992 peaked above 300 m^3/s, possibly due to heavy rainfall events, as October is one of the wettest months (precipitation records were not available for this time period).

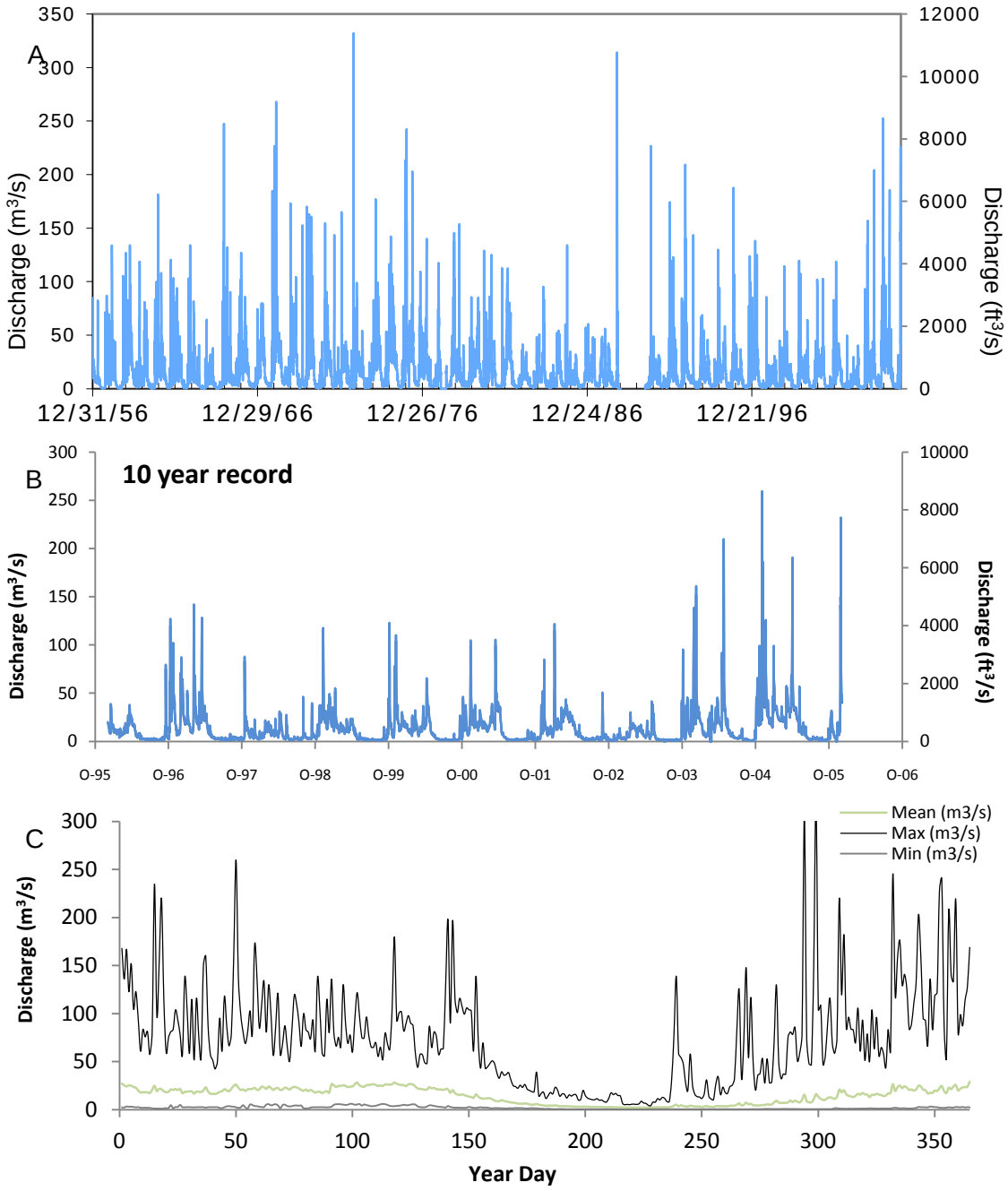

Figure 1.4 Flow statistics for the Golo River, 1961-2009 (hydro.eaufrance.fr). A) Daily flow value for the entire record B)Ten year record showing peak flows in the spring and fall C) Maximum, minimum and mean flows for the 48 year record with high variability of peak flows above the mean in the fall, winter and spring with the summer months containing lower and less variable flow.

Quaternary Paleoclimate and Sea-level

Studies in the Alborán Sea, near the Strait of Gibraltar, have shown the sensitivity of the western Mediterranean to changes in the conditions of the North Atlantic on millennial scales related to changes in sea-surface temperature associated with Dansgaard-Oeschgar (D/O) events and Heinrich Events (HE) (Cacho et al., 1999). Planktonic foraminifera assemblages from throughout the Mediterranean Sea indicate that sea-surface temperatures during the Last Glacial Maximum (19-23 cal. yr BP) were coldest in the western Mediterranean Gulf of Lyon (~7º C) and the warmest near the eastern Mediterranean Aegean and Levantine Sea (~16ºC) (Hayes et al., 2005).

Because the Mediterranean is directly connected to the North Atlantic Ocean through the Strait of Gibraltar, the western Mediterranean sea-level record is similar to the global eustatic curve (Figure 1.5) (Waelbroeck et al., 2002). Relative sea level and shorelines in the western Mediterranean during the LGM were approximately 120-150 meters below present day sea level and ~135 m below present in Corsica based on hydro-isostatic predictions (Stewart and Morhange, 2009). In western Sardinia, OSL dating of Pleistocene coastal deposits show a succession of four unconformity-bounded units with three sea-level highstands at 186 ± 13 ky (OIS 7, 2.5 ± 1 m asl), 120 ± 10 ky (OIS 5e, 5.2 ± 1 m asl), and 100 ± 5 ky (OIS 5c, 1.5 ± 1 m asl) and a final unit associated with sea-level fall and the beginning of the last glacial phase (OIS 4) (Andreucci et al., 2009).

Calculations of equilibrium line altitudes (ELA's) from glacial moraines, hypsometry, and isolines indicate that the average ELA for the Corsican mountains was at ~1600 m asl and temperatures were ~9.5°C cooler during the last glacial maximum (LGM) (Krumrie, 2009). Glacial termini extend to elevations as low as ~850 m asl along the Tartagine River within the Golo River watershed (Kuhlemann et al., 2005). Large valleys in northern Corsica show higher Würmian (OIS 2) ELA's on south-facing slopes relative to north facing slopes, most likely due to less precipitation and greater insolation (Kuhlemann et al., 2005). Large differences in ELA's along northwest flanks of the Corsican mountains between the cold phases of the late Würmian is explained by a intensified moist and cold conditions during the LGM resulting from a southward shift of the polar jet (Krumrie, 2009). Due to the steep ELA gradients, Corsica is regarded as an extremely sensitive area for paleoclimatic reconstructions (Krumrie, 2009). Conchon (1988b) estimated that deglaciation within the Corsican mountains occurred 12,000 years ago through a comparison of sediment cores and palynological and radiocarbon dating. Pollen studies using ^{14}C to date lake sediments just above a sand and gravel layer at Lac de Creno (1,310 m asl) in central Corsica show a steady rise in *Pinus nigra* ssp. *laricio* (typical of modern Corsican forests) starting at 14,560 ± 100 yr BP (17,255-18,008 cal yr BP) (Figure 1.1) and indicate the end of Younger Dryas glaciation in Corsica at 10,035 ± 85 yr BP (11, 261-11, 829 cal yr BP) (Reille et al., 1997).

Previous Work

The bulk of previous work on Quaternary deposits in Corsica was conducted by Conchon (e.g. Conchon 1972, 1975, 1977, 1978, 1979, 1984, 1985a, 1985b, 1986, 1987, 1988a, 1988b, 1999; Conchon et al., 1986). She used soil characteristics to map and correlate alluvial deposits assuming that an island-wide correlation between river catchments is possible. Seven alluvial terraces were identified and differentiated based on soil-profile characteristics including the degree of clast weathering, clay content, soil color and clast composition. Alluvial landforms were mapped as terrace units N1-N7, with N1 representing the oldest terrace (Figure 1.6). Following Conchon's work, the Bureau de Recherche Géologiques et Minières (BRGM) produced similar maps of the Golo River catchment (Lahondère et al., 1994). For comparison of F-series units, refer to Table 1.1, which synthesizes all the previous mapping nomenclature used for the fluvial terraces in Corsica as well as that of this study.

Although seven, coarse grained, alluvial terraces were mapped by Conchon (1977) on the Marana Plain, the oldest terrace (N1) is not attributed to the Golo River and is found 4.5 km south of the Golo River along the small tributary (ruisseau de Novale) near the mountain front (60-80 m asl). Conchon assigned relative ages for fluvial deposits based on an assumed 4-tier glacial chronology. Deposits were correlated to the Würm (OIS 2-4) (N6-N4), Riss (OIS 6) (N3), Mindel (OIS 8), (N2) and Güntz (OIS 10) (N1) glaciations. Relative correlation of terraces based on soil color and weathering characteristics of

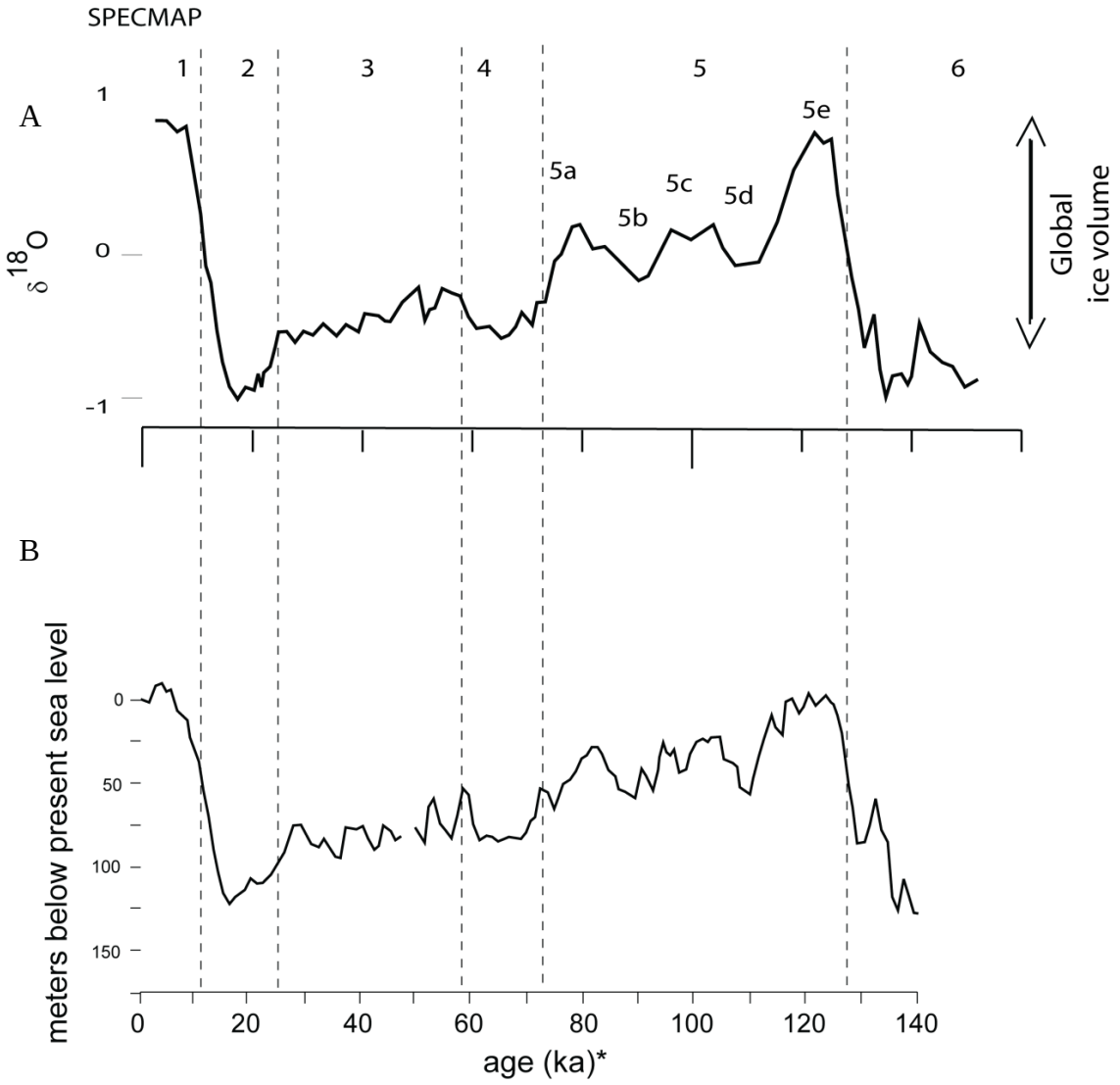

Figure 1.5 Record of A) global ice volume as a function of δ18O where positive values indicate warm conditions (less ice) and negative values indicate cold conditions (more ice) and B) sea-level over last glacial cycle (from Waelbroeck et al., 2002). Dashed lines indicate boundaries between oxygen isotope stages (OIS).

alluvial clasts (with particular emphasis on diabases) was a centerpiece of Conchon's correlation and chronology. Conchon found that iron monosiallitisation was the primary type of weathering found within the clasts of N1-N3 terraces and display decreasing intensity towards the younger units. These clasts range from highly weathered and altered rhyolites, grusified granites, and many completely disintegrated, ghost stones in N1 to thinner and less common weathering rinds on clasts in the N3 terrace deposits (Conchon, 1978) (refer to Appendix A for more details). Conchon described soils on the N1-N3 terraces as characterized by a well-developed red (Conchon 1977, 1986). N4 and N5 terraces are characterized by brown soils. N6 and N7 terraces have grey, poorly developed soils.

This previous work, however, did not utilize geomorphic principles. For example, paired terraces at the same height on each side of the river were mapped as different surfaces because younger capping overbank and marine onlap sediments produced soils with different degrees of weathering. Furthermore, age constraints for fluvial and coastal deposits on Corsica are limited. Available age control for interpreted correlative fluvial deposits includes : sediment cores off the coast of Ajaccio, interbedded fluvial (N4) and marine sediments near Santana and ^{14}C ages for the on the Aleria Plain (Conchon, 1978, 1986a, 1986b, 1999).

More recent work on the Golo River includes OSL ages on fluvial deposits from two terraces in the Francardo basin, one terrace on the Asco River and two

alluvial terraces on the Marana Plain (Sømme et al., 2011). On the Marana Plain, Sømme et al. (2011) obtained ages of 0.89 ± 0.07 ka and 0.58 ± 0.06 ka from the N6 terrace surface and is assigned to Younger Dryas deposition with recent overbank deposits accounting for the young ages. OSL Ages of 76 ± 5 ka (OIS4) and 45 ± 3 ka (OIS3) were determined for the N3 terrace surface and was used as the cornerstone to construct a depositional sequence for the Golo River (Sømme et al., 2011). Upstream on the Golo River in the Francardo alluvial reach, he obtained ages of 58 ± 4 ka (OIS 3) for a strath terrace mapped as the N4 terrace and 8.4 ± 0.5 ka and 4.7 ± 0.4 ka for a deposit mapped as the N5; on the Asco River, he obtained ages of 7.0 ± 0.4 ka and 8.8 ± 0.6 ka for terrace mapped as the N5.

These previous OSL results are problematic. For example, despite N6 ages pointing to 900-600 yrs, Sømme et al. (2011) correlate the N6 to the Younger Dryas. In addition, the younger- than- expected- ages for the N5 and N4 strath terrace deposits likely reflects recent deposition, as there is flood debris in the trees above these low terrace deposits. Sømme et al. (2011) associate the N5 surface to the LGM (OIS2) based on a relationship between climatic stability and the lateral extensiveness of the deposit as well as the correlation of the N4 with OIS 3-4. Although not discussed in detail, Sømme et al. (2011) conclude an OIS 6 (150 ka) age for the N2 surface based on height above the modern river and an assumed steady long-term incision rate.

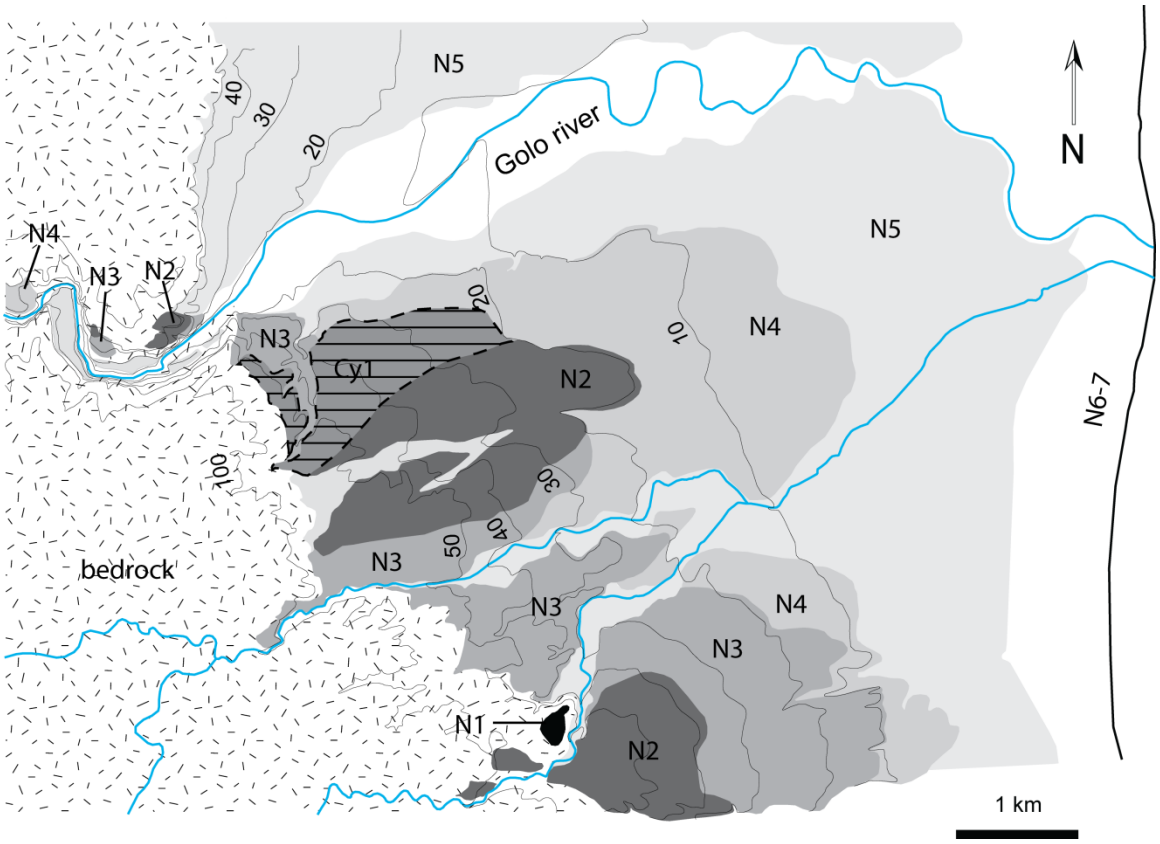

Figure 1.6 Map of fluvial deposits along the Golo River, Marana Plain after Conchon (1977) nomenclature.

Previous work by Conchon (1977, 1978, 1985, 1986) suggested there have been four glacial advances. Similar to the relative age designation of fluvial deposits, Conchon used soil development and color to map glacial deposits in the highlands and to correlate them to fluvial deposits within the river valleys and on the coastal plains across Corsica. The same numbering system was used in order to easily identify the time equivalent deposits; for instance, the G5 glacial deposit is correlative with the N5 fluvial deposit (Table 1.2) (Conchon 1986, 1987).

Table 1.1 Synthesis of nomenclature used in reference to Corsican and Golo River Quaternary deposits.

Conchon terrace nomenclature[1]	Geologic Map Unit[2] (BRGM)	Correlative glacial deposit/advance[1] (Conchon, 1978)	Assigned $\delta^{18}O$ Stage[3] (Conchon)	Climate/Glacial Period[4] (Conchon)	Soil color[1] (Conchon)	Degree of weathering[1] (Conchon)	This Study: Range in height above river (m)[5]	This Study: Golo River and Marana Plain	This Study: Assigned $\delta^{18}O$ Stage
N7	F_z	G7	1	modern to Holocene	Grey	not altered	*0-2.5*	modern floodplain	1
N6	F_{y3}	G6	2	late Würm	Grey	not altered	*0.5-4*	lower and upper Canonica (Qat1 and Qat2)	2
N5	F_{y2}	G5	3	middle Würm	10YR 5/4 yellowish brown	slightly altered	*2.5-10*	Poretta (Qat3)	3-4
N4	F_{y1}		4-5e	early Würm/last interglacial	10 YR 6/6 brownish yellow	altered			
N3	F_x	G3	6	Riss (penultimate glacial)	7.5 YR 6/6 reddish yellow	strongly altered	--	Revinco Alluvial Fan (Qaf3)	3
N2	F_w		8	Mindel (antepenultimate glacial)	7.5 YR 6/6 reddish yellow	strongly altered	*20-40*	Torra (Qat4)	6 or 8
N1	F_v (not seen in Golo terraces)		10	Güntz (oldest glacial)	Red	strongly altered (highest terraces)	--	--	--

[1] Nomenclature based on soils mapped by Conchon (1972, 1977, 1978)
[2] As mapped on BRGM Vescovato 1/50 000 geologic map, Lahondère et al., 1994
[3] Assigned marine isotope stages based on Conchon (1986)
[4] Alps glacial periods following original terminology of Penck and Bruckner (1909)
[5] Elevations taken from IGN Vescovato 1/25,000 topographic map, 2009

Table 1.2 Comparison of results from Conchon (1978, 1989) and Krumrie (2009).

Glacial Deposit/Advance[1]	$\delta^{18}O$ Stage[1]	Glacial Period[2]	Krumrie (2009)[3]
G7	1	modern to Holocene (13-5 ka)	Younger Dryas (13-11 ka)
G6	2	late Würmian (24-19 ka)	Older Dryas (17-14 ka)
G5	3	middle Würmian (60-25 ka)	Last Glacial Maximum (24-19 ka)
	4-5e	early Würmian/last interglacial	
G3	6	Riss (penultimate glacial)	
	8	Mindel (antepenultimate glacial)	
	10	Güntz (oldest glacial)	

[1]Glacial advance and assigned marine isotope stages based on Conchon (1986)
[2] Alps glacial periods following original terminology of Penck and Bruckner (1909)
[3] Based on ^{10}Be dating of moraines

More recent research by Krumrie (2009) has improved the glacial chronology of Corsica. ^{10}Be cosmogenic surface exposure dating of boulders on glacial moraines has constrained four glacial advances during OIS 2-4 (Würmian). These include large valley glacier advances at ~30 ka (OIS3/2) and 24-19 ka (LGM, last glacial maximum) while smaller valley glacier advances occurred at 17-14 ka (Heinrich event 1/Older Dryas) and 13-11 ka (Younger Dryas) (Krumrie, 2009). Evidence of more extensive glaciations prior to the Würmian are present however these deposits have yet to be dated due to poor preservation of datable material. Krumrie (2009) modified Conchon's previous proposed glacial chronology and determined that the age of most glacial deposits

were overestimated, in some cases by ~10 ky and exemplifies the importance of absolute dating (Table 1.2).

Fluvial response to external forcing

Rivers are important geomorphic agents responsible for sculpting landscapes. Fluvial dynamics and resultant deposits and landforms are controlled by three primary external forces: tectonics, climate and base-level (Holbrook and Schumm, 1999; Blum and Törnqvist, 2000). Changes in base-level can be controlled by eustacy, tectonic uplift, or subsidence, resulting in either base-level rise or fall. However, the relative extent to which these forces influence a river system at particular times is not easily determined. Fluvial adjustments to these external forces include changes in stream power and sediment transport, channel gradient and concavity, bedload and vegetation. The relative proportions of these factors and how they interact affect whether a system is constructive or destructive. Evidence for past shifts in the fluvial regime can be seen in the form of terraces. Stream terraces form in response to crossing a geomorphic threshold, where there is a change balance between sediment load and stream slope allowing for aggradation, degradation or equilibrium conditions (Bull, 1991). Main types of terraces include fill terraces formed by valley alluviation followed by incision; fill-cut terraces formed by incision into an older fill deposit; and strath terraces formed by the lateral erosion and planation of bedrock followed by incision (Bull, 1991).

In general, base-level fall due to tectonic uplift drives incision and leads to terraces stranded above the active channel (Bull, 1991). Strath terraces, like those along the lower bedrock reach of the Golo River, have a thin mantle of alluvium over a planar bedrock strath (Bull, 1991; Hancock and Anderson, 2002) and they are commonly found in tectonically active regions and rapidly incising systems (Bull, 1991). Studies of terrace formation in tectonically active landscapes of western North America are good analogues to the Golo River. The studies of Merritts et al. (1994) and Snyder et al. (2003) on small watersheds (up to 655 km^2) in California focus on catchments that are influenced by changes in sea-level, tectonics and climate. Merritts et al. (1994) found that the formation of strath terraces is dependent on uplift rates while aggradational fill terraces in the lower reaches are controlled by sea-level high stands followed by incision during low stands.

Modeling of strath terrace formation suggests that lateral planation rates and vertical incision are in competition and their balance changes as a result of stream competency and sediment supply (Hancock and Anderson, 2002). These simulations suggest lateral planation during glacial times when sediment production was high, whereas transition to inter-glacial times sparks incision and terrace abandonment (Hancock and Anderson, 2002).

Sea-level fluctuations influence both coastal geomorphology and terrace records (Figure 1.7). The rate of change associated with sea-level rise and fall will directly affect the response of a river system. During base-level lowering, minor changes and slow rates of change are expected to result in lateral

migration, minor channel adjustment and reconfiguration, and channel elongation to meet the new sea-level, whereas relatively large changes and higher rates of sea-level fall will result in river incision (Schumm 1993; Koss et al., 1994). A large magnitude, rapid lowering of sea-level may cause river incision to continue upstream even if sea-level returns to its original position due to headward migration of knickzones (Schumm, 1993). In contrast, raising sea-level may result in the aggradation of sediment in order for the river system to compensate and maintain the same transport gradient (Schumm, 1993). Using flume experiments, Koss et al. (1994) found that fluvial aggradation only occurred during periods of base-level still stand or rise.

An additional factor that influences fluvial response to sea-level change is the slope of the coastal plain compared to the slope of the continental shelf, which will control whether a system aggrades or incises (Blum and Törnqvist, 2000) (Figure 1.7). Sea-level during the Pleistocene was ~80-125 meters lower than Holocene conditions (Figure 1.5) causing Pleistocene river gradients to be steeper, with respect to a steep continental slope and shelf. Marine onlap is seen where older Pleistocene deposits are buried by Holocene deposits due to sea-level rise. In the case of the Golo River, the modern gradient of the continental shelf is steeper than that of the Marana coastal plain, as in Figure1.7B. During OIS 2 and OIS 6, it is expected that the sea-level lowstand caused true base-level fall and increased the effective gradient of the Golo River, resulting in incision, as seen in Figure 1.7B.

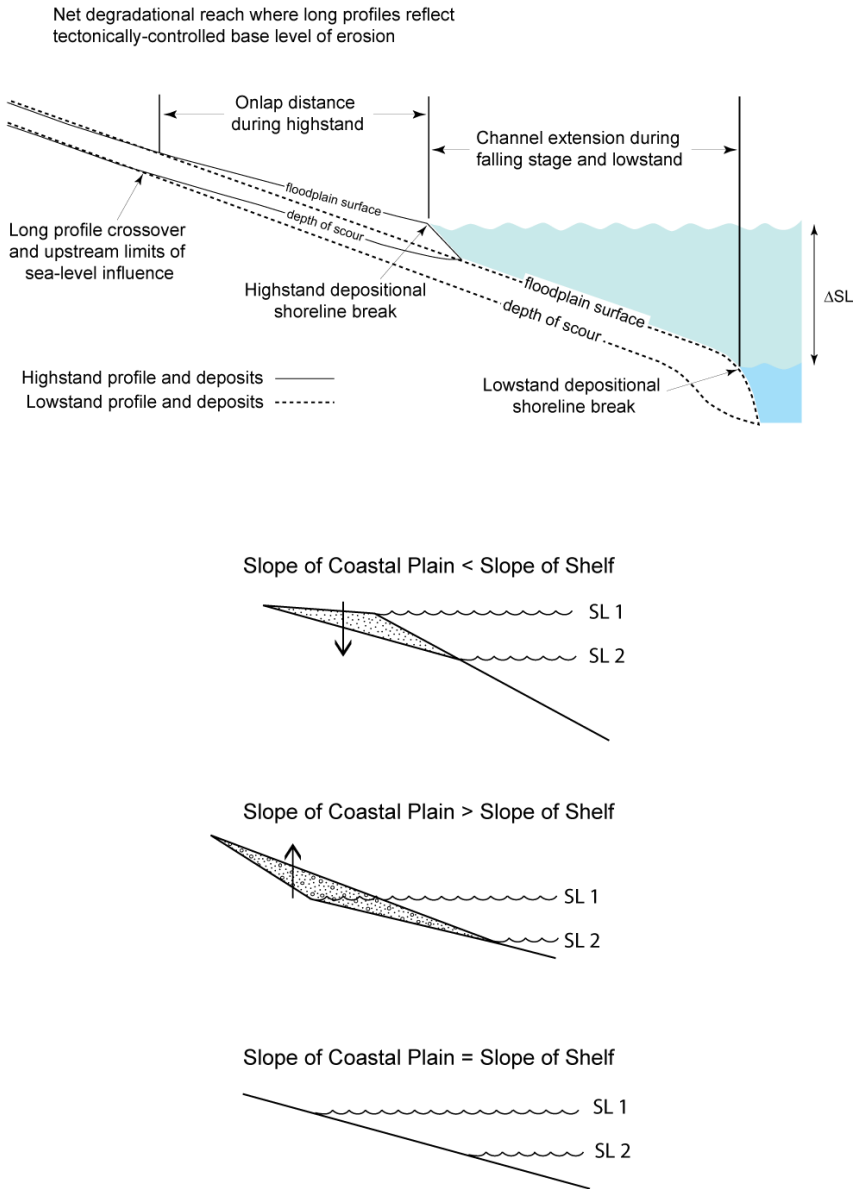

Figure 1.7 Fluvial response to base level change and coastal geometries (modified from Blum and Törnqvist, 2000). A) Channel response to highstand and lowstand levels as well as directions of change (incision/aggradation) and limits of influence. ΔSL indicates changes in sea-level. B) When the gradient of the coastal plain is less than the gradient of the shelf, lowering sea level with cause extensive incision and channel extension. C) When the gradient of the coastal plain is greater than the gradient of the shelf, channel extension and aggradation will occur. D) When the gradient of the coastal plain and shelf are equal, channel extension with little to no incision or aggradation will occur.

Research Objectives

The objectives for this study are to assess the impacts of sea-level, climate and tectonics on the geomorphology and terrace development of the coastal plain.

The research objectives include:

1. Mapping and describing the Quaternary deposits of the Marana Plain associated with the Golo River to provide insight into fluvial response to climate and sea-level change.
2. Provide age control for terrace deposits using OSL to determine the timing of alluvial deposition relative to local and regional sea-level and paleoclimate records.
3. GIS/geomorphic analysis of longitudinal profiles and hypsometry of the Golo drainage basin to assess potential tectonic and climate signals.

Research Strategy

Here, a collection of geomorphic and geochronologic data are used to help interpret the primary forcings responsible for deposition and alluviation on the Golo coastal plain. Problems with previous work highlights the importance of good age control of deposits on the coastal plain. This research is important because it is provides on-shore to off-shore correlation and ties together the large-scale dynamics of this source to sink record. For example, results from this research can be used to compare onshore deposits to offshore deposits and

understand their formation in relation to sea-level, climate and fluvial dynamics in sequence stratigraphy context. The Golo catchment is a good location for this assessment due its small size with direct influence of base-level changes, tectonic activity and Quaternary climate change on the fluvial record.

Although mapping by Conchon and the French Geological Survey apply consistent N-series and F-series map units throughout the Golo River and other catchments in Corsica, it is not certain that the terrace chronology developed on the coastal plain should be applied to the higher and more numerous strath terraces of the upper Golo River watershed. This study applies surface descriptions and an OSL derived chronology only to the Marana Plain deposits in the vicinity of the Golo River.

CHAPTER 2

GEOMORPHIC AND OSL RECORD OF THE RESPONSE OF THE GOLO RIVER TO CLIMATE AND SEA-LEVEL, MARANA PLAIN, NORTHEASTERN CORSCA, FRANCE

Age control on the Golo River terrace deposits is needed to assess river response to climate (glaciation) and sea-level change over recent glacial cycles. This chapter aims to improve previous soil-development based correlations and interpretations of alluvial deposits of the Golo River on the Marana Plain and improve the age estimates for these deposits through geomorphic mapping and optically stimulated luminescence (OSL) dating of fluvial and alluvial terraces, alluvial fan and beach deposits.

Methods

Geomorphic Mapping and Relative Dating

Mapping of the Marana Plain was conducted using a topographic base map and was facilitated by the use of geologic maps. Analysis of aerial photo stereo-pairs and Google Earth imagery was used to identify subtle changes in topography. In addition, soil profiles and weathering rinds on clasts were examined to corroborate previous work as well as to compare the relative degree of weathering between surfaces (Appendix A). In October 2010, new road construction in a roughly N-S transect created exposures cutting across Golo River deposits and a locally sourced alluvial fan on the Marana coastal plain.

The fortuitous timing of our fieldwork created an opportunity to examine deep, continuous outcrops and allowed for greater selection in sampling sites.

All deposits were assigned relative ages based on landscape position and stratigraphic relationships. Although the area had been previously mapped by Conchon (1977) and later again by Lahondére et al. (1994), they assumed that landforms with surface soil properties *and* similar elevations were the same geologic map unit (Figure 1.6). To avoid confusion with the previous 'N' and 'F' series terraces names, local place names were used here to identify map units and surface deposits.

Optically Stimulated Luminescence Dating

The primary method used to provide age control on the Quaternary and Holocene alluvial deposits in this study was optically stimulated luminescence (OSL) dating. Previous applications of OSL dating on Corsica focused on dating glacial, glacio-fluvial and some fluvial deposits (Krumrie, 2009; Sømme et al., 2011). However these attempts were largely unsuccessful possibly due to feldspar contamination of the quartz samples, lack of sensitization of the quartz or poor selection of sediment for sampling.

In total, 15 samples were collected from the six major alluvial and colluvial units within the study area. Exposures due to active road construction served as the basis for most sample site selection due to the excellent lateral and vertical exposures. Two samples for OSL were collected from each surface/deposit, with the exception of the Canonica Terrace where three samples were taken. Only

one sample was collected from one of the oldest Holocene beach ridges. Multiple samples were taken from sediment underneath each surface in order to provide a higher degree of confidence in age results as well as to serve as a backup if any problems were encountered. OSL results for each location can be found in Table 2.1 and dose rate information associated with each sample can be found in Table 2.2. Site descriptions refer explicitly to the surfaces found on the Marana Plain and correlation upstream throughout the valley or island-wide was not attempted or intended in this study. For detailed OSL equivalent dose distributions and data refer to Appendix B.

OSL Background

The OSL technique provides an age for sediment deposition by determining the amount of time that has passed since the sediment was last exposed to sunlight, presumably during transport. Minerals, such as feldspars, can be used for luminescence dating, however, due to properties such as anomalous fading and internal dosimetry, quartz is the primary mineral used in this study.

During sediment transport, exposure to sunlight ‘bleaches’ the sediment and resets the luminescence signal. The process of resetting occurs as a result of the eviction of electrons trapped within defects in the crystal lattice of the minerals (Huntley, et al 1985). Once deposited, the sediment begins to re-accumulate a signal as a result of radioactive decay of Potassium-40, Rubidium-87, Thorium and Uranium and exposure to cosmic rays (Aitken, 1998). Ionizing

radiation from alpha particle (α) decay penetrates 3 μm into grains while beta decay (β) can extend 3 mm into a grain. Gamma rays (γ) travel much further and influence sediments within a 30cm radius of each grain. The radioactive contribution from alpha, beta and gamma particles and cosmic rays (c) is collectively referred to as the dose rate environment for a sample and is expressed as grays per thousand years (Gy/ka) (Aitken, 1998).

$$Dose\ rate = D\alpha + D\beta + D\gamma + Dc \quad (1)$$

Additional factors that contribute to dose rate are depth, sediment density, and moisture content. Moisture content can highly influence dose rate calculation. Water filling pore space within the sediment will attenuate and absorb a portion of the incoming radiation and if unaccounted for will result in an age underestimation (Aitken, 1998). Ionizing radiation expels electrons from atoms within the crystal lattice. These electrons diffuse through the crystal lattice until they encounter a defect that is attractive to electrons (such as substitution or point defect) known as a 'trap' (Aitken, 1998). The longer the sample is exposed to ionizing radiation, the more electrons can accumulate in the traps until stimulation by light or heat evicts the electrons (Aitken, 1998). Eventually, due to the filling of available traps, electrons become in competition with each other and eventually reach a point where no more electrons can be stored. This is referred to as saturation and the saturation level of a mineral grain limits the maximum age attainable.

Table 2.1 OSL results for Marana Plain alluvial and colluvial samples

location	USU #	depth (m)	# aliquots[1]	dose rate (Gy/ka)	Equivalent Dose[4] (Gy)	OSL age[5] (cal kyr)
Lower Canonica Terrace (Qat1)						
Paduloni	USU-861[2]	2.3	20 / 57	2.83 ± 0.13	2.31 ± 0.73	0.58 ± 0.16
Paduloni	USU-862[2]	2	35 / 71	2.39 ± 0.18	2.61 ± 0.89	0.70 ± 0.21
Paduloni	USU-863[2]	3	21 / 87	2.85 ± 0.13	2.89 ± 0.63	1.02 ± 0.23
Poretta Terrace (Qat3)						
Gravel Pit	USU-797	1.9	31 / 83	3.31 ± 0.20	165.90 ± 16.96	50.2 ± 6.4
Old Golo Canal	USU-798	1.95	19 / 81	3.23 ± 0.19	185.66 ± 32.12	57.5 ± 10.8
Torra Terrace (Qat4)						
Torra Pit	USU-868[3]	4	34 / 64	4.04 ± 0.19	209.57 ± 13.34	52.0 ± 6.0
Torra Pit	USU-869[3]	4.5	20 / 53	3.38 ± 0.16	211.11 ± 20.03	63.0 ± 12.0
Revinco Alluvial Fan (Qaf_o)						
Canavaja	USU-866	2.3	22 / 37	2.23 ± 0.10	96.21 ± 7.84	43.2 ± 7.5
Canavaja	USU-867	5	18 / 51	1.48 ± 0.08	77.33 ± 7.64	52.2 ± 10.9
Sant Antone	USU-870	5	22 / 58	2.75 ± 0.12	80.86 ± 5.36	29.4 ± 4.3
Sant Antone	USU-871	5.4	16 / 53	2.40 ± 0.16	132.04 ± 13.85	55.1 ± 12.3
Torra reworked alluvium (Qac)						
Torraccia	USU-864	1.9	16 / 59	3.82 ± 0.19	124.22 ± 6.17	32.6 ± 3.9
Torraccia	USU-865	2	21 / 76	3.14 ± 0.14	128.97 ± 7.62	41.1 ± 3.7
Torra Pit	USU-872	2	22 / 49	3.80 ± 0.18	108.77 ± 7.35	28.6 ± 4.3
Biguglia Holocene Beach Ridge (Hb)						
Biguglia	USU-860[2]	1.4	22 / 69	2.17 ± 0.11	8.22 ± 2.55	3.13 ± 0.98

[1] numbers of aliquots accepted/number of aliquots analyzed

[2] MAM-3 age model used for age calculation of Paduloni samples (see Appendix B) (Galbraith et al., 1999)

[3] interpreted as minimum ages due to dose-rate and saturation problems

[4] Calculated at 2 standard error

[5] Early background subtraction (EBG) (Cunningham and Wallinga, 2010), Central age model (CAM) (Galbraith et al., 1999) used for calculation of equivalent dose based on 2-sigma

Table 2.2 Dose rate information[1] for OSL age calculation

location	USU #	grain size (μm)	in situ H_2O%	K (%)	Rb (ppm)	U (ppm)	Th (ppm)	Cosmic Contribution (Gy/ka)[3]	Dose rate (Gy/ka)
Lower Canonica Terrace (Qat1)									
Paduloni	USU-861	75-150	0.12	2.28 ± 0.06	107.7 ± 4.3	1.8 ± 0.1	9.7 ± 0.9	0.15	2.83 ± 0.13
Paduloni	USU-862	75-150	0.29	2.35 ± 0.06	80.3 ± 3.2	2.0 ± 0.1	8.2 ± 0.7	0.16	2.39 ± 0.18
Paduloni	USU-863[2]	150-250	7.50	2.55 ± 0.06	108.8 ± 4.4	1.7 ±0.1	7.9 ± 0.7	0.14	2.85 ± 0.13
Poretta Terrace (Qat3)									
Gravel Pit	USU-797	150-250	0.20	3.01 ± 0.08	146.0 ± 5.8	2.7 ± 0.2	11.7 ± 1.1	0.16	3.31 ± 0.20
Golo Canal	USU-798	150-250	0.10	2.89 ± 0.07	146.0 ± 5.8	2.5 ± 0.2	12.4 ± 1.1	0.16	3.23 ± 0.19
Torra Terrace (Qat4)									
Torra Pit	USU-868[2]	125-250	6.50	3.04 ± .08	162.7 ± 6.5	3.1 ± 0.2	15.95 ± 1.4	0.12	4.04 ± 0.19
Torra Pit	USU-869	125-250	0.12	3.05 ± 0.08	165.1 ± 6.6	2.9 ± 0.2	12.45 ± 1.1	0.12	3.38 ± 0.16
Revinco Alluvial Fan (Qaf_0)									
W Canavaja	USU-866	90-150	0.10	1.75 ± 0.04	72.8 ± 2.9	1.5 ± 0.1	7.1 ± 0.6	0.15	2.23 ± 0.10
W Canavaja	USU-867	90-150	0.15	1.42 ± 0.04	34.3 ± 1.4	0.7 ± 0.1	3.8 ± 0.3	0.11	1.48 ± 0.08
Sant Antone	USU-870[2]	90-150	7.50	2.39 ± 0.06	106.5 ± 4.3	1.4 ± 0.1	8.7 ± 0.8	0.11	2.75 ± 0.12
Sant Antone	USU-871	75-150	0.23	2.59 ± 0.06	78.8 ± 3.2	1.1 ± 0.1	7.1 ± 0.6	0.10	2.40 ± 0.16
Torra reworked alluvium (Qac)									
Torraccio	USU-864	75-180	0.13	2.92 ± 0.07	139.7 ± 5.6	2.7 ± 0.2	15.6 ± 1.4	0.16	3.82 ± 0.19
Torraccio	USU-865[2]	125-250	4.70	2.77 ± 0.07	136.4 ± 5.5	1.8 ± 0.1	10.35 ± 0.9	0.16	3.14 ± 0.14
Torra Pit	USU-872[2]	75-150	4.80	2.72 ± 0.07	148.2 ± 5.9	2.5 ± 0.2	16.4 ± 1.5	0.16	3.80 ± 0.18
Biguglia Beach Ridge (Hb)									
Biguglia	USU-860	150-212	0.16	2.17 ± 0.05	103.8 ± 4.2	1.1 ± 0.1	5.2 ± 0.5	0.17	2.17 ± 0.11

[1] Dose rate determined by elemental concentration by ICP_MS and converted to dose rate using conversion factors of Guérin et al. (2011).
[2] Water content assumed to be closer to 10 % (to calcualate dose rate and age)
[3] Cosmic contributions calculation by Prescot and Hutton (1995)

The amount of radiation a sample has acquired over time is referred to as the equivalent dose, D_e, and is determined by comparing the natural luminescence of the sample to the luminescence produced in the laboratory by applying a sequence of known doses. The age of the sample is determined by the equation where

$$Age\ (ka) = \frac{Equivalent\ Dose\ (Gy)}{Dose\ Rate\ (\frac{Gy}{ka})} \quad (2)$$

The single-aliquot regenerative dose (SAR) protocol (Murray and Wintle, 2000) is a method for determining the D_e through multiple cycles of heating, dosing, stimulation and measurement on the same aliquot, as well as a test dose that corrects for any sensitivity changes during measurement cycles (Table 2.3). During stimulation, the amount of photons released during blue-green LED light stimulation is proportional to the amount of radiation a sample has received since the time of deposition and thus is related to the age of the deposit and dose-rate environment.

The SAR protocol typically involves six cycles where differing doses are given and measured in order to create a dose-response curve that is used to determine the D_e (Figure 2.1). In the first cycle, no dose is given because the aliquot already contains the natural burial dose. Aliquots are then preheated for 10 s (160-300° C) to release geologically unstable traps (such as the 110° thermoluminescence (TL) trap) that would otherwise contribute to the measured luminescence. Next stimulation with blue-green light (470 nm) at 125°C for 40 s (to keep the 110° TL traps from refilling) is applied and luminescence is

measured. A test dose is given followed by applying a cut heat of 160-220°C for 0 s (to empty the 110°C TL traps) and measurement of this dose at 125°C for 40 s. Because the same low test dose is given at the end of each cycle, this measurement is used as a monitor for sensitivity changes. The cycle is repeated with three regenerated doses that aim to bracket the natural signal measured in the first cycle. A zero-dose cycle is applied to identify if the sample has a recuperated signal. At the end of each SAR sequence, a repeated dose, typically the same as the first dose, is applied to determine if the test-dose sensitivity corrections are adequate to produce the similar results for the same dose given at different times within the protocol.

During light stimulation and OSL decay, a shine-down curve is created as the more easily bleached traps quickly evict their electrons and decay towards a lower rate of eviction until the aliquot reaches an asymptotic background level (Figure 2.2). The shape of this curve is seemingly a simple single exponential decay. However typical OSL signals are a modulation of three to five components with different decay rates: ultrafast (sometimes), fast, two medium components and two to three slowly decaying components (Aitken, 1998). The ultrafast component is associated with a shallow electron trap that is thermally unstable with a very short lifespan (~1.5 yrs) that is responsible for its absence in the natural signal (Jain et al., 2003). In order to isolate the most readily bleached fast component of the OSL signal, it is necessary to subtract the slowly decaying component at the end of the signal from the quickly decaying component at the beginning (calculated as the first 0.64 s minus the average of the last 5 s of

Table 2.3 Single aliquot regenerative dose protocol (after Murray and Wintle 2000).

Step	Treatment	Observed
1	Give dose[1], D_i	-
2	Preheat (260, 240° C for 10s)[2]	-
3	Stimulate for 40s at 125° C	L_i[3]
4	Give test dose, D_T	-
5	Heat (220, 160° C)[2]	-
6	Stimulate for 40s at 125° C	T_i[3]
7	Return to Step 1 for five regen dose cycles (N, R1, R2, R3, R0, R1')	-

[1] For the natural sample, *i*=0 and D_0 is the natural dose
[2] (USU 797-798 and 864-869, USU 860-863)
[3] L_i and T_i are derived from the stimulation curve, typically the first 1-10 s of initial OSL signal, minus a background estimated from the last part of the stimulation curve.

decay). In some cases, unwanted and potentially unstable intermediate components are included in the initial signal. For these cases, an alternative approach of integration time is necessary. A modified equation following Cunningham and Wallinga (2010) integrates the signal as the sum of the first two channels minus two times the average of the following four channels (3-6) in order to isolate the fast component. This technique is referred to as early background subtraction (EBG).

Because D_e can be dependent upon preheat temperature, it is important to determine where the D_e form a plateau and variation is at a minimum (Murray and Wintle, 2000). A dose-recovery test assesses the accuracy of the SAR protocol in reproducing an applied dose. The chosen applied dose should be similar to the expected natural dose of the sample and the ratio of the measured dose to the known dose should result in unity, ± 10% (Wintle and Murray, 2006). When plotting the ratio of the given dose to the recovered dose as a function of

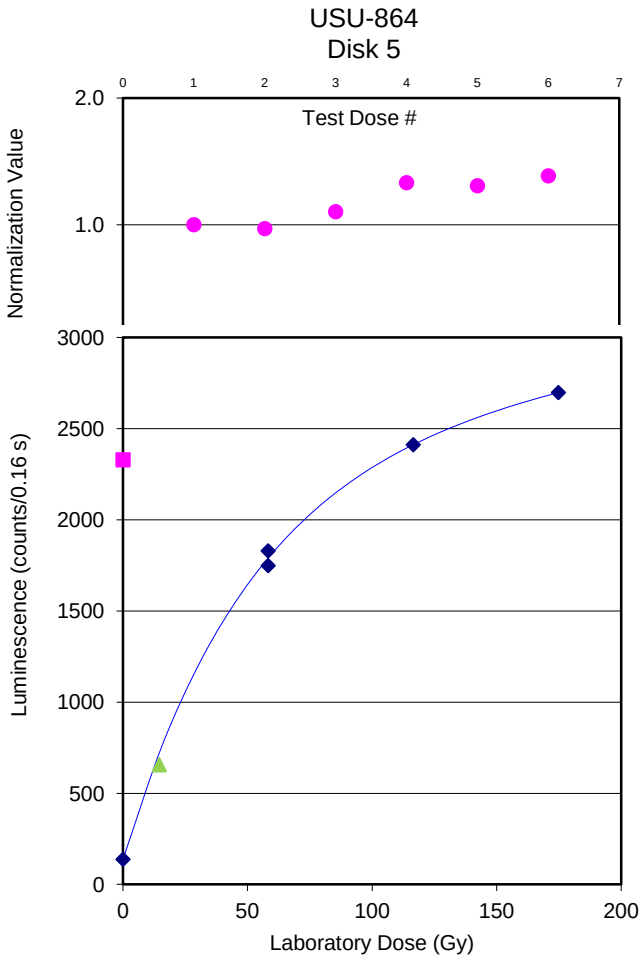

Figure 2.1 Test dose plot and dose response curve for sample USU-864. Test doses are seen as pink circles on the top graph and show that the SAR sequence is capable of correcting for sensitivities to within two standard deviations for this aliquot. The dose response curve is constructed using regenerated laboratory doses (blue diamonds) to interpolate the natural OSL signal (N, pink square) of each aliquot. Three regenerative doses (R1, R2, R3), one zero dose (R0), and one repeated dose (R1') bracket the natural dose to determine an equivalent dose. Low recuperation (R0 signal) and a good recycling ratio (R1:R1') contribute to a good saturating exponential plus linear fit for this aliquot. The green triangle represents the luminescence signal from the first test dose. Test dose 1 corresponds with the measurement of the natural dose while test dose 6 corresponds with R1'.

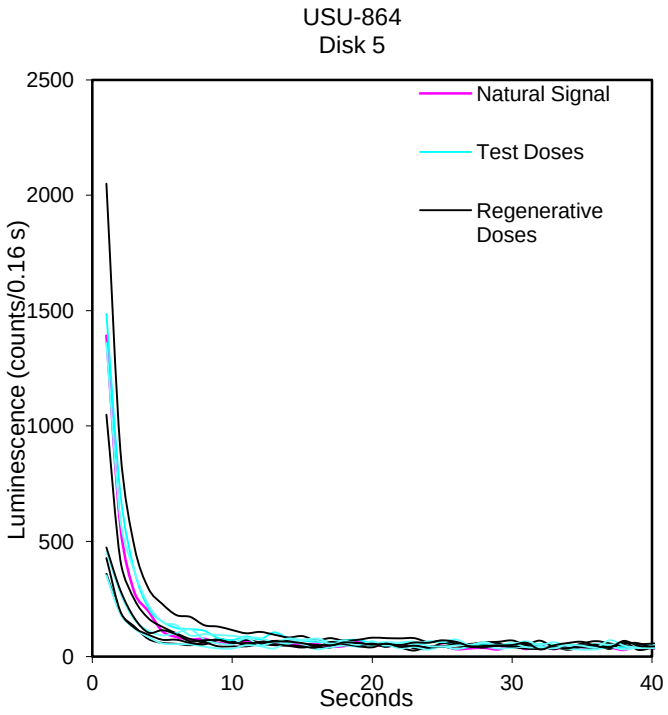

Figure 2.2 Shinedown curve with the response signals for the various steps throughout the SAR protocol. This curve shows the first 40 out of 250 channels. The natural signal is shown in pink.

preheat temperature, the least error and closest reproduction of the given dose indicate the best fit preheat temperature for the sample.

In this study, two preheat-plateau dose-recovery tests were completed on two samples of differing age, USU-798 and USU-863 with temperatures ranging from 200-300°C and 180-280°C (Figure 2.3). Thirty-five aliquots of USU-863 were given ~7.3 Gy of radiation. A rough plateau in D_e results emerged between 240 and 260°C. Recuperation of the signal as well as the recycling ratio were lowest at 180°C and 220°C; however, dose recovery was best at 200°C and

240°C with less error associated with 240°C. A 240°C preheat and 160°C cut heat was used for USU-863,-862 and -861, which were collected from the youngest terrace deposit. Thirty-five aliquots of USU-798 were given ~129.19 Gy of radiation. A rough DR-PH plateau emerged between 220 and 260°C. This sample returned the lowest recuperation at 220°C and a recycling ratio near unity at 220°C and 260°C with lower error associated with the 260°C preheat. During analysis, it was suspected that there was some contribution from an unstable ultrafast component so the cut heat was raised to 220°C following Jain et al. (2003). A 260°C preheat and 220°C cut heat was applied to all samples except those from the youngest terrace.

Additional factors affecting D_e and age determination include partial bleaching or incomplete resetting of the OSL signal prior to burial. This becomes especially important in the fluvial system due to either turbidity in the water column inhibiting penetration of light to grains, transport at night and erosion and rapid transport of sediment from river banks of older deposits (Olley et al., 1998; Rittenour, 2008, and references within). Incomplete resetting of the signal results in the contribution of a residual signal being included in the measurement.

Due to the proximal distribution of sediments and influence of glaciation in the headwaters of the Golo River, partial bleaching was anticipated. When graphed, partial bleaching can be recognized as an asymmetrical distribution of equivalent doses skewed towards higher D_e values (Olley et al., 1998). Where there is a high degree of asymmetry, the lowest doses are thought to represent

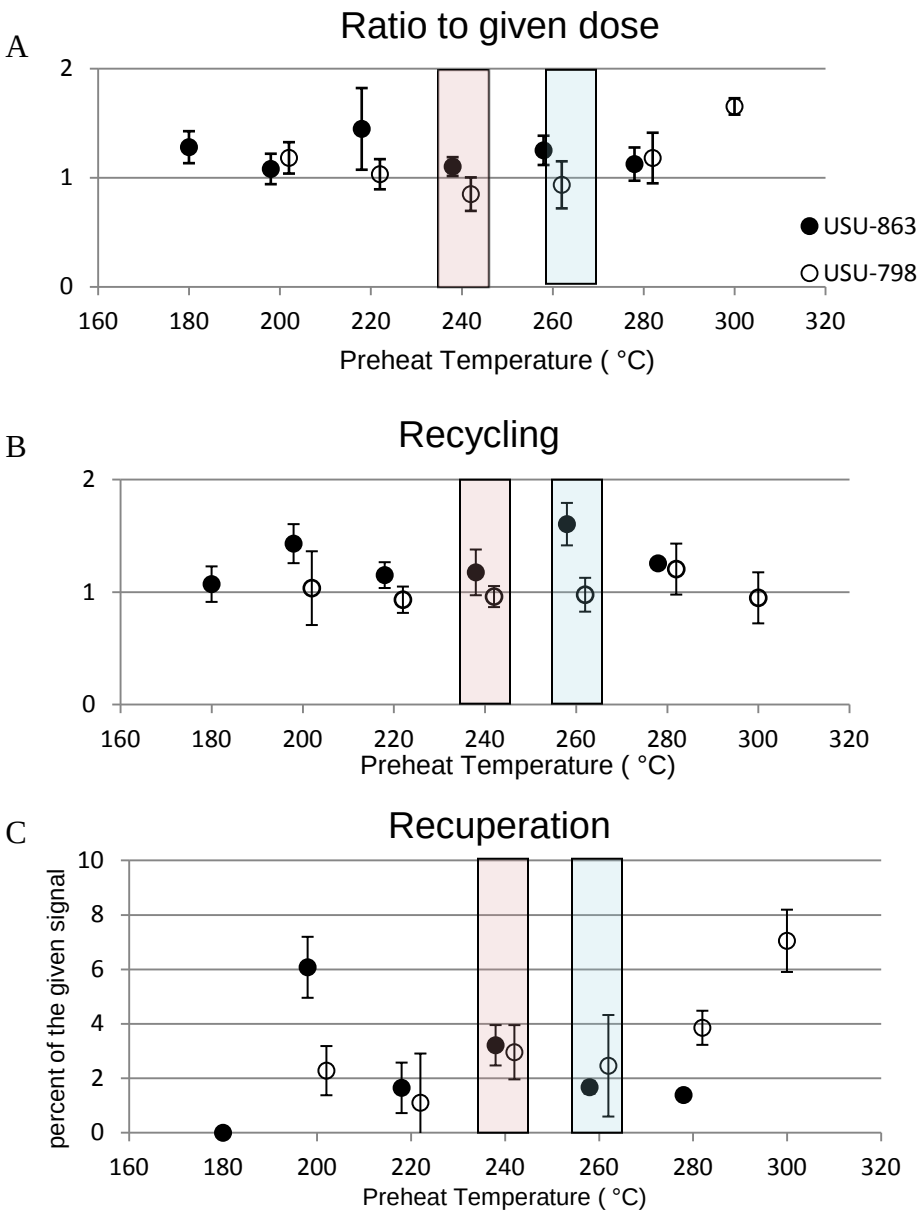

Figure 2.3 Dose recovery, recycling and recuperation results from USU-863 (filled in circles) and USU-798 (hollow circles). A) Dose recovery test shows that 240°C is nearest unity with the least error for USU-863 while 220-260°C are likely candidate preheat temperatures for USU-798. B) The recycling ratio (R1'/R1) for USU-863 is lowest from 220-240°C with the least error on 220°C. USU-798 has good recycling and low error from 220-260°C. C) The percent of the given signal recuperated is lowest between 220-260°C for both samples. Light red bars indicate the preheat temperature chosen for USU-863 and the light blue bars indicate the temperature chosen for USU-798.

the true burial age (Olley et al., 1999). Statistical age models have been developed to address dose distributions in a variety of depositional environments. These include the central age model (CAM) and the minimum age model (MAM) (Galbraith et al., 1999).

Sample Collection and Analytical Preparation

Fifteen samples were collected from eight sites on the Marana Plain near the Golo River. In general, multiple samples were taken from different depths and/or lenses of each deposit to reinforce the validity and reproducibility of the OSL-derived ages and monitor for problems with individual samples.

Samples were collected using opaque steel tubes hammered into sandy interbeds. Sediment from a 30 cm diameter around the sample tube was collected for dose-rate calculation and moisture content. Elevation, latitude, longitude and sample depth were recorded for the calculation of the cosmic contribution to the dose rate (following Prescott and Hutton, 1988). All samples were processed under dim amber light conditions (~590 nm) at the Utah State University Luminescence Lab, Logan, Utah, USA. Elemental analyses for dose-rate calculation were performed at ALS CHEMEX Labs, Sparks, Nevada, using ICP-MS and ICP-AES procedures. Small aliquot age estimates on quartz sand were determined using the single-aliquot regenerative-dose (SAR) protocol of Murray and Wintle (2000).

In order to reduce the potential of incorporating exposed or mixed-origin grains into the target sample, outcrops were cleared back in the field before

sampling and in the lab ~2 cm of sediment was discarded from the ends of each tube to remove sediment exposed to light during sampling. Samples were wet sieved to target grains between 75-250 µm (eg. 75-150, 90-150, or 150-250 µm, see Table 2.2 for grain size used for each sample). All samples were treated in 10% hydrochloric acid to remove carbonates followed by household bleach to remove organic material. Heavy minerals were removed from the remaining material using sodium-polytungstate (2.7 g/cm^3). The lighter suspended minerals (mostly quartz and feldspars) were then treated in 47% hydrofluoric acid for a total of three thirty-minute treatments with the hydrofluoric acid decanted and replenished following each treatment. The hydrofluoric acid step is aimed to dissolve feldspars and to etch the outer 5-10 µm of the quartz grains to remove any contributions from alpha radiation as well as any iron staining of the grains. This was followed by a 37% hydrochloric acid rinse to remove any precipitated fluorides. After rinsing and drying, the samples were dry sieved to remove partially dissolved feldspar and quartz grains <75 µm.

Aliquots of the remaining quartz sand were adhered in a monolayer to stainless steel disks using a silicon spray. All samples were loaded within a 2 mm diameter area in the center of the disk and consist of ~120 grains for samples sieved to 75-150 µm and ~45 grains for samples sieved to 150-250 µm. Due to low luminescence response, sample USU-870 was loaded using a 5 mm diameter area mask and consists of ~500 grains for the 90-150 µm grain size fraction. All optical measurements were performed at 125° C on Risø TL/OSL DA-20 readers with blue-green light emitting diode (LED) stimulation (470 nm)

and an intensity of 40 and 50 mW/cm^2, using a 7.5 mm Hoya U-340 detection filter, with 90% diode power and a ^{90}Sr/^{90}Y β-irradiation source (dose rates of 0.1458 and 0.1276 Gy/s).

Results

Geomorphic Mapping

Using geomorphic principles and OSL dating, results of this study suggest that there are four discernible Golo River terrace surfaces on the Marana Plain (Figure 2.4). During the course of this study, several inconsistencies and problems with previous mapping were addressed and modified. These include four major changes, described as numbered on Figure 2.5: 1) The BRGM Fy1 and Fy2 map units of Lahondére et al. (1994) were combined here into one unit, mapped as the Qat3, Poretta Terrace. 2) The BRGM Fy3 and Fz units were modified to reflect younger terraces (Qat1 and Qat2) that are much wider than originally mapped and incorporated some of the Fy2 on the southern side of the Golo River. In addition, part of the Fy2 was modified to reflect a gently seaward dipping marine onlap overlying the Qat3 near the coastal margins. 3) The BRGM geologic map has the Fx unit mapped on the north and south side of the Golo River. The Fx unit on the southern side of the Torra Terrace is an inset terrace (mapped here as Qat_L) that is not associated with the Golo River. On the northern side of the Golo River, the Fx unit is a fan shaped deposit that consists of angular, poorly sorted, locally sourced Schistes Lustrés and is referred to as the Revinco Alluvial Fan, Qaf_o. 4). On the southern side of the river near the

mountain front, the Fw unit was revised as Qac (Quaternary alluvium-colluvium) with additional local tributary sediments cross-cutting this unit now mapped as Qal (Quaternary alluvium).

Sample Descriptions and Locations

Golo fluvial gravels are differentiated from other coarse-grained alluvial deposits on the Marana Plain by the presence of granites and rhyolites sourced from the Hercynian basement rocks found in the headwaters. Field investigations identified four terraces of the Golo River, described below (Figure 2.4, Table 2.4). Local tributaries and stream catchments emerging onto the coastal plain originate in the Schistes Lustrés and consist primarily of angular fragments of metabasalts and schists. Within the canyon reach of the Golo River just upstream of the coastal plain, terraces are discontinuous strath terraces and difficult to correlate. However on the Marana Plain, there are fill terraces that are more easily identified and correlated and are the focus of this study. Good natural exposures of terrace deposits are rare due to the low gradient of the Marana Plain but the aforementioned road cuts proved vital in OSL sample collection. In addition to samples from three of the four terraces, OSL samples were taken from two alluvial/colluvial deposits, one laterally continuous sandy unit beneath an alluvial fan and from the farthest inland beach ridges in the region (Table 2.1, Figure 2.4, Appendix B).

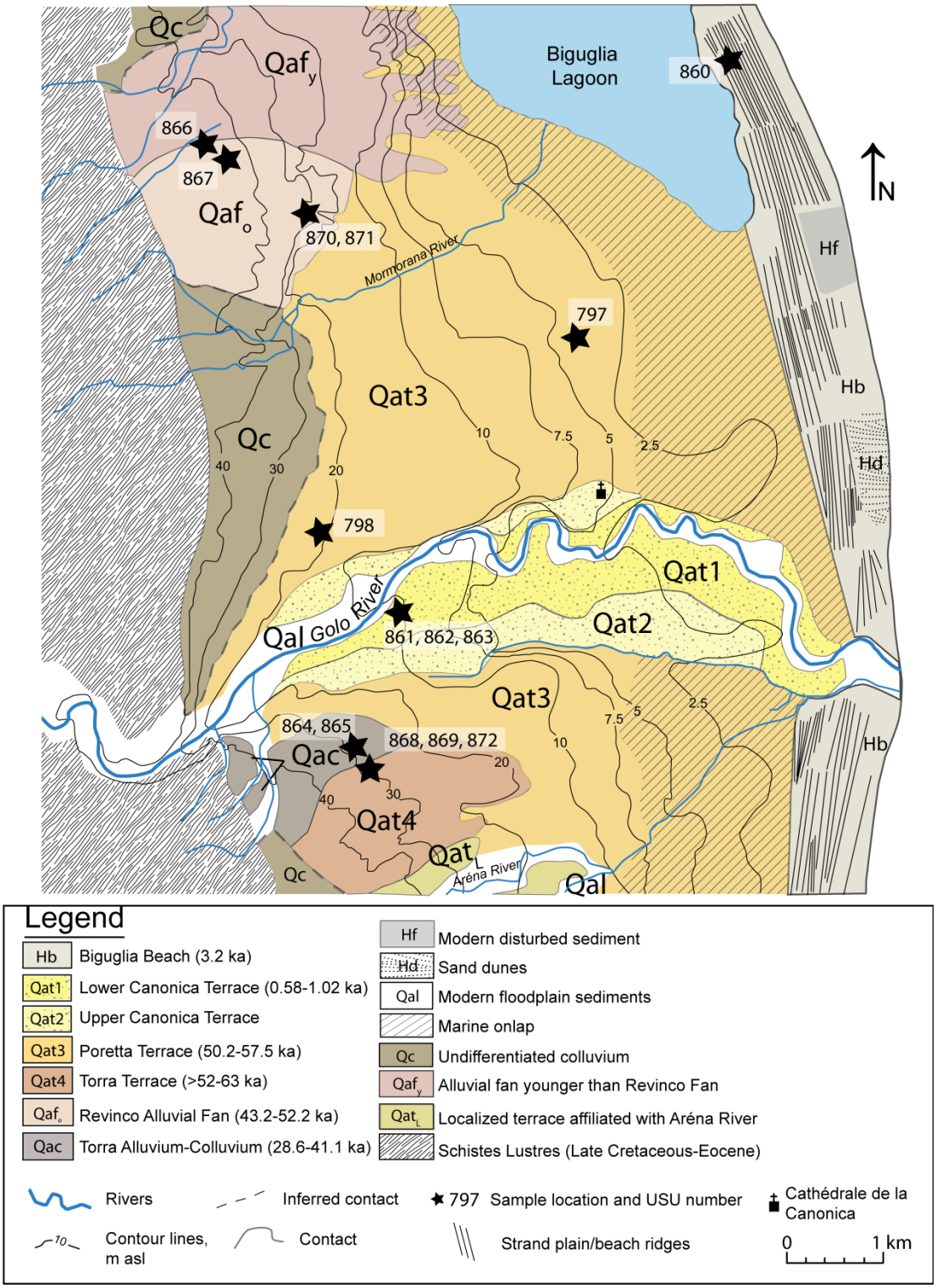

Figure 2.4 Geologic map of the central Marana Plain (from this study).

Table 2. 4 Geologic map descriptions

Unit	Name	Description
Qat1	Lower Canonica Terrace	gray soil with fine grained overbank silts, cobble to pebble channel deposits with sandy interbeds
Qat2	Upper Canonica Terrace	"
Qat3	Poretta Terrace	brown soil with laterally and vertically extensive imbricated gravel deposits and thick lenticular medium to coarse grained sand lenses
Qat4	Torra Terrace	red soil with highly weathered, weakly imbricated cobbles and fine to coarse sand lenses
Qac	Torra alluvium-colluvium	clast supported, poorly sorted, highly weathered, rounded clasts to massive fine grained deposit with angular fragments of locally sourced rocks
Qaf_o	Revinco Alluvial Fan	poorly sorted rubified sediment consisting of matrix to clast supported, weakly imbricated angular to subrounded clasts of locally sourced metamorphic rocks; some massive, homogenous medium to coarse grained sand lenses with silt and clay
Qaf_y	Alluvial fan younger than Qaf_3	younger alluvial fan cross-cutting the Revinco Fan and radially extending seaward
Qc	Undifferentiated colluvium	covered and vegetated hillslope sediments along the mountain front
SL	Schistes Lustrés	metabasalts, metagabbros, mica-, calc- and greenschists and serpentinites
Qal	Alluvium	Quaternary to modern inset floodplain sediments from localized ephemeral to perennial tributaries
Qatl	Localized alluvial terrace	alluvial terrace associated with deposition along the Aréna River
Hd	Holocene sand dunes	
Hb	Holocene beach ridges	
Hf	Modern fill/disturbed area	modern development and disturbance

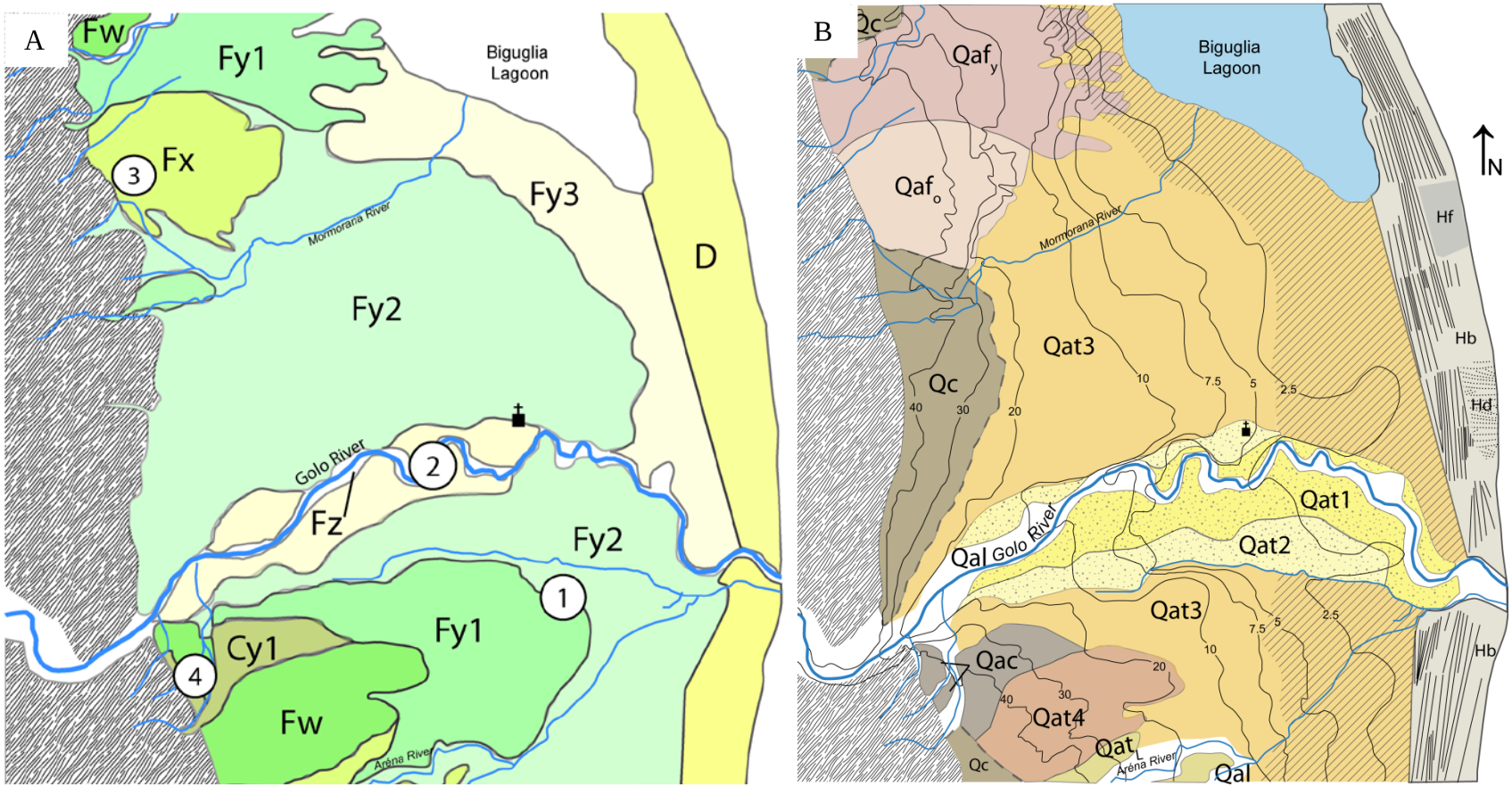

Figure 2.5 Comparison of modifications from original geologic map A) geologic map of Lahondére et al. (1994), where numbers represent the locations of major changes discussed within the text B) geologic map from this study.

Canonica Terrace (Qat1-Qat2)

The upper and lower Canonica fill-cut fluvial terrace ranges from 0.5-4 m above the modern river. These terraces are interpreted to be inset into an older OIS 2 alluvial fill deposit when the Golo River was graded to a lower sea-level (Figure 2.6). The upper Canonica terrace is host to a historic 12th century church, Cathédrale de la Canonica, on the north side of the river ~3.5 km from the river mouth. Levees were built on this terrace to mitigate modern flooding. The upper Canonica surface (Qat2) is more extensive on the southern side of the river; however no samples were collected from this deposit in this study, as there were no adequate exposures other than the historic site previously sampled by Sømme et al. (2011). A map of the Marana Plain from 1866 AD shows a portion of the river in a more southern position and as a braided stream (Figure 2.7). The lower Canonica Terrace (Qat1) may represent an inset floodplain due to northward migration of the Golo River.

On the south side of the Golo River, the Paduloni site is on the lower Canonica terrace (Qat1) and is located ~500 m from the modern river and 3 m above the modern river (Figure 2.8). Approximately 3 meters of soil and alluvium are exposed at this. This deposit is characterized by weakly imbricated cobble to pebble gravels with sandy interbeds overlain by ~2m of gray silty sandy loam (10YR 4/4) interpreted to be overbank deposits and weakly developed soil horizons. Three samples were taken at the Paduloni road cut and represent a suite of depositional ages, ranging from terrace building to overbank silt

deposition. Sample USU-861 was collected near the base of the overbank silts 2.3 m depth from a dark brown (7.5 YR 3/4) medium lower sand-rich bed and produced an age of 0.58 ± 0.16 ka. USU-862 was taken 2 meters below the present surface in a cobble to pebble gravel unit within a ~0.4 m thick dark yellowish brown (10YR 5/3) medium upper to medium lower sand lens. This sample produced an age of 0.70 ± 0.21 ka. The stratigraphically deepest sample, USU-863, was taken 3 meters below the surface in a fine upper to medium lower sand lens within a cobble to gravel unit. This sand lens contains a humic layer with iron staining near its upper boundary, although no identifiable samples for ^{14}C were found. USU-863 produced an age of 1.02 ± 0.23 ka.

Poretta Terrace (Qat3)

The Poretta terrace is the most extensive surface on the Marana Plain (Figure 2.9). The tread of the Poretta terrace ranges from 2.5-10 m above the modern river. The range in height is due to the Poretta terrace having a steeper gradient than the modern river. The Poretta terrace is evident at the mouth of the Golo River, and fans out across the coastal plain with the steepest gradients near the mountain front. This surface was once a large, braided fan of the Golo River as indicated by its surface characteristics, clast provenance, and sedimentary structures. Imbricated cobbles and gravels with frequent lenticular sandy interbeds characterize the Poretta alluvial deposit. It has well a developed mollic soil (7.5 YR 4/4) with a ~1m Bt horizon. Multiple operating gravel pits exist on this surface with one exposure on the seaward side of the Bastia-Poretta airport

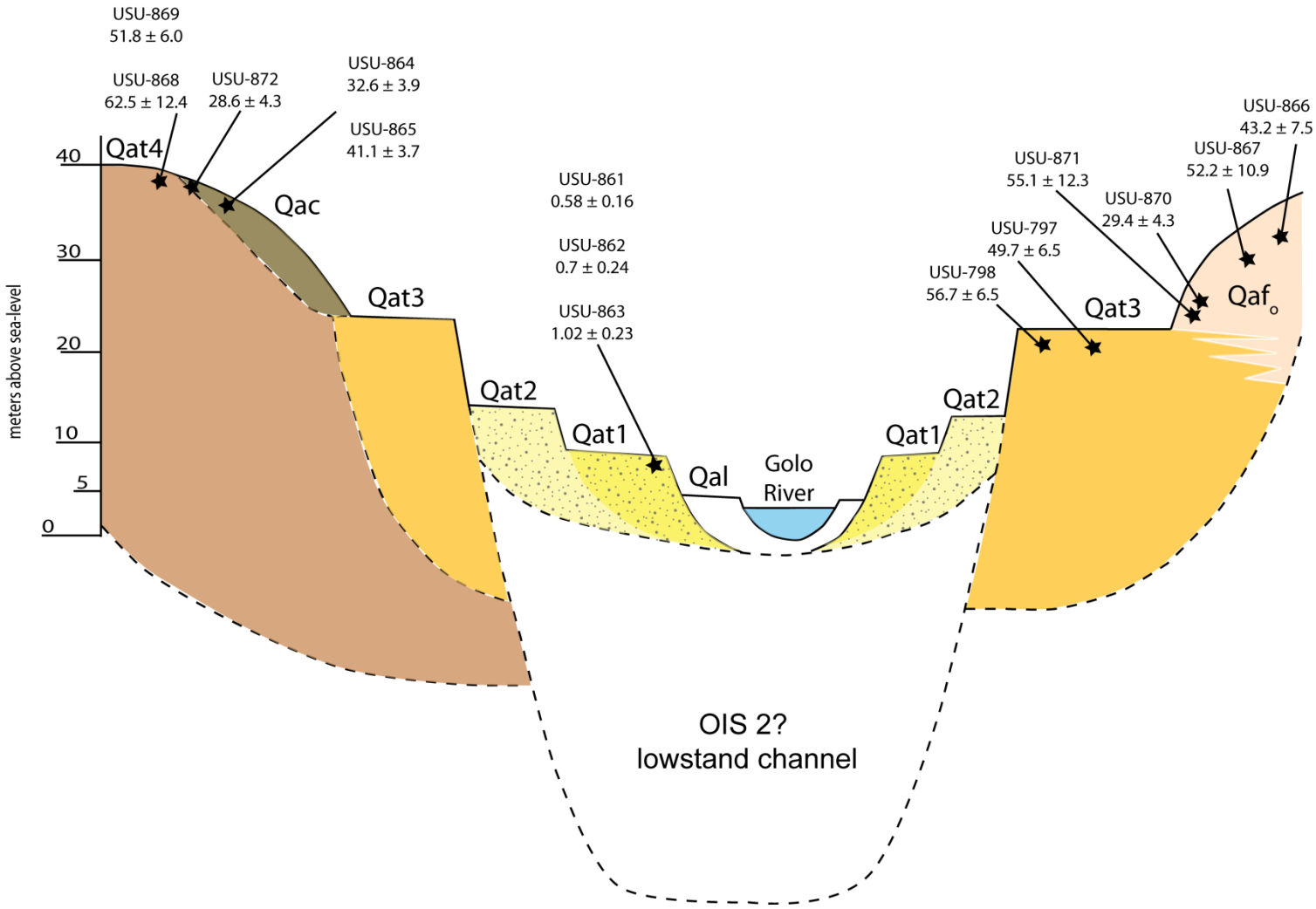

Figure 2.6 Cross-section view of the Marana Plain and associated OSL ages. Not to horizontal scale

Figure 2.7 Map of the Marana Plain from 1866 AD, Bureau de Recherche Géologiques et Minières (BRGM). The blue line represents the course of the modern day Golo River. The black star is the location of the three samples taken from the lower Canonica terrace (USU 861-863) and the church symbol on the north side of the river is the location of Cathédrale de la Canonica.

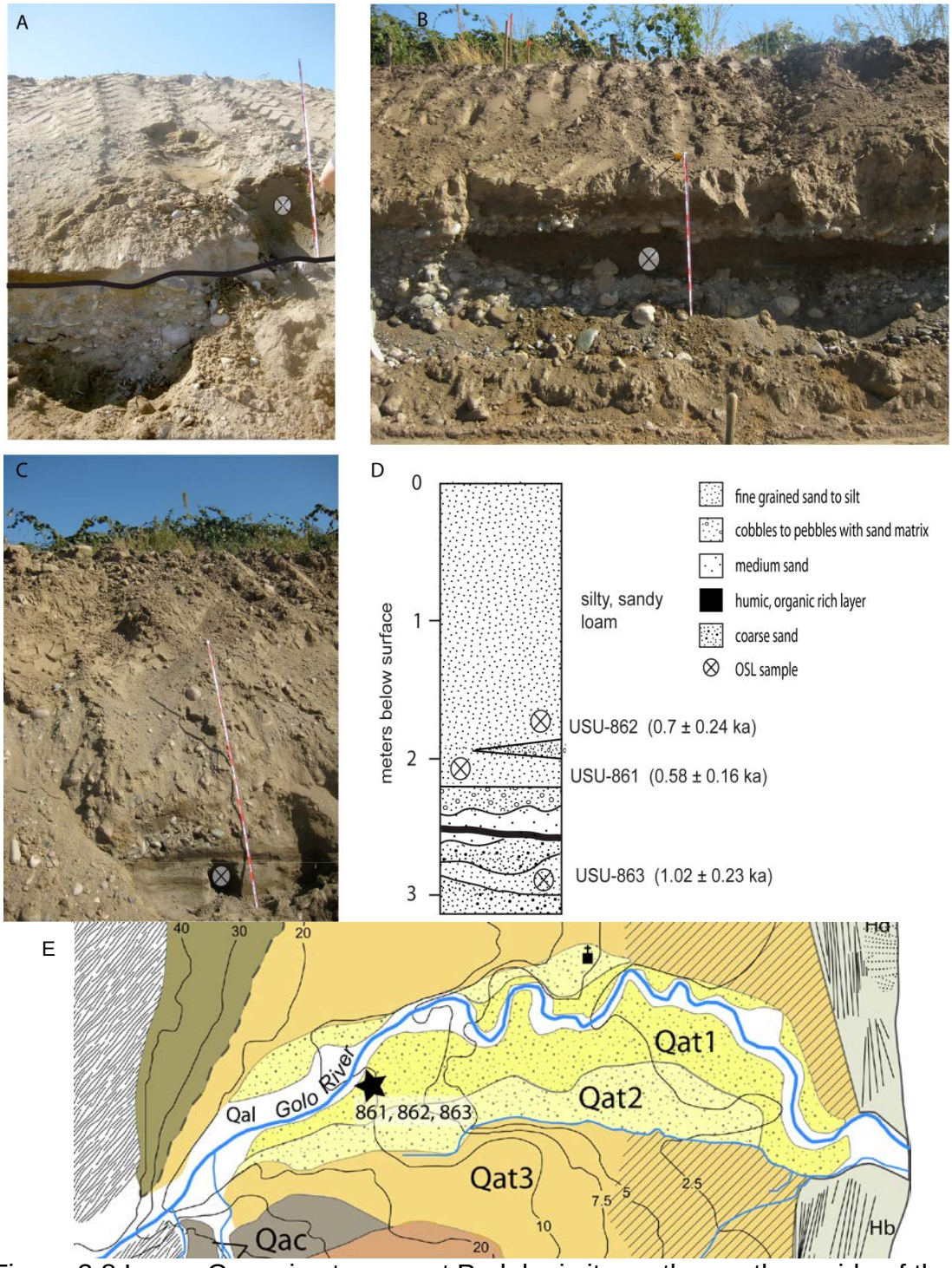

Figure 2.8 Lower Canonica terrace at Paduloni site on the southern side of the Golo River. Three samples were taken and were OSL dated to 0.58-1.02 ka. A) USU-861. Dark black line indicates the transition from fine overbank sediments to fluvial channel deposits. B) USU-862 C) USU-863 D) Composite stratigraphic column of Qat1 E) Location map of samples.

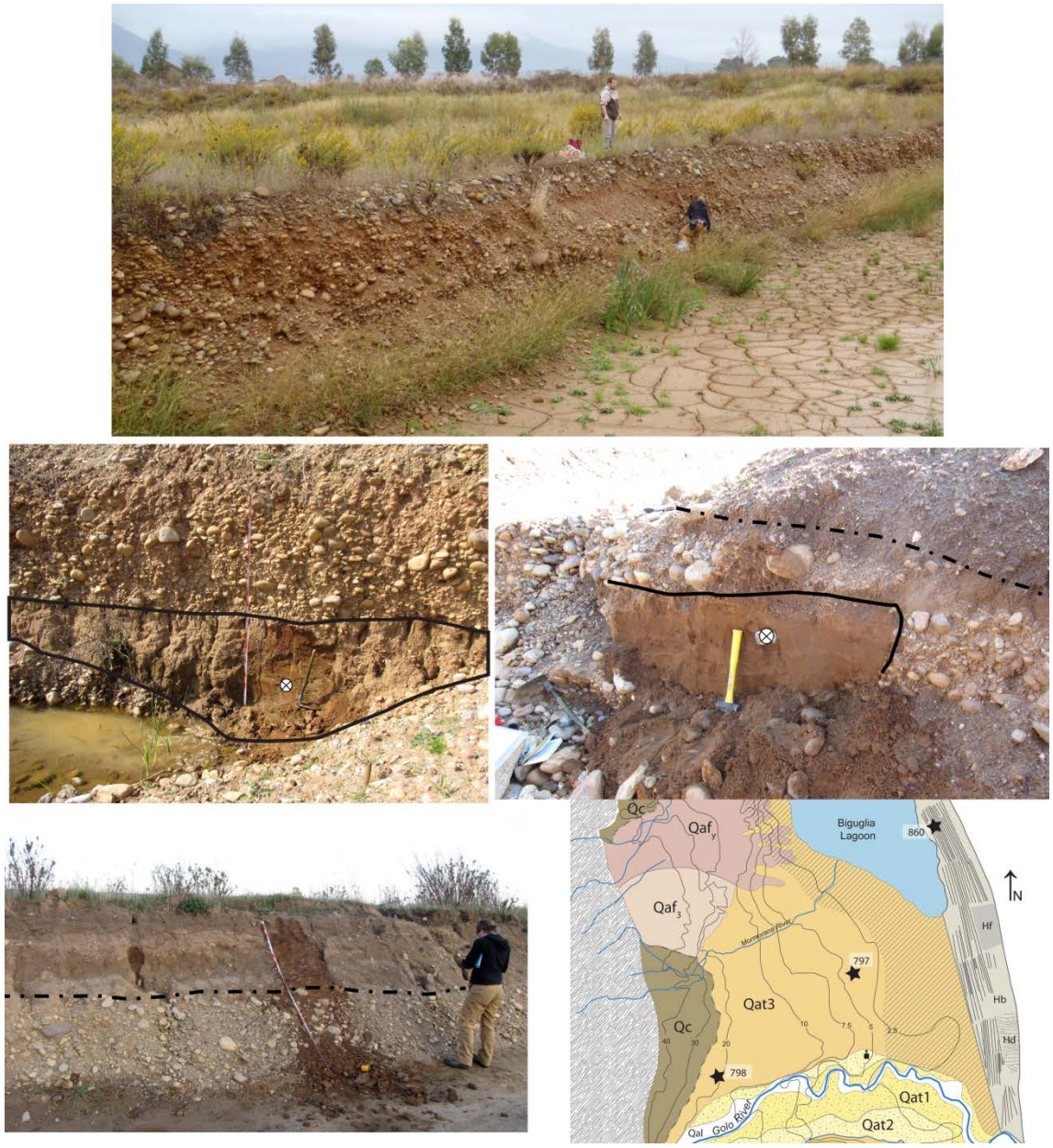

Figure 2.9 Two Poretta terrace (Qat3) exposures on the northern side of the Golo River. A) Two-meter thick continuous exposure within the Betag gravel pit B) Solid black lines indicates sand lens sampled (USU-797) within the gravels C) USU-798 sand lens (solid black line). Dashed line separates disturbed soil above Qat3 D) Exposure of an intact soil profile in overbank fines overlying rounded fluvial cobbles of the Qat3 (separated by the black dotted line) E) Location map for Poretta terrace samples and Biguglia beach ridge sample denoted by stars.

exposing more than 5 meters of gravel in steep-walled trenches. The Poretta terrace is buried by Holocene coastal sediments and overbank deposits near the coast, with the onlap point up to 2.5 km inland from the current shoreline.

Betag Gravel Pit

The Betag gravel pit is located on the north side of the river and exposes the upper ~2 meters of imbricated, rounded cobbles with occasional sand lenses (Figure 2.9 A). The original land surface and soil profile at this site has been modified by erosion and anthropogenic influences; however there is still a soil profile visible in places. Sample USU-797 was taken from a meter thick sand lens with redoximorphic features. This sample was taken 1.9 m below the original surface (near the water line in the pit) and produced an OSL age of 49.7 ± 6.5 ka.

Old Golo Canal

An old canal runs parallel to the mountain front on the north side of the river connecting the Golo River to the Mormorana River. The original surface at the sample location was removed; however, less than five meters to the east, an exposure of the 0.9 m intact brown soil profile with the underlying fluvial gravels is visible (Figure 2.9 B). The soil exhibits increasing clay content with depth and clay films on angular to columnar ped faces (Bt horizon). The soil is highly micaceous with small pebbles and medium to coarse sand and few to no roots. Neither the soil nor the matrix of the fluvial gravels reacts to HCl. The canal exposes ~4 meters of clast supported, imbricated river cobbles. Sample USU-

798 was taken within a 0.4 m thick, medium to coarse grained sand lens ~1.95m below the original surface. OSL results for USU-798 produced an age of 56.7 ± 6.5 ka.

Torra Terrace (Qat4)

The Torra Terrace is the highest of the alluvial terraces associated with the Golo River on the Marana Plain (Figure 2.10). This terrace ranges from 20-40 meters above the modern river and is only preserved on the southern side of the river. This unpaired terrace is the least aerially extensive Golo River terrace on the Marana Plain. The Torra terrace is cross-cut by the Poretta terrace but neither the base of this deposit nor the contact between these two terraces were seen. The slope of the Torra terrace is much steeper and distinctly different than that of the other terraces. This terrace is highly dissected by gullies and channels and its riser is abutted by a thick alluvial/colluvial apron (Qac) composed of reworked gravels along the terrace riser to the north.

The Torra pit, a small deep pit (50m x 20m x 5m) on the north side of road D237 exposes a contact between fluvial gravels and fine-grained alluvial slopewash. Approximately 5 meters of cobbles and gravels is exposed. The surface has been modified through cultivation and erosion with approximately 2 m removed (but is included in the total depth for OSL determination of USU-868 and 869). Deposits are interpreted to represent channel facies of the Golo River based on the nature of the deposits and clast provenance. Fluvial gravels consist of rounded clast-supported boulders, cobbles and pebbles with

uncommon thin sand lenses no more than 30 cm thick. These gravels contain intensely grusified granites, and weathered calcschists, micaschists and metabasalts. OSL sample USU-868 was taken from a 0.25 m coarse-grained sand lens 2.5 meters below the present land surface. USU-869 was taken from 2 m depth in a structureless 0.3 m fine to medium sand lens with highly weathered pebbles. OSL age results for USU-868 and USU-869 are 51.8 ± 6.0 and 62.5 ± 12.4 ka. These results are thought to be minimum ages due to the extensive weathering and uncertainties in dose rate (see Discussion section).

Torra reworked alluvium (Qac)

On the southern side of the river, there is a composite alluvial-colluvial deposit mapped as a colluvial apron along the terrace riser off the northwestern side of the Qat4 (Figure 2.11). Near the Qat4 terrace tread-riser break, this deposit is poorly sorted, clast supported with a coarse grained matrix and predominantly consists of rounded Golo River clasts. Further upslope and stratigraphically higher, this deposit becomes finer and contains angular clasts.

Torra pit

Within the Torra pit, an inset surficial deposit of poorly sorted, coarsening upwards, medium to fine sand containing angular clasts abuts the paleo-erosional scarp of the Torra terrace and thickens away from the contact with fluvial cobble gravels of the Torra terrace deposits (Figure 2.11A). This deposit also contains layers of matrix supported, poorly sorted, weakly stratified alluvium near the top of the outcrop and may interfinger with the Torraccia road cut further

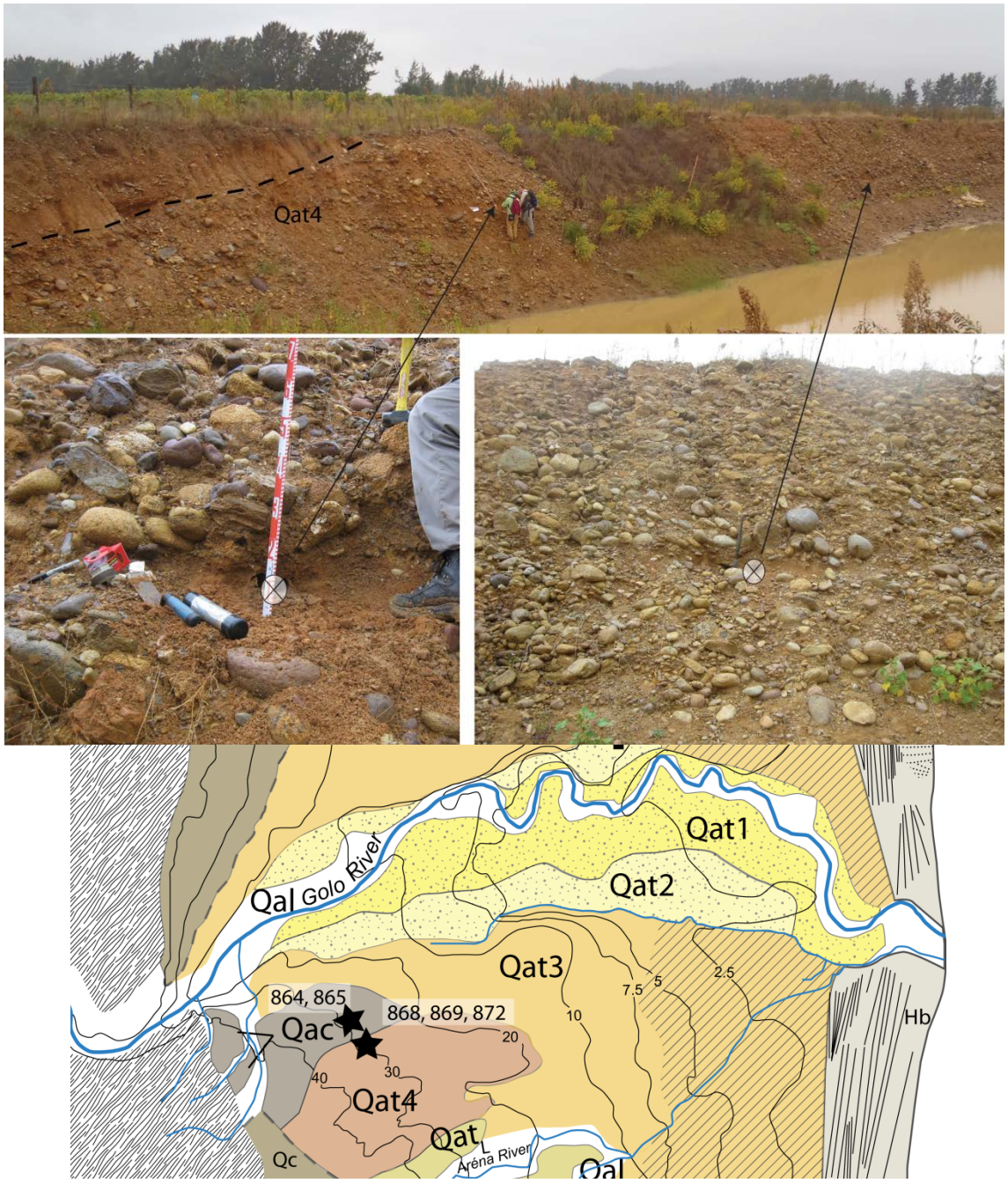

Figure 2.10 Torra pit exposure of the Torra terrace (Qat4). Dashed black lines represent the contact between the fluvial and colluvial deposits A) Torra terrace exposure in the Torra pit B) USU-869 C) USU-868 D) Location map, stars denote sample locations.

downslope. Soil development into this deposit is less than with the Torra alluvium and there are manganese stains within and along rootlets and pores. USU-872 was taken from 2 m depth from a brownish yellow (10YR 6/6) medium to fine grained sand and produced and age of 28.6 ± 4.3 ka.

Torraccia road cut

Near the toe of the Torra Terrace, a road cut near Torraccia (17 m asl) has exposed reddened matrix supported gravels and sand (Figure 2.11 B, C). This exposure is just north of the Torra Pit exposure along the terrace riser between the Torra and Poretta terrace. Within the 2.5 meters of exposure, a thin (~0.6 m) horizon of cultural fill overlies poorly sorted, yellowish red, 5YR (5/6) matrix supported, rounded boulders and coarse gravels with sparse, subangular to subrounded, fine upper to very coarse upper sand (177-2000 μm) interbeds. This deposit is interpreted to be reworked alluvium of the Torra deposit draping the terrace scarp down to the Poretta terrace. Two sample tubes were collected for each sample due to the coarse-grained nature of the available sand lenses. USU-864 was collected from 1.35 m depth within sandy gravel and OSL results return an age of 32.6 ± 3.9 ka. USU-865 was collected at 2 m depth from a 0.4 m thick, fine to medium sand lens exhibiting massive structure to weak stratification with some pebbles. OSL results for USU-865 suggest an age of 41.1 ± 3.7 ka.

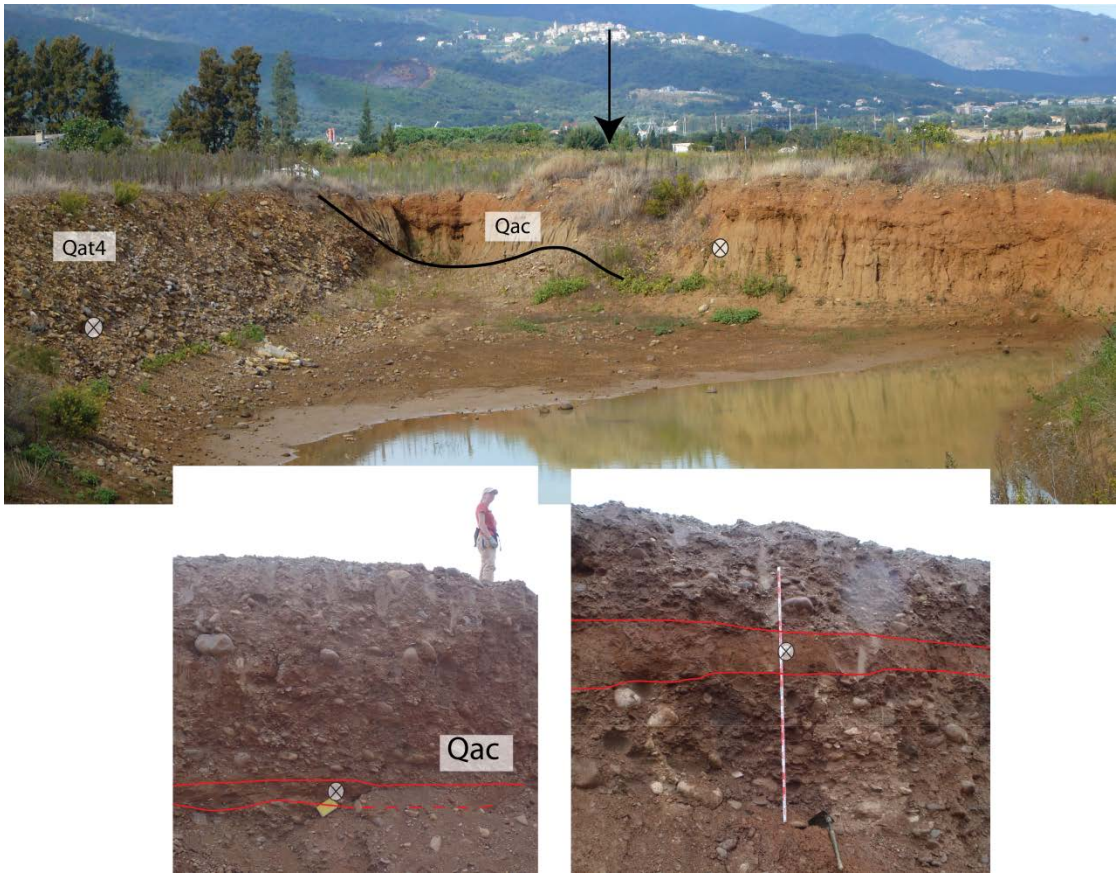

Figure 2.11 Torra reworked alluvium (Qac) localities on the southern side of the Golo River. A) View north-northwest towards Golo River of the Torra pit. OSL locations are noted by white circles with the X. The black line indicated the contact between the Qat4 and the Qac_3. Arrow in the background indicates approximate location of photos in B and C near the trees (~200 m). B) USU-865 C) USU-864 Red lines indicate boundaries of internal sand lenses in which OSL samples were taken from and dashed red line is where the contact is inferred.

Revinco Alluvial Fan (Qaf_o)

On the north side of the Golo River, various local tributaries form a radial alluvial fan with elevations ranging from 20-80 m asl over 2.2 km. This landform has a steep toe and overlays, and potentially interfingers with, the Poretta terrace (Figure 2.12). Deposits are typified by debris flow deposition with poorly sorted, angular clasts of the Schistes Lustrés interspersed with sheet flood deposits of fine to coarse grained sand, with some silt and clay (Figure 2.12A). This deposit lacks well rounded, far traveled lithologies indicative of Golo River provenance. Samples for OSL were collected from the Canavaja and Sant Antone site.

Canavaja site

Near the mountain front, a shallower road cut exposure revealed that approximately 1 meter of soil and colluvium has been removed by construction leaving 1.7 m of colluvium exposed at this site. The upper 1.1 m of this exposure consists of clast supported angular to subrounded cobbles and boulders as well as matrix supported subrounded pebbles to cobbles with a coarse grained matrix of Schistes Lustres. USU-866 was sampled at 1.3 m depth in angular, poor to moderately sorted, clay rich, fine grained sand at 51 m asl (Figure 2.12B).
A fresh road cut exposes ~6 meters of a dark red alluvial. Most of the exposure consists of angular clasts of the Schistes Lustrés interfingered with silty to sandy, moderately-sorted units ranging from fine to coarse grained while near the base of the exposure there is a ~1m thick lens of fine grained sand with some silt and iron manganese nodules. USU-867 was taken 5 m below the surface at 41 m asl in the lower meter of the outcrop (Figure 2.12C). The sand lens sampled was a

homogenous, dark yellowish brown (10 YR 4/6) subrounded to rounded, very fine lower to very fine upper sand with some silt and iron and manganese nodules. OSL results from USU-866 and USU-867 produced OSL ages of 43.2 ± 7.5 and 52.2 ± 10.9 ka, respectively.

Sant Antone site

Near the toe of the Revinco alluvial fan, a continuous road cut reveals a 3.4 m thick and laterally continuous silty-sandy basal unit with an erosional upper contact with an overlying ~2.5 m of locally sourced alluvial fan gravels (Figure 2.12D). The alluvial fan surface overlying this tabular silty-sandy bed is 30 m asl. Two samples were collected from a unique ~6m thick tabular unit exposed in this roadcut. USU-870 was collected 2.5 m below the contact from a yellowish red (5YR 4/6) matrix supported, subangular to subrounded, medium upper to very coarse upper sand with abundant pebbles >1mm. USU-871 was collected at 2.9 m depth below the contact from a deeper recently trenched, exposure saturated due to recent rains (Figure 2.12E). Within the 0.9 m exposed lower profile, there are manganese oxide stains on sub-blocky ped faces with few manganese oxide stringers. This unit is poorly sorted with subrounded, very coarse upper sand grains in a very fine lower sand to silt micaceous matrix. Both samples were taken from homogenous units with no evidence of bedding or stratification; however, clast supported, locally derived sediment is exposed immediately below the tabular silty-sand bed (5.9 m below the alluvial fan surface) (Figure 2.12F). USU-870 and USU-871 produced OSL ages of 29.4 ± 4.3 and 55.1 ± 12.3 ka.

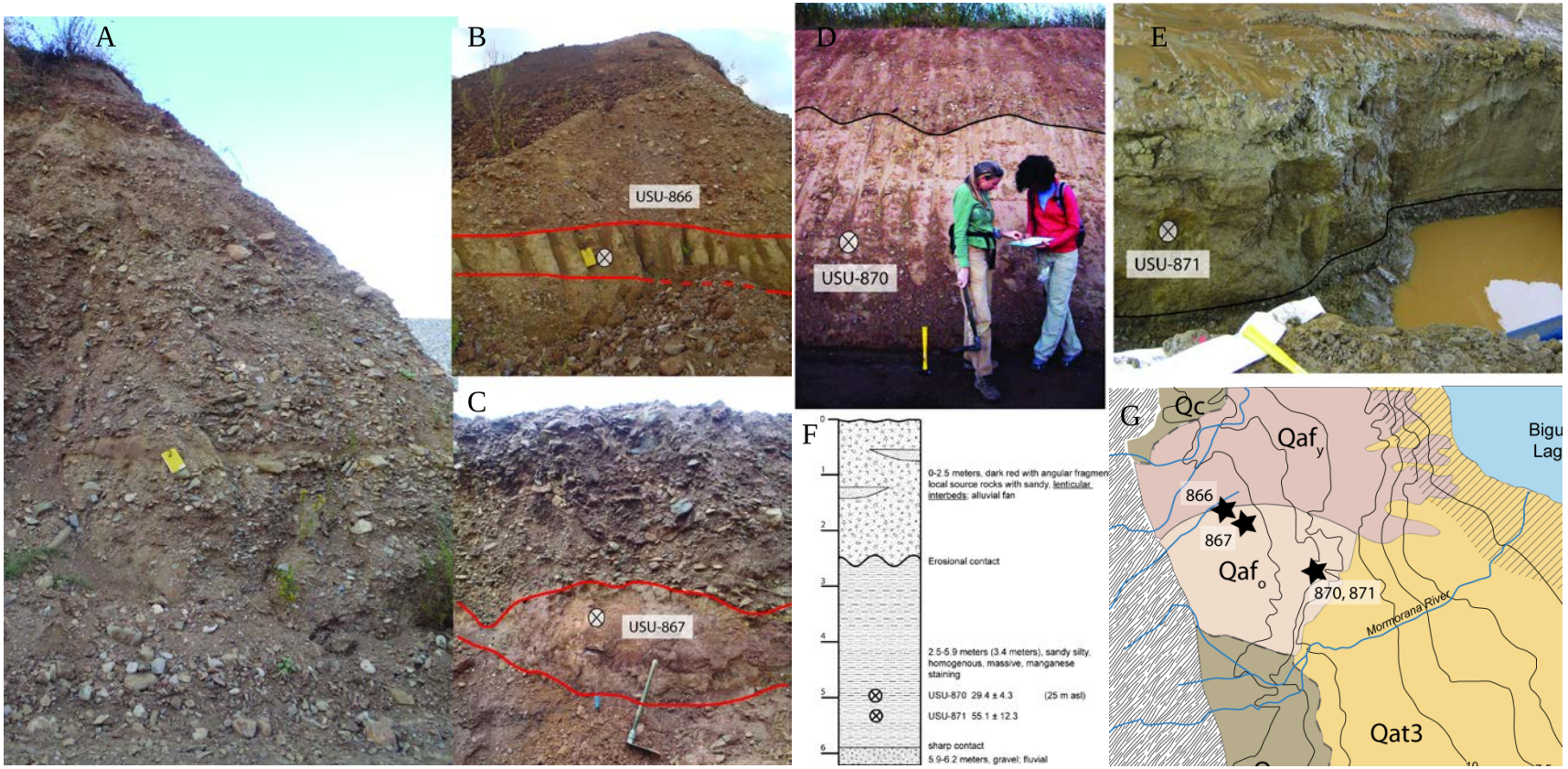

Figure 2.12 Revinco Alluvial Fan (Qafo) A) Outcrop directly across from the photo in B in which the upper 5 m of colluvium is exposed B) Thick sand lens within weakly imbricated locally derived sediment C) poorly sorted alluvial fan debris with irregular sand lens D) Homogenous, massive exposure of lower alluvial fan sediments E) sandy, silty deposit directly above fluvial cobbles and pebbles F) Stratigraphy of the Sant Antone site G) Location map.

Biguglia Beach Ridge (Hb)

The coastline of the Marana Plain contains beach deposits that extend ~500 m inland. Beach ridge deposits and strand plains enclose the Biguglia Lagoon and are found on the north and south side of the mouth of the Golo River. Elevations range from 0-3 m asl. In some locations, multiple cross-cutting beach ridge sets are seen especially near the mouth of the Golo River, indicating progressive formation.

Near the southeastern tip of the Biguglia Lagoon (Etang de Biguglia), USU-860 was sampled from a beach ridge at ~1 m depth from homogenous gray sand below a brown to red sand with rooting and pedogenesis. This deposit is one of the oldest, most landward beach ridge features along the baymouth bar separating the Biguglia Lagoon and the Tyrrhenian Sea. Sampling occurred under very wet conditions and was close to the water table preventing description of sedimentary structures. USU-860 produced an OSL age of 3.18 ± 0.98 ka.

Discussion

In most cases, OSL was useful for age determination. In the following discussion, problems with the OSL ages for the Qat4 will be discussed as well as proposed depositional influences in response external forcings.

Age of the Qat4

The Qat4 is the highest and oldest terrace of the Golo River alluvial terraces on the Marana Plain. OSL age estimates from the Qat4 produced OSL

ages ranging from 52 ± 6 to 63 ± 12 ka (OIS 3). Current OSL ages overlap with the Qat3 (50.2 ± 6.4 and 57.5 ± 10.8) suggesting a similar depositional age for both terraces. However it is thought that these Qat4 age results are underestimates based on geomorphic characteristics, evidence for sediment weathering, and changes in dose rates. Lines of evidence for age underestimates include the following: 1) there is a significant difference between the degrees of dissection on the Qat4 terrace surface compared to the Qat3 surface. 2) There is an extensive reworked alluvial deposit in addition to the infill of dissected channels. 3) The Qat4 surface is sloping/tilted at a higher angle than that of the Qat3 surface. 4) Additions and losses of soluble elements are apparent in the chemical signatures of the sediment (Figure 2.13). 5) Intense weathering of the rhyolite cobbles within the Qat4 deposit (Appendix A). Based on these observations, there is reason to believe that the OSL results are inaccurate and that there are inherent problems with quartz OSL dating in the older deposits. These can arise from problems with intrinsic OSL properties of the sediment and dose-rate calculation.

In order to test the relative age of the Qat3 vs. Qat4 terraces, the soluble and insoluble elemental content of each sample was examined. Insoluble elements should have a higher concentration in older samples than soluble elements due to weathering of the sediments. If the Torra terrace were similar in age to the Poretta terrace, one would expect the two deposits to have similar chemical signatures. Figure 2.13 shows a moderate increase in Potassium while becoming depleted in Sodium and Calcium with increasing age. When

comparing the ratio of resistant Titanium to other elements, Calcium depletion stands out as an indicator of a difference in age between the terraces with a ratio that is more than twice that of the other two terraces, suggesting significant age difference for the two terraces.

OSL techniques depend on a luminescence signal dominated by fast decaying components. Some quartz OSL signals are dominated by the intermediate or slow OSL decay components and can result in age

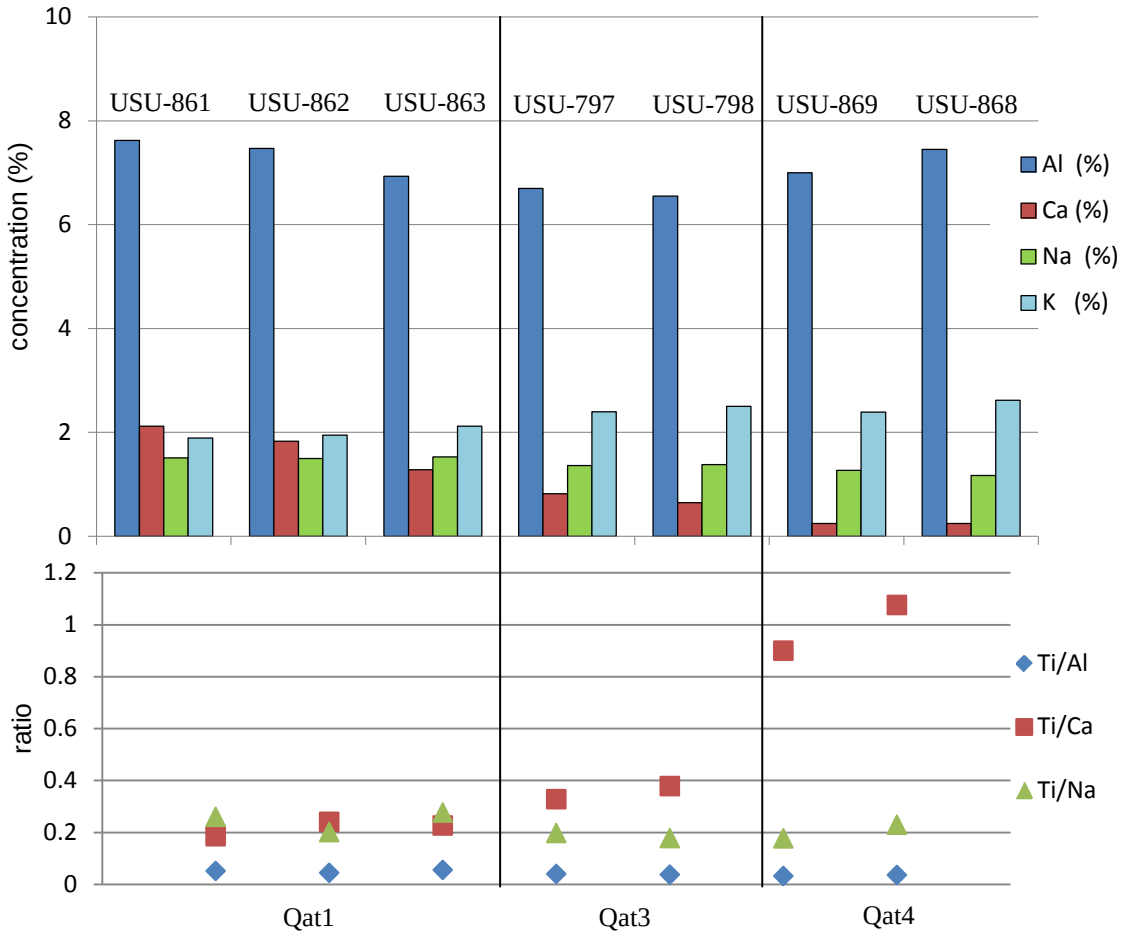

Figure 2.13 Chemistry for fluvial terrace samples on the Marana Plain.

underestimates (i.e. Jain et al., 2003). The ratio of the fast component to the intermediate and slow components should be greater than 20 (Durcan and Duller, 2011). Marana Plain samples have ratios that range from 6-24 with an average of 11-13 and few very aliquots over 20. This low ratio suggests that these samples are not necessarily dominated by the fast component. Furthermore, thermally unstable intermediate components can be identified when the dose equivalent is plotted versus stimulation time, D_et plots (Wintle, 2010). This ratio will decrease and show falling D_et plots if the medium component is not thermally stable (Wintle, 2010; Bailey, 2000). The older Qat4 samples show this general trend and indicate that the medium component is contributing to the OSL signal and may require an alternative OSL analysis method. Early background subtraction helps to mitigate the effects of these unwanted components by isolating the fast component (Cunningham and Wallinga, 2010) and was performed on all OSL samples, excluding the youngest samples.

Age determination of this terrace could also be complicated as a result of luminescence saturation of the sample or the overall sensitivity of the quartz. Sediment within the Golo River valley and its tributaries only has a short distance to travel (~90 river km, at most) with limited storage potential in the bedrock and alluvial reaches, with the exception of the coastal plain. It is possible that the quartz traveling within this system has not experienced enough cycles of exposure to light and subsequent burial to 'sensitize' the imperfections within the crystal lattice and acquire a representative luminescence signal. A measurement of the quartz sensitivity within the Golo system averages 75 counts per Gray,

which is sufficient for luminescence dating. These older samples, while not fully saturated, may be approaching saturation (based on examination of the saturating exponential growth curves) however, this may not be the only contributing factor to age underestimation.

A number of factors could lead to an age underestimation of this surface such as overestimation of dose rate. Over time, soil and sediment weathering can increase the dose rate due to additions, losses and translocations of minerals (Jeong et al., 2007). If the dose-rate measured at the time of sample collection is higher than the mean dose-rate over the length of burial, it will result in an age underestimate. This variability in dose rate through time makes it difficult to correctly deduce which rate adequately represents the system. Microdosimetry can also lead to uncertainty in dose-rate calculation and occurs when some quartz grains are deposited near more radioactive particles and increase the dose rate in a localized region. Secular disequilibrium in the decay series between Uranium and Thorium, two major components of radioactive decay, can also affect the dose-rate calculation; however the ratio of these two elements ranges from 4-5 in the Qat4 samples and does not indicate disequilibrium.

Overestimated, high dose-rates associated with the two Qat4 samples may be contributing to age underestimation. For the Golo River samples, the dose-rate progressively increases as the sample age increases (Figure 2.14). The younger samples from the Qat1 have dose rates that range from 2.4-2.85 Gy/ka while older samples from the Qat4 have dose rates that range from 3.38-

4.02 Gy/ka. However, samples from the Sømme et al. (2011) study on the Marana Plain (Qat2) also returned high dose rates ranging from 3-3.95 Gy/ka. Dose-rate problems and saturation are thought to be the primary causes of age underestimation for the Qat4. Assuming that the dose-rates were too high, an average of dose-rate of 3.0 Gy/ka was used and yielded an age of ~70 ka (OIS 4).

Given the geomorphology discussed earlier, this surface is likely older than suggested by the OSL age. In addition to reasoning discussed above, there is considerable overlap of OSL ages (and their associated error) for the Qat3 and Qat4 (Figure 2.15), thus there is good reason to believe that the ages for this

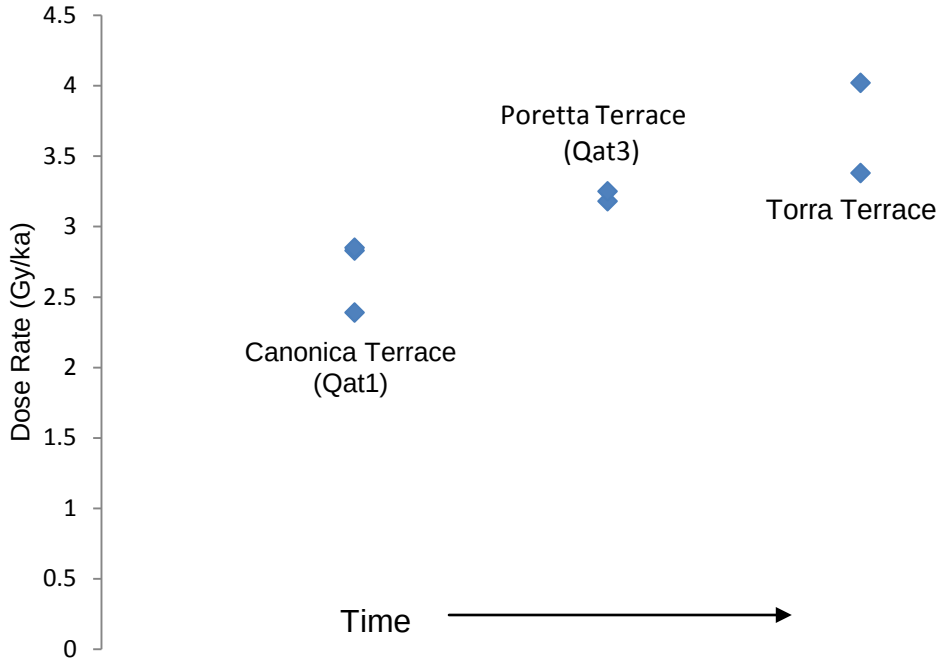

Figure 2.14 Plot of the dose-rate of individual samples from three Golo River terraces studied vs. relative age. Note that dose-rate increases with older terraces.

terrace can only be regarded as minimum ages and deposition occurred pre-OIS4.

River response to climate

Evidence of glaciations throughout the high mountains of Corsica is substantiated by moraine complexes and wide, U-shaped valleys. Although there is a lack of dated glacial sediments in the headwaters older than the LGM, evidence of older glaciations further down valley from dated LGM deposits suggest that Corsica experienced more extensive glaciation during older glacial periods, such as OIS 3-4, 6 and 8. Glacial processes scouring, plucking and abrading bedrock in the headwaters would have resulted in increased sediment production. The Qat3 terrace is the most laterally extensive surface on the Marana Plain. During the deposition of this unit, the Marana Plain would have been an extensive coastal braid plain. The expanse of the coarse gravel deposit suggests sustained high sediment load and transport capacity that may have been in response to changes in the hydrologic system, such as changes in glaciation, vegetation or climate. Fluctuations in glacial advance and retreat at the transition from OIS4 to OIS3 are interpreted to have had increased sediment supply to the Golo, causing aggradation and deposition of the broad Qat3 braidplain.

During OIS 3, there was also increased hillslope activity at the mountain front. OSL ages from the Qaf_o suggest coeval alluvial fan deposition with the Qat3 throughout OIS 3, and progradation slightly into OIS 2 (Figure 2.15).

Sometime after the main deposition of this unit, avulsion resulted in the northern Qaf_y unit, which was not sampled in this study. Also, deposition of the reworked Qac near the Qat4 terrace suggest mobilization of sediment as a result of increased activity from local tributaries, most likely due to increased precipitation in eastern Corsica during OIS 3.

River response to sea-level

The slope of the modern continental shelf (~11 m/km) is steeper than that of the modern Golo River as it flows across the coastal plain (~2.5 m/km) and coastal terrace gradients. While this geometric configuration exerts a primary control on the occurrence of degradation or aggradation, other factors to consider are the magnitude and extent of base-level change (Schumm, 1993). Based on present-day geometry in which the slope of the coastal plain is less steep than that of the shelf, one would expect that the Golo River would respond to sea-level fall with localized incision of the coastal plain, such as that represented in Figure 1.6B.

With respect to the present morphology of the continental shelf margin, only sea-level lowstands more than 120 m below sea-level (lower than the present-day shelf break) would drive incision across the coastal plain, which occurred during OIS 2, 6, and 8. Sea-level lowstand during OIS 2 was ~120 m below present sea-level (Waelbroeck et al., 2002). During sea-level lowering, there would have been localized incision of the channel; however, progressive channel extension to meet the new base-level eventually resulted in extension

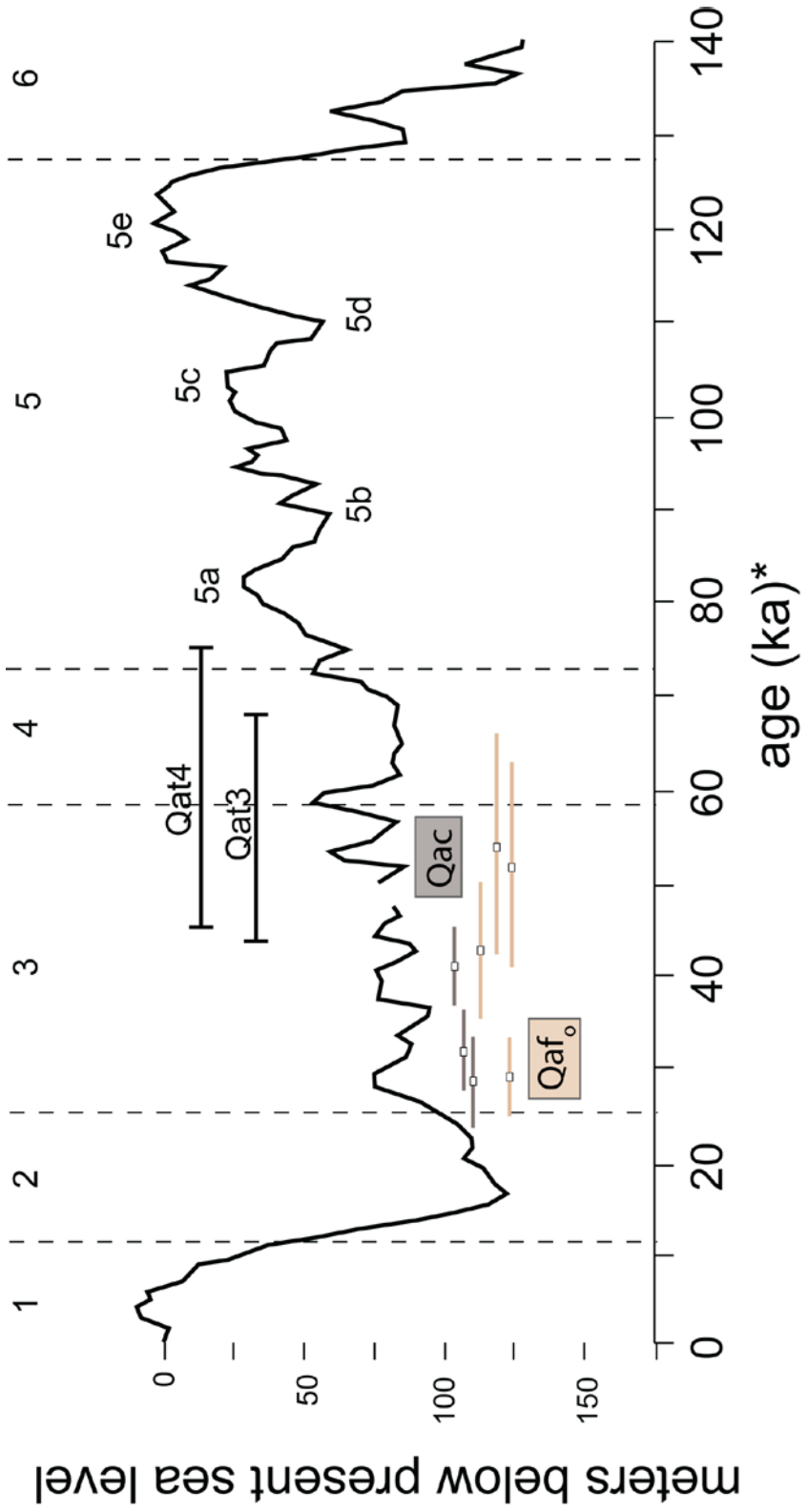

Figure 2.15 Sea-level curve with ages of the Qat3, Qat4, Qaf$_o$ and Qac.

across the shelf break. A rapid increase in channel gradient would have driven incision across the coastal plain and fixed the incised OIS2 Golo River channel. Extensive glaciation in the headwaters would have likely maintained an elevated level of sediment supply and discharge contributing to a steepened gradient. OIS 2 deposits are hypothesized to be well below the modern channel that has since aggraded and backfilled with sediment during sea-level rise as the river gradient shallowed but maintained high sediment supply from the headwaters. With respect to the position of the present day Golo River and Canonica terraces, it is further likely that the total width of the Qat1 and Qat2 represent the valley width of the incised LGM Golo River.

During OIS3/4, sea-level was ~80 m below present sea level (Waelbroeck et al., 2002). The channel gradient during OIS 3-4 may have been slightly steeper than the modern gradient due to a larger grain size fraction bedload; however extension of the river channel most likely did not connect to the shelf break (Figure 2.16). A braidplain encompassing most of the Marana Plain would have been the result of high sediment load of the Golo River, leaving extensive channel gravel deposits and some sandy interbeds. Post LGM sea-level rise led to the onlap of Holocene sediments (up to 2 km inland) and created a wedge that makes the Qat3 and Qat1-2 gradients appear to flatten sea-ward. A depositional setting for the Qat4 is difficult to hypothesize without accurate OSL ages. If Qat4 deposition is associated with a glacially dominated signal, ie OIS 6 or 8, what were the governing factors that preserved it onshore abutted to the mountain front? This suggests that the Qat4 could have undergone major

uplift after deposition or that it could be an OIS5 or OIS7 highstand deposit where accommodation space would allow for large aggradation.

The OSL ages of the Biguglia beach ridge suggests that the modern coastline of the Marana Plain was established by at least ~3 ka. Marine onlap of sediments on top of the steeper dipping Poretta Terrace resulted in a gentle seaward dipping gradient near the coast. With stabilization of sea-level, beach ridges and strand plains formed along the wave dominated eastern margin of the Marana Plain and continued prograding seaward (Johnston et al., 2007).

Response to tectonics

Although the mountain front of the Marana Plain has triangular facets typical of extensional faults, the Qat4 terrace maintains a notably steeper terrace tread profile, opposite of what would be expected from normal faulting. On the northern end of the Marana Plain, just south of Bastia, there is a pop-up structure with exposed (questionably) Pliocene to middle Pleistocene (OIS 6) tilted gravels (Fellin et al., 2005b). The tilted surface of the Qat4 has been linked to the left-lateral transpressional reactivation along the mountain front responsible for the pop-up structure (Conchon, 1977 and Fellin et al., 2005b). Results in this study suggest that 1) The Qat4 is older than OIS 4 and has undergone considerable uplift and tilting or 2) The steeper gradient is reflective of a steeper gradient river channel during deposition. An OSL sample from the gravels within the pop-up structure would be a good start for constraining the timing of related events.

Conclusions

This study identified four Golo River alluvial terraces on the Marana Plain and is pivotal in shifting away from the previous paradigm set in place. Revised mapping of the coastal plain centered on the Golo River is based on geomorphic principles and geochronologic results. While OSL results have not resolved the age of the Qat4, these results have helped refine the chronology of the other alluvial terraces and deposits on the Marana Plain. The expanse of the OIS 3-4 Qat3 is the end result of the combination of an increase in stream power and sediment supply in tandem with base-level lowering that did not cross the shelf break. In contrast, the OIS 2 deposits are buried and onlapped by Holocene sediments due to sea-level fall that resulted in channel extension beyond the shelf break and subsequent incision of the river channel. While sediment production and river discharge is governed by climate in the headwaters, preservation potential near the mouth is constrained by coastal geometry and eustacy.

All colluvial deposits in this study are dated to OIS 3 (Figure 2.15 B) suggesting that while glaciers were forming and receding in the headwaters of the Golo River, there was also increased hillslope activity from local tributaries along the mountain front on the Marana Plain. Both the Qaf_o and Qac deposits overlie the Poretta Terrace (Qat3) indicating that fan building continued well through OIS 3 and potentially into OIS 2.

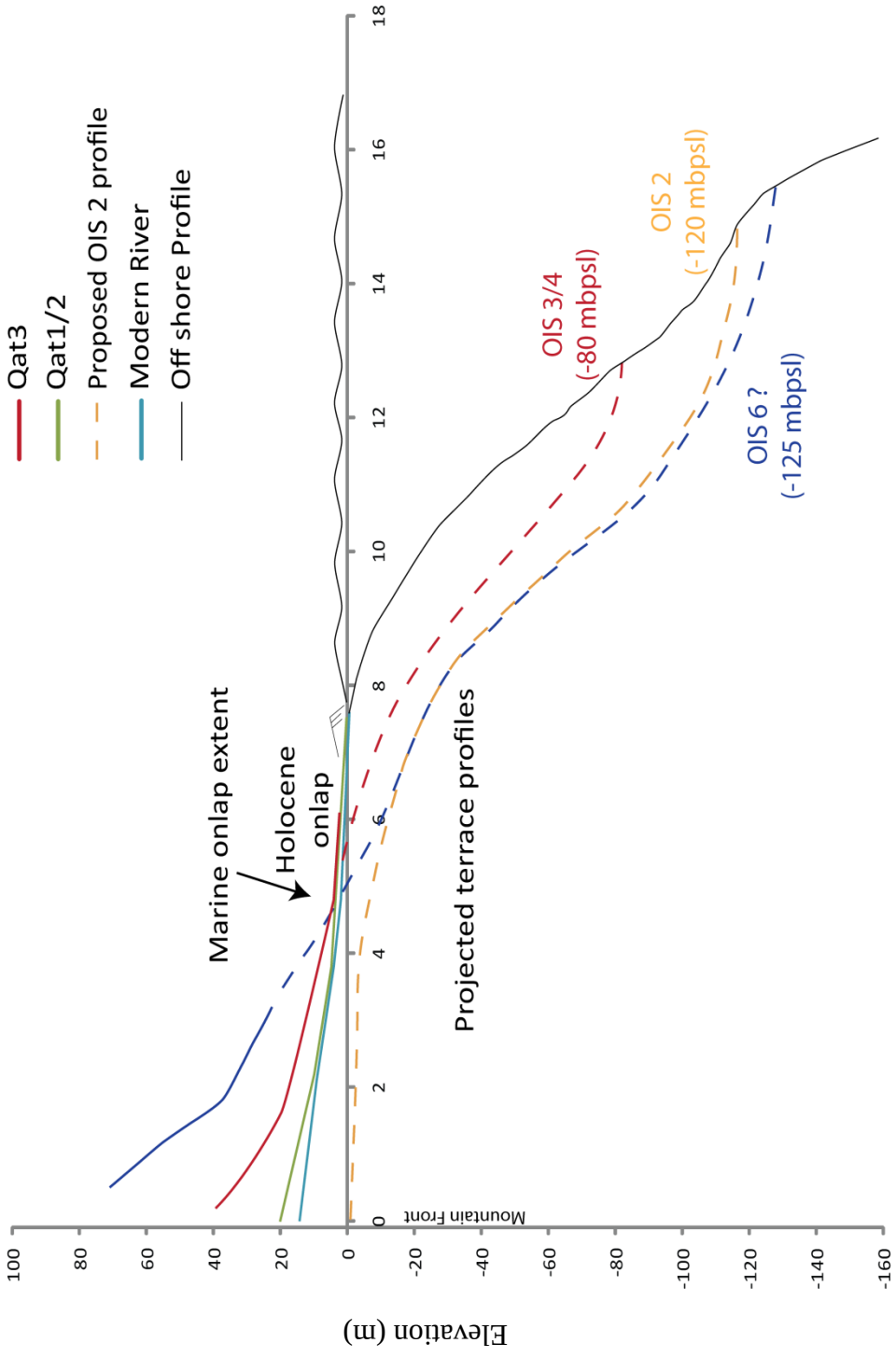

Figure 2.16 Terrace tread profile projections offshore.

CHAPTER 3

WATERSHED ANALYSIS OF THE GOLO RIVER, NORTHEASTERN CORSICA, FRANCE

The primary external variables of tectonics, sea-level and climate along with internal hydrologic and geologic characteristics govern the evolution of a drainage basin. These controls can generate various fluvial responses depending on the rate and location of change. In this study, topography and geology are assessed in a GIS-based analysis to help understand landscape evolution of the Golo River watershed (~1000 km^2). The Golo River drainage network consists of five major tributaries and sub-basins: the Lagani, Tartagine, Asco, Upper Golo and Casaluna (Figure 1.1 and 1.2). All major tributaries converge with the Golo River at Ponte Leccia, 42 km upstream from the mouth. (See Chapter 1 for a review of the geologic history of Corsica.)

Previous Geochronologic and Thermochronologic Studies

Long-term exhumation, erosion, uplift and incision in northern Corsica have been investigated by a number of researchers over the last few decades. In general, there is no age-elevation relationship throughout Corsica, which is thought to be a result of intense tectonic adjustment after cooling of the basement during the Early Miocene (Fellin et al., 2005a; Danišík et al., 2007). Apatite fission track (AFT) and apatite (U-Th)/He (AHe) dating from the Tenda Massif record rapid exhumation at rates greater than 1 m/ky (1000 m/My) during the early to middle Miocene, but decreased to less than 0.4 m/ky (400 m/My)

after the middle Miocene (Fellin et al., 2005a). In comparison, detrital AFT on a pebble in the Saint Florent Basin in northeastern Corsica inferred upland erosion rates of 0.12-0.20 and 0.05-0.17 m/ky (Fellin et al., 2005a). Quaternary erosion rates were reconstructed s using in situ ^{10}Be surface exposure dating of granitic bedrock and indicate Pleistocene valley incision rates (0.25-0.45 m/ky) are an order of magnitude higher than on the relict summit surfaces (0.05-0.024 m/ky) (Kuhlemann et al., 2008)

Longitudinal Profile Analysis

The longitudinal profile of a river represents the relationship between slope and elevation and commonly is concave in profile with decreasing slope as drainage area increases. Two variables for quantifying the shape of a longitudinal profile include the steepness index and concavity. The normalized steepness index (k_{sn}) is a generalized form of the stream-length gradient index of Hack (1973) that allows broad comparison between drainages based on a reference profile concavity, θ_{ref}. The calculation of profile concavity and k_{sn} assumes that the profile is in steady-state and that uplift rate and erosion are uniform throughout each reach (Snyder et al., 2000). In order to first quantify the change of river-bed elevation, the difference between uplift and erosion is expressed as:

$$\frac{\delta z}{\delta t} = U - E = U - KA^m S^n, \quad (3)$$

where $\frac{\delta z}{\delta t}$ is the time rate of change of river-bed elevation, *U* is uplift rate, *K* is a

dimensional coefficient of erosion, *A* is upstream drainage area, *S* is slope, *E* is erosion rate, and *m* and *n* are variables related to basin hydrology, hydraulic geometry, and erosion processes (Whipple and Tucker, 1999; Snyder et al., 2000; Wobus et al., 2006). In a steady-state landscape, in which $\frac{\delta z}{\delta t} = 0$, $E = U$, equation (1) can be solved to give the equilibrium slope, S_e:

$$S_e = \left(\frac{U}{K}\right)^{1/n} A^{-m/n}, \quad (4)$$

where *m/n* is a measure of profile concavity, θ, and $\left(\frac{U}{K}\right)^{1/n}$ is a representation of profile steepness, k_s (Snyder et al., 2000; Kirby and Whipple, 2001). Assuming reach uniformity of *U* and *K*, this power function can then be written as:

$$S = k_s A^{-\theta}, \text{ and} \quad (5)$$

Finally, k_s is normalized according to a representative reference concavity, θ_{ref}, to give the normalized steepness index, k_{sn}:

$$S = k_{sn} A^{-\theta_{ref}}. \quad (6)$$

The value of θ_{ref} is chosen based on the characteristic concavity of stream profiles, and typically $0.4 \leq \theta_{ref} \leq 0.6$ in steady-state landscapes (Wobus et al., 2006; Kirby and Whipple, 2012).

Longitudinal profiles tend to have prominent convexities in tectonically active environments (Burbank and Anderson, 2001) and are useful for identifying zones of irregularity (convexities or knickzones) along the river profile. Knickpoints are the inflection points separating steep reaches (knickzones) along the longitudinal profile from lower gradient reaches. Knickzones may occur as a

result of more resistant bedrock, a localized coarsening of the bedload (Knighton, 1998) or bedrock bedding orientation (Frankel et al., 2007); however they may also point to lowered base-level by way of tectonic uplift or eustacy (Merrits et al., 1994; Pazzaglia, 2003; Wobus et al., 2006). Knickzones retreat headward due to focused energy expenditure and migrate and diffuse through the system (Seidl and Dietrich, 1992; Crosby et al., 2005; Crosby and Whipple, 2006; Wobus et al., 2006; Hayakawa and Oguchi, 2009), the rate of which is proportional to discharge (Burbank and Anderson, 2001).

Although high k_s can indicate active tectonic influence, normalized steepness values (k_{sn}) are more useful for interpreting regional patterns, whereas concavity values can indicate small-scale changes along the channel profile (Wobus et al., 2006). In a tectonically active setting, Snyder et al. (2000) found that concavity was uniform throughout the study area regardless of uplift rate while the ks values vary in step with rates. In contrast, the concavity of a profile is greatly influence by mean annual rainfall intensity-peak annual discharge while steepness values have no correlation to climatic influences (Zaprowski et al., 2005).

Fellin et al. (2005a) attribute the large-scale convexity in the lower Golo River profile to farfield stresses and/or Pliocene-Miocene tectonic perturbations resulting in differential uplift and suggest that these convexities do not correlate to changes in lithology. Collectively, the vast disconnect between exhumation, erosion and incision rates coupled with the presence of knickpoints imply that this area is not operating under steady-state conditions, where incision and

exhumation are balanced (Fellin et al., 2005a; Kuhlemann, et al., 2008; Sømme et al., 2011).

Aerial analysis

Hypsometric analysis provides a representation of how elevations are distributed throughout a basin. A hypsometric curve is a cumulative area-altitude expression that turns basin topography into a normalized unitless form, making it possible to compare basins of different sizes and properties (Strahler, 1952). In general, hypsometric curves follow three shapes: concave (mature landscapes), S-shaped (equilibrium), and, less commonly, convex (youthful) (Strahler, 1952; Hurtrez et al., 1999). In the past, analysis of hypsometric curves had been primarily focused towards understanding the basic stage of topographic evolution, or maturity, of a given basin (Strahler, 1952). Some recent studies have shifted to using hypsometric curves to provide clues about tectonic activity (Hurtrez et al., 1999; Pérez-Peña et al., 2009) as well as the topographic signature of glaciation (Brocklehurst and Whipple, 2004). Slope histograms can be used in conjunction with longitudinal profiles and slope-area analysis to help interpret landscape evolution (Wolinsky and Pratson, 2005).

Project Goals

This investigation aims to incorporate longitudinal profile analysis, hypsometry and slope histograms to assess the tectonic and bedrock influences within each tributary catchment of the Golo River watershed. Specifically, the

influence of the Alpine Fault in western Corsica and uplift and folding in northeastern Corsica on river profiles are investigated.

Methods

Longitudinal Profile

The relationship between the slope and elevation of a river channel can be expressed in the form of a longitudinal profile. In order to create longitudinal profiles and compute concavity and steepness values for the Golo River and its tributaries, the Stream Profiler tool was used (Whipple et al., 2007). ASTER (Advanced Spaceborne Thermal Emission and Reflection Radiometer) data (http://asterweb.jpl.nasa.gov/gdem.asp) were used for the 30-m DEM in ArcGIS. The cell size of 26.863 pixels was derived directly from the DEM and dependent on the resolution of the ASTER data set.

User-defined parameters were established to obtain unique steepness (ksn) and concavity (θ) values (Whipple et al., 2007). Theta ref (θ_{ref}) refers to a chosen reference concavity that best represents the area in question (Wobus et al., 2006). The smoothing window length averages the elevation data and removes DEM artifacts before slope values are calculated (lower resolution requires a longer window) (Wobus et al., 2006). To test for sensitivities to these two input parameters, the model was iterated five times (three to test the sensitivity of the initial theta_ref value and twice to test the influence of the smoothing window). The smoothing window has little to no effect for values of

250 and 500, so a 250 m window was chosen. In contrast, the θ value has dramatic effects on the outcome of steepness values. Reference values of θ=0.4 reduced the anomaly of steep reaches while reference values of θ=0.5 enhanced the steepness values of less steep reaches. For this analysis, I chose to run a reference concavity of 0.45 in order to capture a middle ground. The sampling interval is the specified change in vertical distance between slope calculations and 12.192 m (40 feet) was chosen. Auto k_{sn} is also a moving window used to calculate normalized steepness indices along the river profile at a 5 km interval. The normalized steepness values (k_{sn}) themselves are relative to the chosen θ_{ref} (Wobus et al., 2006). A minimum (min) accumulation value of 10 pixels was used to define how much contributing area leads to channel initiation. After these parameters are set in ArcMap, channel profiles were exported to MATLAB. In MATLAB, the longitudinal profiles, steepness, and concavity plots were created. Elevations for river origins were taken from topographic maps and river lengths were calculated based on data extracted using the Stream Profiler Tool. Positive concavity values indicate a concave-up profile, negative values represent a convex profile and values near 0 resemble a straight line.

For stream profile analysis, the main stem Golo River was broken into four primary reaches based on geologic substratum and the Golo River above the Alpine contact was additionally divided into four sub-reaches. Reach selection in the upper Golo River and other sub-catchments were identified based on groupings of steepened reaches and

knickzones on slope-area plots to identify average values for these components of the profiles.

Hypsometry

Hypsometry for each sub-catchment was extracted in ArcGIS using CalHypso (Pérez-Peña et al., 2009). Histogram bins of elevation display the frequency and distribution of elevation within a catchment. A cumulative hypsometric curve plots elevation (h) relative to the total relief (H) on the y-axis ($\frac{h}{H}$) and the ratio of the cumulative area (a) upstream of a point relative to the entire area (A) of the basin on the x-axis ($\frac{a}{A}$), both on a normalized scale of 0-1 (Strahler, 1952). The hypsometric integral, the area below the ground surface that has not been eroded, is calculated in order to quantitatively assign stages of 'maturity' and typically vary from 0.25-0.7 (Strahler, 1952).

Slope Histograms

Slope histograms were created using the same DEM that was used for longitudinal profile and hypsometry generation. Slope information was exported using the Spatial Analyst extension in ArcGIS and reclassified into 2° slope bins. These data were then imported into Sigma Plot and plotted as a histogram. Statistical values (mean, median, maximum and minimum) were taken from the DEM.

Results

In order to assess tectonic and bedrock controls, each of the sub catchments of the Golo watershed were analyzed in terms of steepness, concavity, hypsometry and slope histograms. Slope-area results for all of the catchments are summarized in Table 3.1.

Longitudinal Profile

The main stem Golo River has four primary reaches based on general lithologic characteristics from the headwaters to the mouth (Figure 3.1): I. Carboniferous Hercynian calc-alkaline granites and Permian rhyolites characterized by steep reaches and fixed stream channels; II. Jurassic terrestrial and marine sediments and Miocene conglomerates in a wide valley with multiple fill terraces (Francardo Basin); III. Late Cretaceous to Eocene Alpine Schist's (Schistes Lustres) with deeply incised meanders; and IV. Quaternary alluvial sediments (Marana Plain) on a low-gradient coastal plain. The Tartagine and Asco Rivers have the same lithology as reach I and II while the Casaluna River lithology is the same as reach III. The Lagani River flows over the Balagne and Nebbio units (ophiolite sequences).

The trunk Golo River originates at 2000 m asl. In the upper Golo profile, there is a prominent convexity near the headwaters associated with mapped glacial deposits (Figure 3.1). Volcano-sedimentary units (350 m asl) within the Scala di Santa Regina stretch of Reach I mark the boundary of continuously preserved alluvium in the river valley. Reach III of the Golo catchment flows

Table 3.1Tributary metrics with steepness and concavity values for the Golo River and its tributaries.

Reach (segment length, km)	Ksn steepness	θ Concavity	Relief (m)	Max/Min Elevation (m asl)	Mean Elevation (m asl)	Contributing Area (km^2)	Gradient (m/km)
Upper Golo			2406	2706/300	1103	341	57
I. Upper (87-84)	67.7	0.34 ± 0.077					
I. Mid Upper (84-82)	200	-1.9 ± 2.9					
I. Niolo Valley (82-67)	92	0.65 ± 0.16					
I. Scala di Santa Regina (67-52)	160	1.1 ± 1.2					
Golo River Catchment			2706	2706/0	900	1000	28
II. Francardo (52-42)	67.1	1.2 ± 1.1					
III. Schistes (42-10)	69.4	-1.3 ± 3					
IV. Quaternary (10-0)	-	-					
Asco			2504	2706/196	1152	161	89
Upper (28-25)	127	0.33 ± 0.021					
Mid Upper (25-21)	132	0.98 ± 0.55					
Mid Lower (21-12)	205	0.57 ± 0.73					
Lower (12-0)	81.9	2.9 ± 1.3					
Tartagine			2175	2400/225	935	137	75
Upper (29-27)	84.9	0.21 ± 0.052					
Mid (27-19)	143	0.17 ± 0.2					
Lower (19-0)	82.9	0.96 ± 0.33					
Lagani			1275	1500/225	566	52	60
Upper (21-20)	56.6	0.36 ± 0.059					
Mid Upper (20-17)	47.7	0.62 ± 0.33					
Mid Lower (17-4)	32.7	87.1 ± 0.34					
Lower (4-0)	87.1	3.7 ± 7.9					
Casaluna			1595	1800/205	825	99	72
Upper (22-21)	68.3	0.059 ± 0.069					
Mid Upper (21-17)	84.3	0.48 ± 0.071					
Mid Lower (17-12)	115	-0.2 ± 0.74					
Lower (12-0)	82.7	1 ± 0.42					

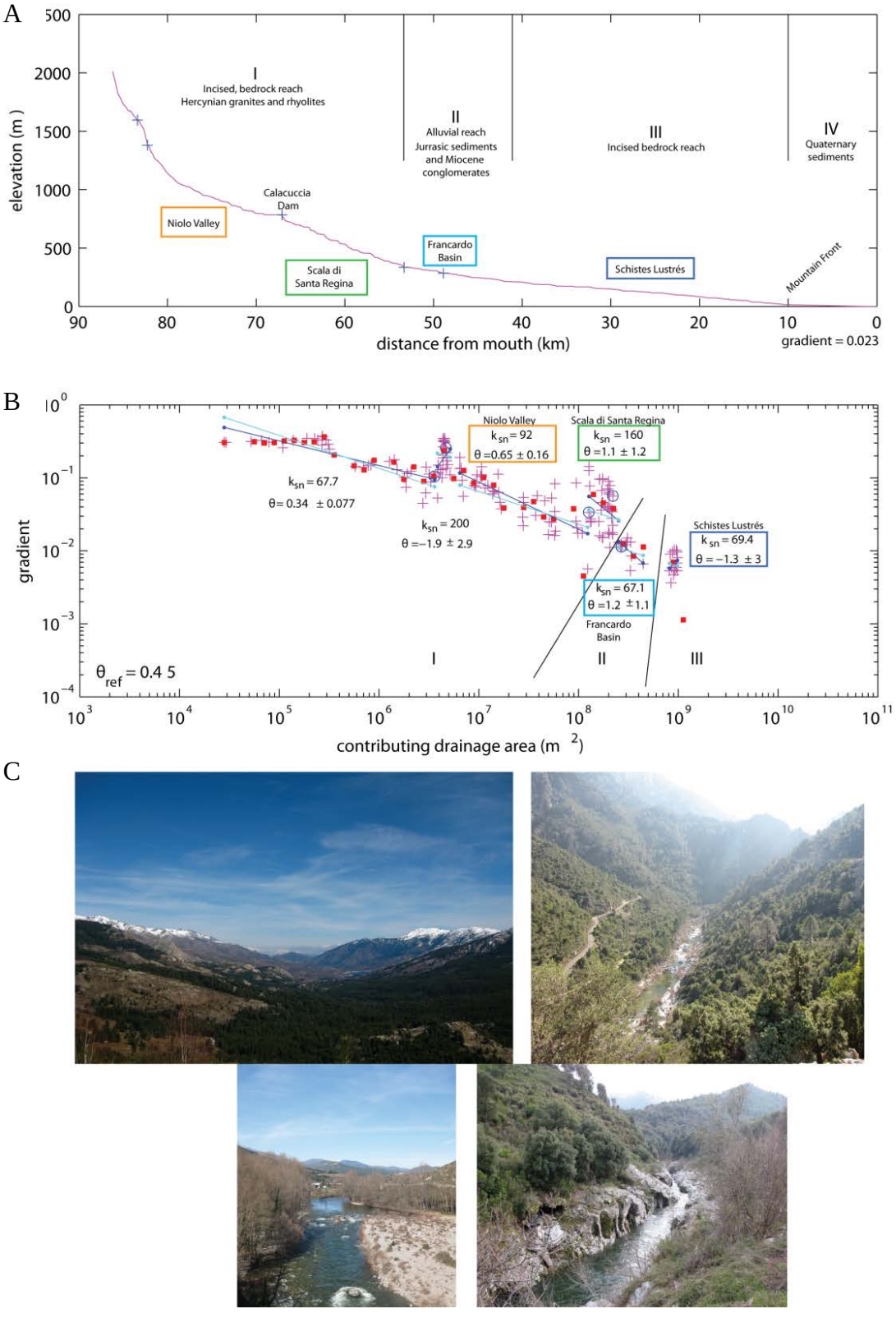
A
elevation (m)
distance from mouth (km)
gradient = 0.023
I
Incised, bedrock reach
Hercynian granites and rhyolites
II
Alluvial reach
Jurrasic sediments
and Miocene
conglomerates
III
Incised bedrock reach
IV
Quaternary
sediments
Calacuccia
Dam
Niolo Valley
Scala di
Santa Regina
Francardo
Basin
Schistes Lustrés
Mountain Front
B
gradient
contributing drainage area (m 2)
Niolo Valley
k sn = 92
θ =0.65 ± 0.16
Scala di Santa Regina
k sn = 160
θ =1.1 ± 1.2
k sn = 67.7
θ= 0.34 ± 0.077
k sn = 200
θ =−1.9 ± 2.9
Schistes Lustrés
k sn = 69.4
θ = −1.3 ± 3
k sn = 67.1
θ =1.2 ±1.1
Francardo
Basin
θ ref = 0.4 5
I
II
III
C

Figure 3.1 Golo River A) Longitudinal profile of the Golo River broken into 4 primary lithologic reaches, labeled I-IV. Reach I is primarily Hercynian granitic bedrock with deeply incised canyons and is divided into 4 sub-reaches identified by changes within the slope-area plot in B). The Alpine Contact serves as the boundary between the bedrock Reach I and alluvial Reach II. Blue crosses on the profile in A) represent knickpoints chosen based on the longitudinal profile and correspond to the open circles on the slope-area plot in B). Box colors in A) correspond to box colors in B). Dark blue lines are the profiles predicted by the regressed channel concavity, θ, and the cyan lines are for the specified reference concavity, θ_{ref}=0.45. Red squares are log-bin averages of the slope area data. Black lines represent the divisions between primary reaches. B) slope-area plot with steepness and concavity values calculated for primary and sub-reaches. Reach III and IV are lumped on the slope-area plots due to the relatively small change in drainage area of Reach IV. C) Photos of corresponding reaches discussed in A) and B).

perpendicular to the Castagniccia anticline axis and is characterized by negative concavity with some stair stepping knickpoints. Reach IV is comprised of Quaternary sediments, however due to its comparatively small elevation change and area, it is indeterminable from Reach III in the slope-area plots and can only be distinguished by the isolated low gradient, high drainage area log-bin average (Figure 3.1B).

The Asco River occupies the valley north of the Golo and originates at 2300 m asl with mapped glacial deposits found at 980-1640 m asl (Figure 3.2). There is continuously preserved alluvium in the river valley below 310 m asl, with minor mapped alluvium appearing in conjunction with volcano-sedimentary units at 360 m asl. The Asco River is characterized by positive concavity, with minor protuberances in the longitudinal profile from 500-1200 m asl. This part of the profile is also correlative with high steepness values. There is a prominent

knickpoint in the profile at the Alpine Contact. Above this knick, the river is deeply incised, similar to the Scala di Santa Regina reach on the Golo.

The Tartagine River is the next tributary to the north of the Asco and it originates at 1780 m asl. The Tartagine River is also mostly concave up with three knickpoints in the upper reaches of the longitudinal profile that can be correlated to mapped landslide deposits. Continuous alluvium is preserved in the river valley at 320 m asl (Figure 3.3). There is also a prominent knickpoint at the Alpine Contact; however, the Tartagine does not have a deeply incised river channel above the knick.

The Lagani River has the most graded, concave up profile of all the tributaries (Figure 3.4). The Lagani River, the northernmost river in the Golo River watershed, originates at 1100 m asl. Cretaceous to Eocene flysch and nappes, and ophiolitic pillow basalts, sheeted dikes and gabbros (Nappe Ophiolitic de Balagne) typifies all reaches, except the lower reach. The Lagani River does not cross the Alpine Contact and has the lowest overall steepness values.

The Casaluna River originates at 1150 m asl and flows parallel to the fold axis of the Alpine units and has a concave up longitudinal profile. The Casaluna River profile has a steepened reach and convexity above a confluence that is also coincident with a major fault on the western limb of the Castagniccia anticline and a change in lithology (Figure 3.5). A knickpoint further upstream is associated with the confluence of a tributary.

All of the profiles exhibit stair stepping knickpoints. Longitudinal profiles of the Golo, Asco and Tartagine Rivers were superimposed to compare convexities and knickpoints based on the similarity of bedrock geology in reach I (Figure 3.6). These profiles all show an increase in steepness values and a broad north-south trending convexity above the Alpine contact. High steepness values are primarily associated with the more resistant Hercynian granites and Mte Cinto rhyolites.

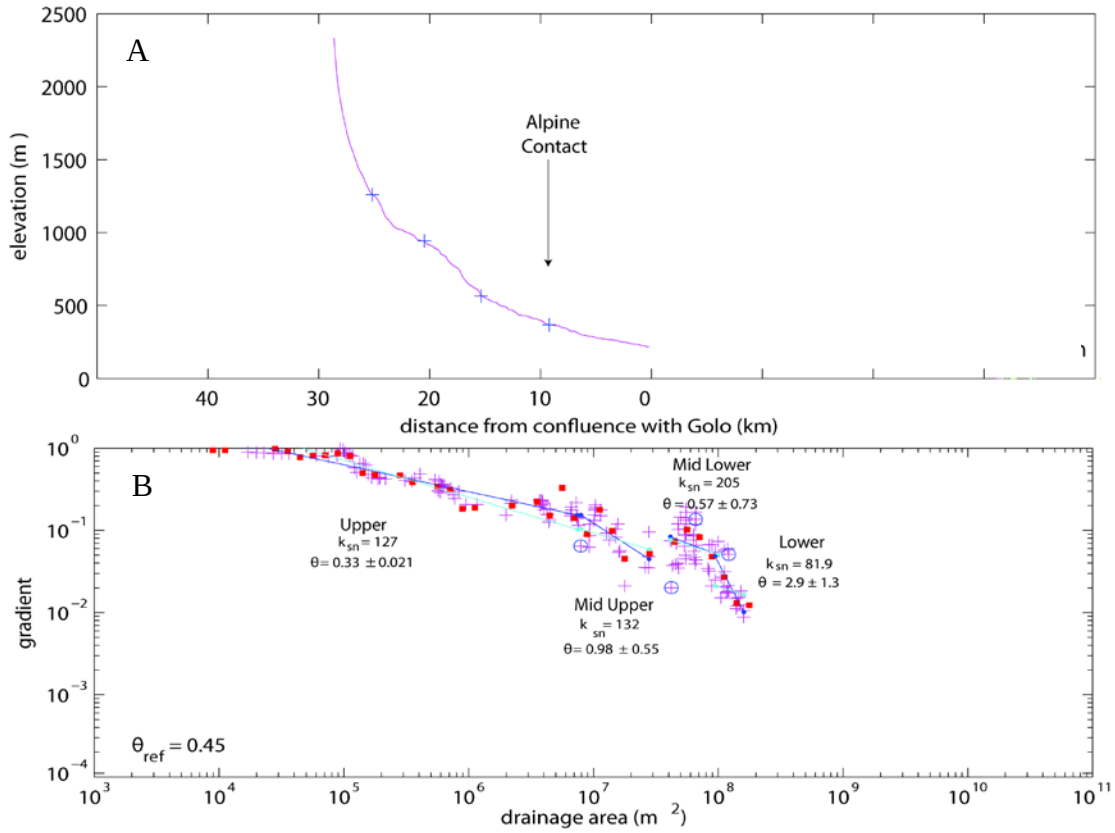

Figure 3.2 Asco River A) Longitudinal profile; crosses represent knickpoints B) Slope-area plot with average steepness values and concavity. Refer to figure caption 3.1 for explanation of symbols.

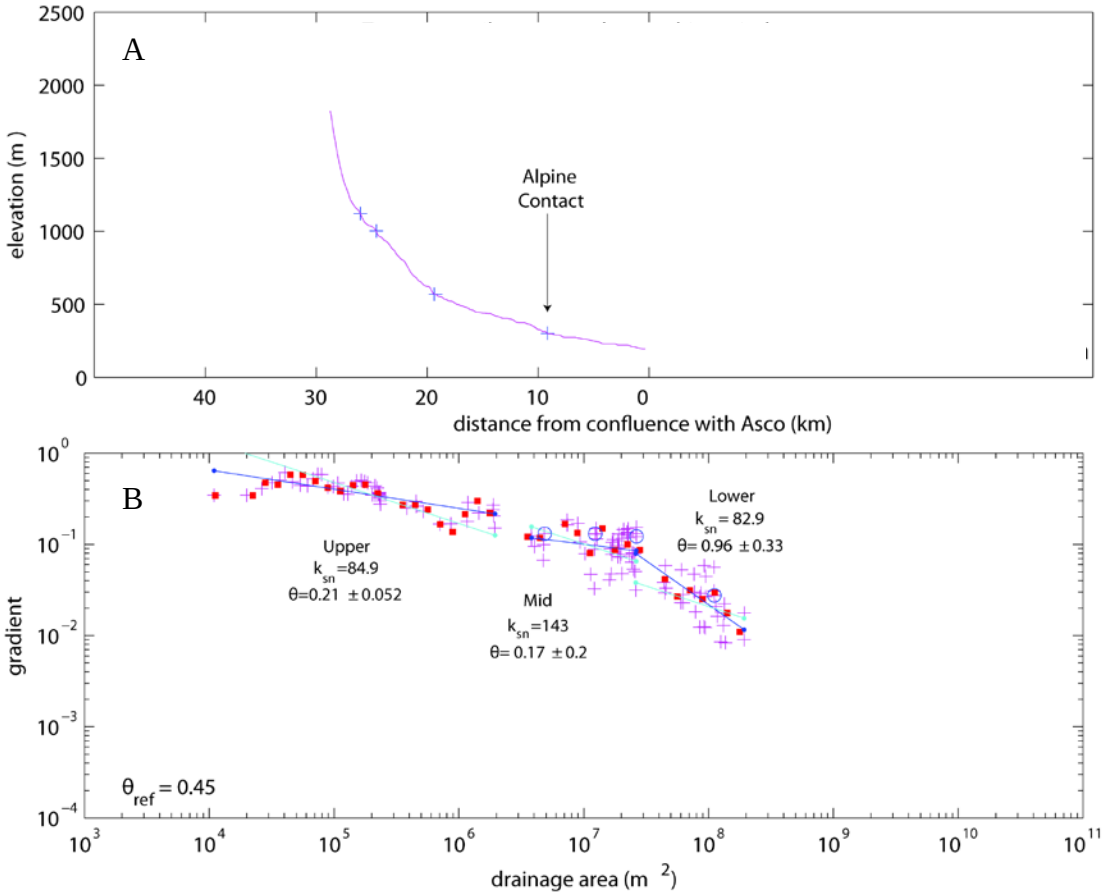

Figure 3.3 Tartagine River A) Longitudinal profile; crosses represent knickpoints B) Slope-area plot with average steepness values and concavity. Refer to figure caption 3.1 for explanation of symbols.

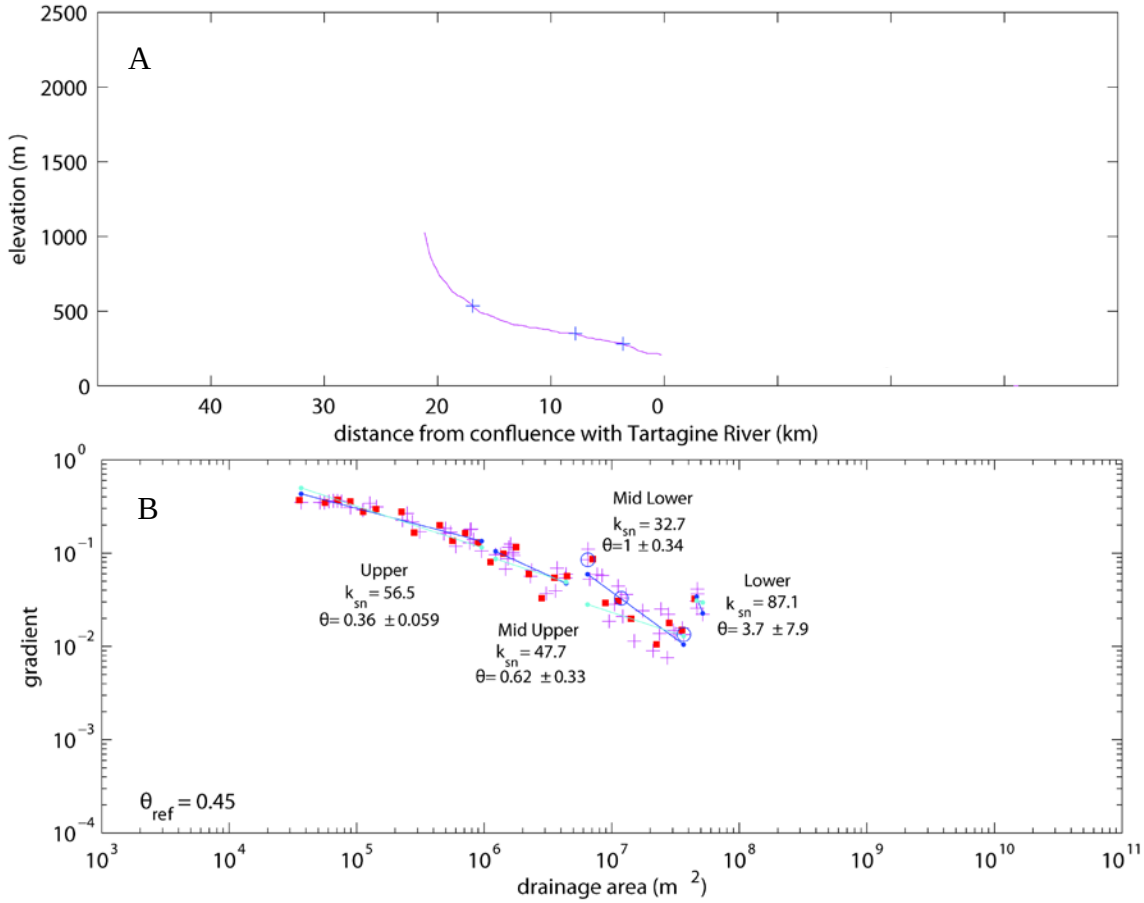

Figure 3.4 Lagani River A) Longitudinal profile; crosses represent knickpoints B) Slope-area plot with average steepness values and concavity. Refer to figure caption 3.1 for explanation of symbols.

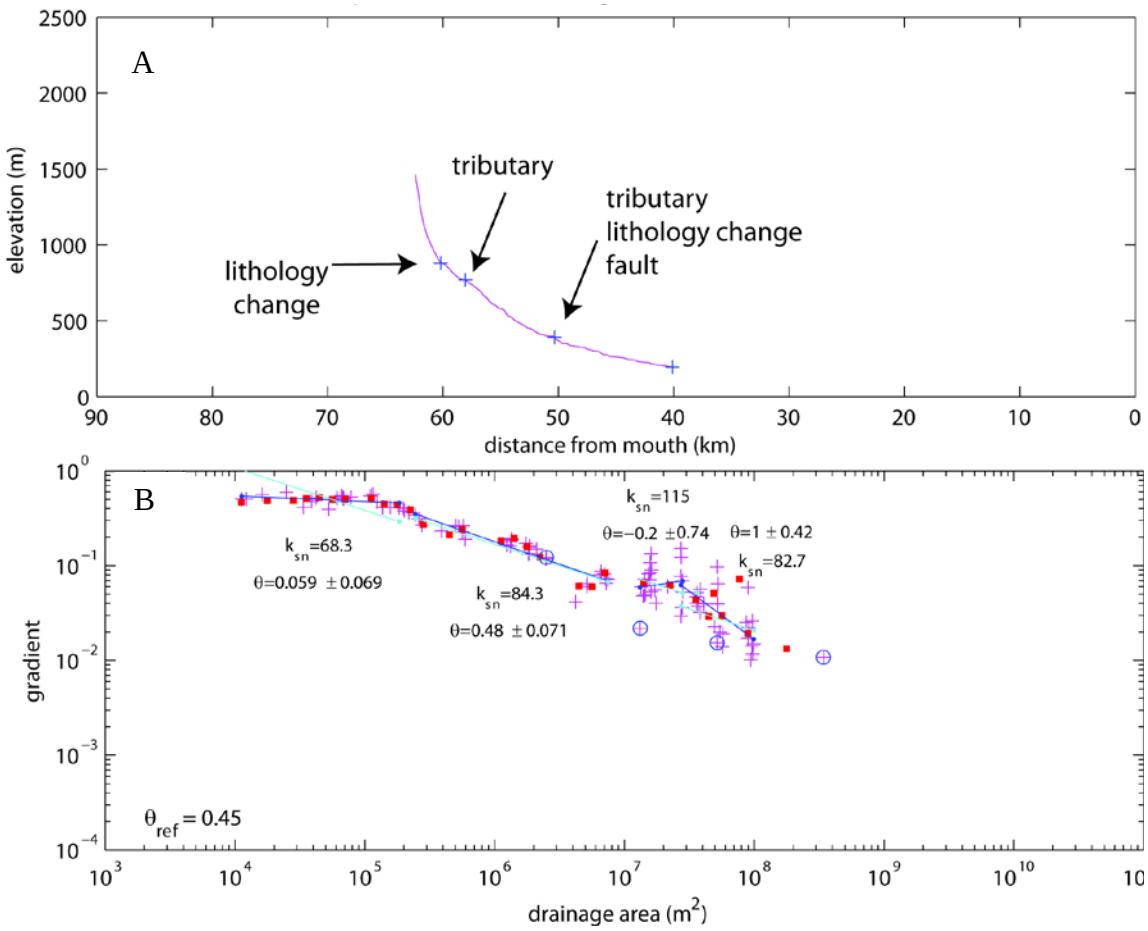

Figure 3.5 Casaluna River A) Longitudinal profile; crosses represent knickpoints B) Slope-area plot with average steepness values and concavity. Refer to figure caption 3.1 for explanation of symbols.

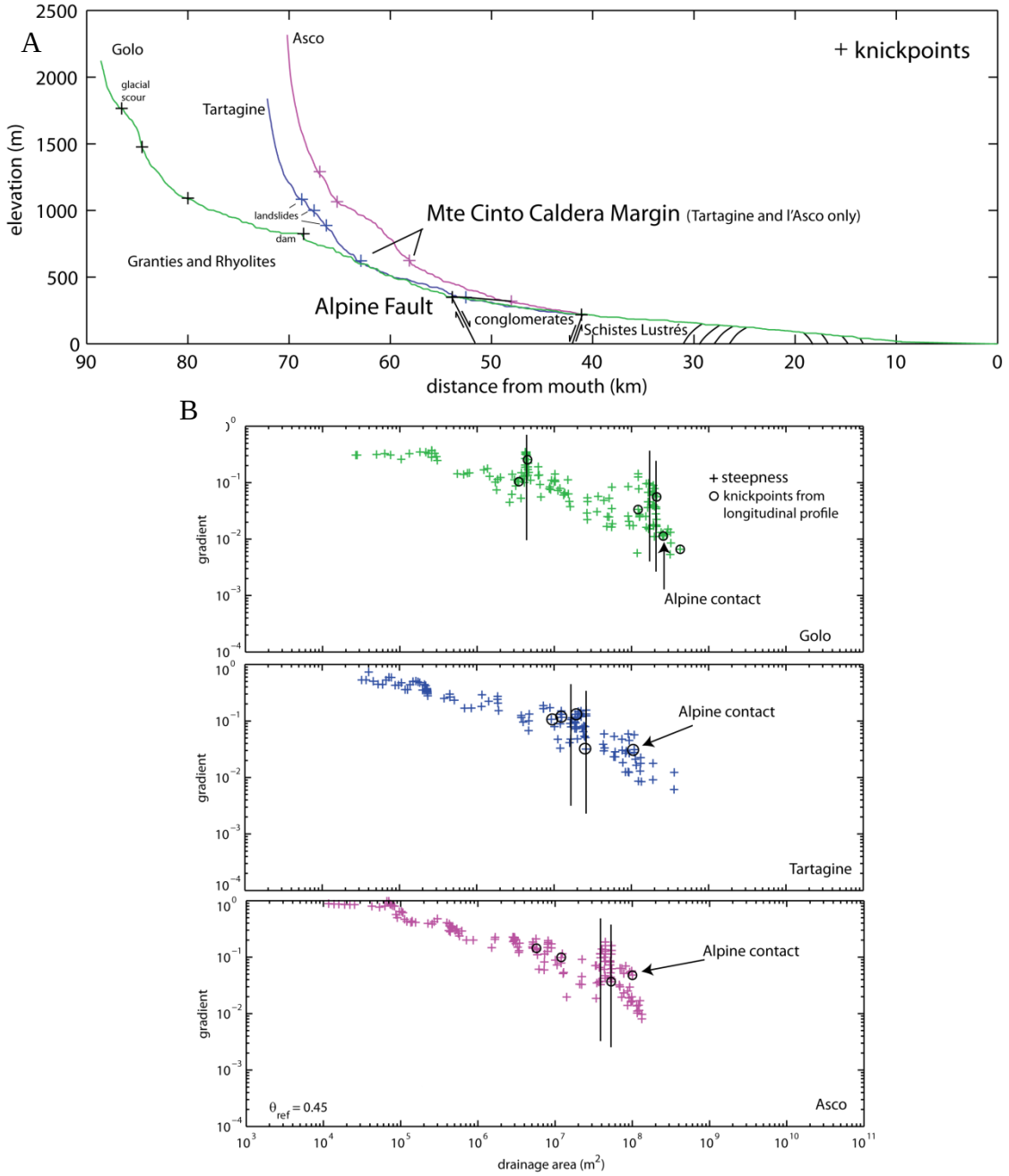

Figure 3. 6 Golo, Asco, and Tartagine correlation A) Longitudinal profiles with knickpoints in relation to lithologic and structural boundaries. B) Slope-area plots with vertical black bars representing steepened reaches above the Alpine contact.

Hypsometric Analysis

Hypsometric integrals range from 0.28-0.42 (Lagani and Casaluna River, respectively). While the hypsometric integrals of the catchments are not significantly different (Figure 3.7A), there are notable differences in hypsometric curves between the catchments (Figure 3.7C). The Upper Golo, Asco and Tartagine constitute a central grouping of similar hypsometric curves that appear to be in transition between concave and S-shaped. These curves also have an unusual merger near ~75% of the area. This central grouping is bookended by the concave Lagani curve and the S-shaped Casaluna curve. The low hypsometric integrals and overall shape of the curves suggest that the tributaries in northeastern Corsica are in the mature stages of development (Strahler, 1952) and most likely have not been subjected to recent large-scale tectonic adjustment.

The elevation distribution within the entire Golo River watershed has a modal distribution centered on 400-500 m asl (Figure 3.7B). When compared to the distribution of each tributary catchment, the Upper Golo River has the highest proportion of high elevations, while the Asco is more evenly distributed, with a broad plateau around ~1700-1000 m asl. The Tartagine and Lagani have a higher proportion of lower elevations and the Casaluna has a broad distribution of average elevation.

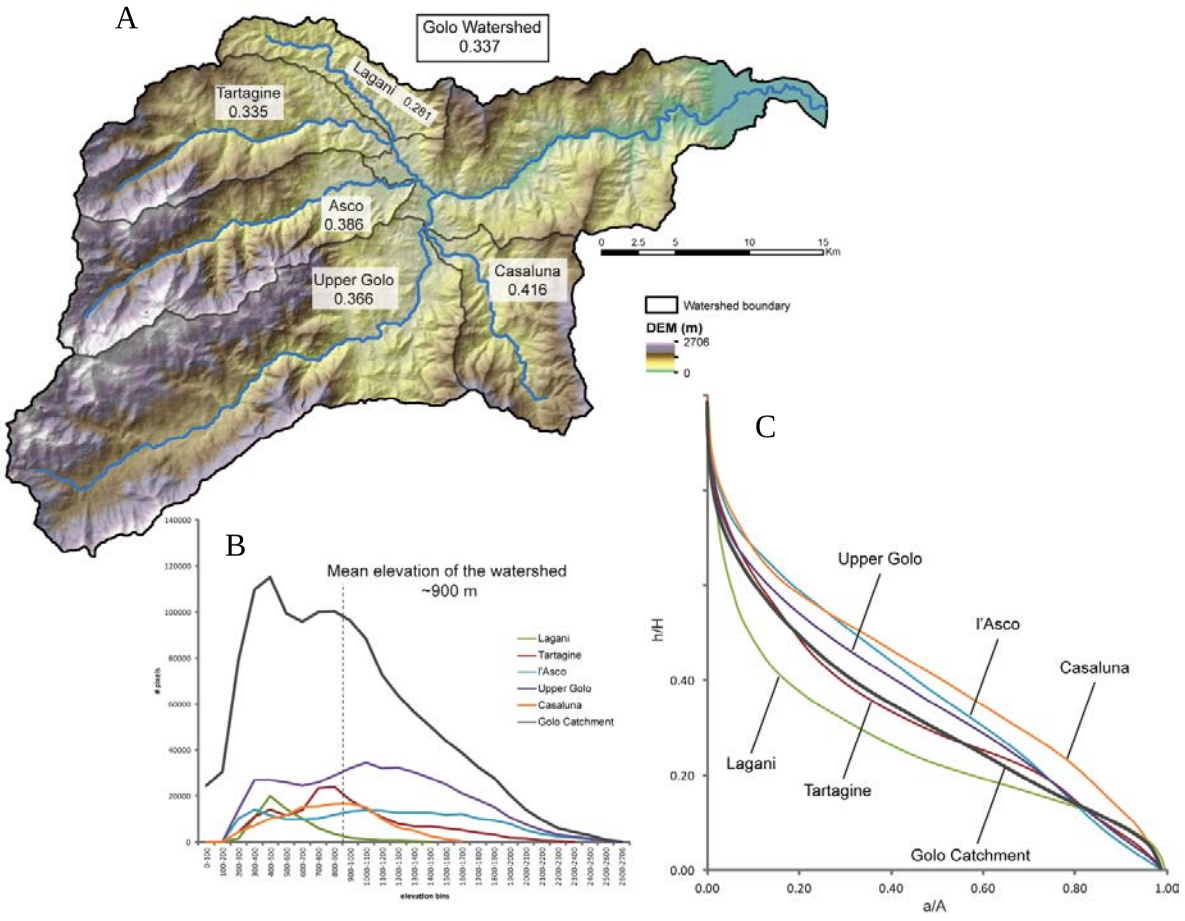

Figure 3.7 Hypsometry of the Golo Watershed. A) Hypsometric integral for catchments of the Golo River watershed. B) Elevation distribution profile for each catchment. Number (#) pixels represent how many pixels from the DEM are accounted for at each respective elevation. C) Hypsometric curves for sub-catchments and entire Golo River watershed.

Slope histograms

Slope histograms for the five sub-catchments of the larger Golo River drainage network are all normally distributed (Figure 3.8). The Asco River has the narrowest distribution and the highest mean and median slope. These data suggest that this watershed has been subject to the most recent perturbation of all the watersheds in the Golo River catchment. Slope histogram distributions of the other four watersheds suggest mature, fluvially dominated systems.

Discussion

Within the Golo River watershed, three groupings emerge that need to be considered individually within the watershed: the Lagani River; the Upper Golo, Asco and Tartagine Rivers; and the Casaluna and lower Golo River (below Ponte Leccia). The mixed bedrock-alluvial Golo River watershed crosses every geologic domain on the island, so it is not inconceivable that lithology will have a large part to play in longitudinal profile response.

The Lagani River is the only river in the watershed that flows over the flysch and ophiolitic Balagne units. These units seem to be easily erodible without presenting much resistance to maintaining a relatively graded profile as suggested by the hypsometry of this sub-catchment, which is the most mature of the group. There are two notable knickpoints present in the longitudinal profile. The upper most knickpoint is associated with a small fault that separates two different units of flysch and the lower knickpoint is at a tributary confluence.

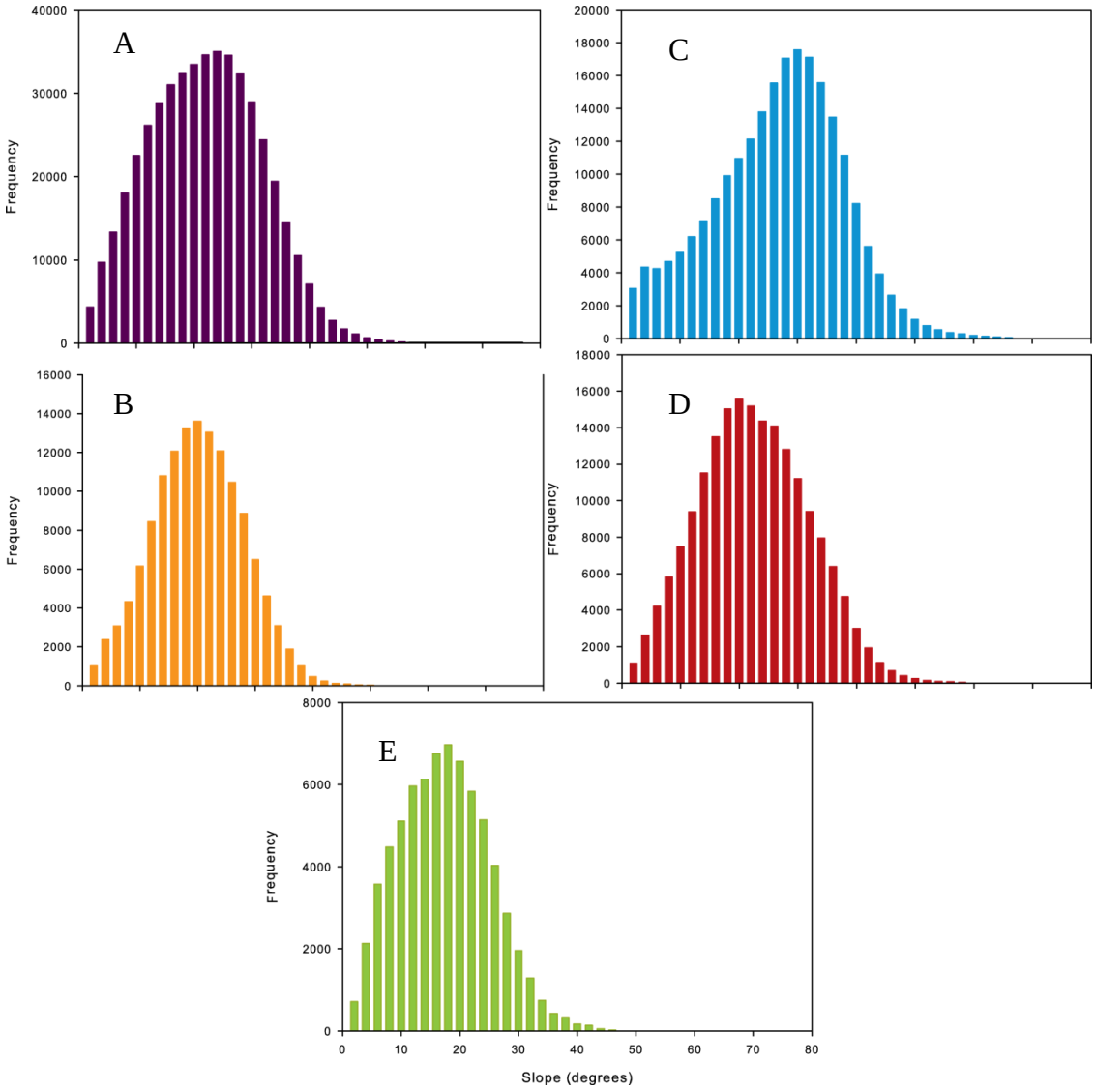

Figure 3.8 Slope histograms A) Upper Golo catchment slope histogram with steep transition from higher angle slopes to a more broad distribution of slopes less than 30° B) Casaluna catchment slope histogram with a more normal distribution of slopes C) Asco catchment D) Tartagine catchment E) Lagani catchment.

The Upper Golo, Asco, and Tartagine Rivers all cross the Alpine contact and they all have major convexities and high steepness values above the Alpine contact (Figure 3.6). In addition both the Asco and the Tartagine Rivers flow over the Mte Cinto caldera margin in the upper reaches. A prominent bulge and an increase in steepness values in both river profiles highlight this margin. Although the Golo River does not flow over the caldera margin, it does have a subdued concavity above the Alpine contact up to ~1100 m asl. When the geology is overlaid with ksn values, the bright red segments of the stream profiles suggest that the more resistant Hercynian granitic and rhyolitic bedrock is able to restrict the upstream migration of knickpoints in the Golo, Asco and Tartagine Rivers resulting in convex profiles (Figure 3.9). While the Golo and Asco Rivers have deeply incised bedrock reaches that are cut into granites/monzogranites, the Tartagine River, on the other hand, is not deeply incised just above the Alpine contact and flows over vertically dipping gneisses. These observations could also be interpreted as either the Alpine contact is controlling knickpoint migration upstream and is getting ‘stuck’ on the caldera margin creating a more prominent bulge or there may be two zones of differential uplift above the Alpine contact.

Below the Mte Cinto margin, the Upper Golo, Asco and Tartagine Rivers show distinct transitions from higher to lower steepness values when crossing the Alpine contact into the Francardo Basin. In all cases there is a broad convexity in the profile upstream. It is noteworthy that there the knickpoints associated with the Alpine contact are all at approximately the same elevation

(~300-330 m asl) and mark the beginning of continuously preserved alluvium in the river valleys and Francardo Basin. This could suggest that either extensional reactivation of the (previously compressional) Alpine contact generated a localized fall in base level resulting in a knickpoint. Alternatively, the change in lithology at the contact could be controlling deposition and knickpoint formation.

In the upper reaches of the Golo and Asco Rivers, there are convexities in the river profile that range from 1100-1300 m asl. The Golo River also has a smaller convexity around 1500-1700 m asl that has a high steepness value (200). Krumrie (2009) mapped moraine deposits at 1450 and 1700 m asl in the upper reach of the Golo River and assigned relative ages of Younger Dryas and Older Dryas to these deposits. Within the Niolo Valley above Calacuccia Dam, Krumrie (2009) mapped six other moraine ridges from 1075-1400 m asl just south of the Golo River (along the Colga River) and one dated to 27.9 ± 5.4 ka. These moraines are interpreted to span from the middle Würmian (OIS 3) to the three advances of the LGM (LGM, Older Dryas and Younger Dryas) (Krumrie, 2009) and most likely account for the upper perturbations in the longitudinal profile. The upper three knickpoints in the Tartagine profile correlate well with mapped landslide deposits in pyroclastics, breccias and tuffs.

The Casaluna River does not cross the Alpine contact and has the same bedrock geology as reach III of the Golo River. These units have been uplifted more recently than the granites and rhyolites in the west (Fellin et al., 2005b).

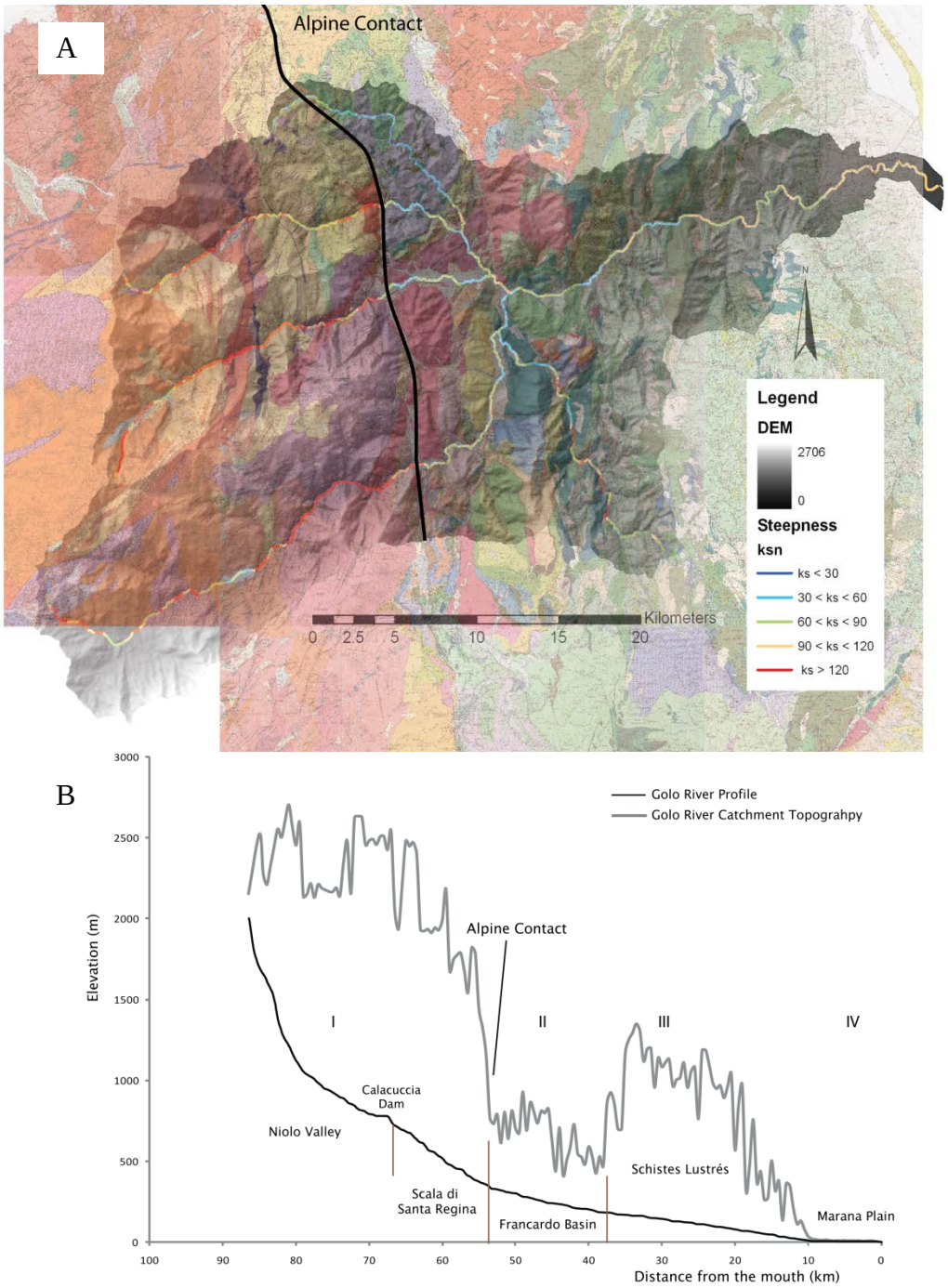

Figure 3.9 Comparison of ksn to geology and topography. A) DEM overlapped with steepness values for all tributaries and 1:50000 geologic maps. High steepness values are noted when transitioning across the Alpine contact into the softer sediments in the Francardo basin. B) Catchment topography also delineates large-scale reaches. Roman numerals refer to primary reaches discussed within the text.

Also, it is subject to a different climate and vegetation regime due to its orographic position in relation to the western rivers and parent rock, to name a few. The Casaluna watershed hypsometric curve has the highest hypsometric integral and youngest expression of all the curves, signifying that it has experienced the most recent perturbation.

Along the lower Golo River profile, there are multiple stair-stepped knickpoints in conjunction with a convexity that could be a response signal due to base-level fall. Approximately 10-15 km upstream from the mouth of the Golo River, there is a ~50 m drop in the river profile of that may be a migrating knickzone associated with changes in sea-level over the last few glacial cycles. However, it may also be associated with range front faulting and basin subsidence along the eastern Corsica margin or strictly due to the change in lithology. Geochronology along the strath terraces along with high resolution GPS data may help resolve this particular piece of the puzzle.

In addition, tributaries flowing into the lower Golo River in Reach III all show an increase in ksn values upon confluence suggesting that the main stem of the Golo River is incising faster than its tributaries (Figure 3.10A). This is also evidenced by the abundance of waterfalls at tributary confluences throughout Reach III (Figure 3.10B).

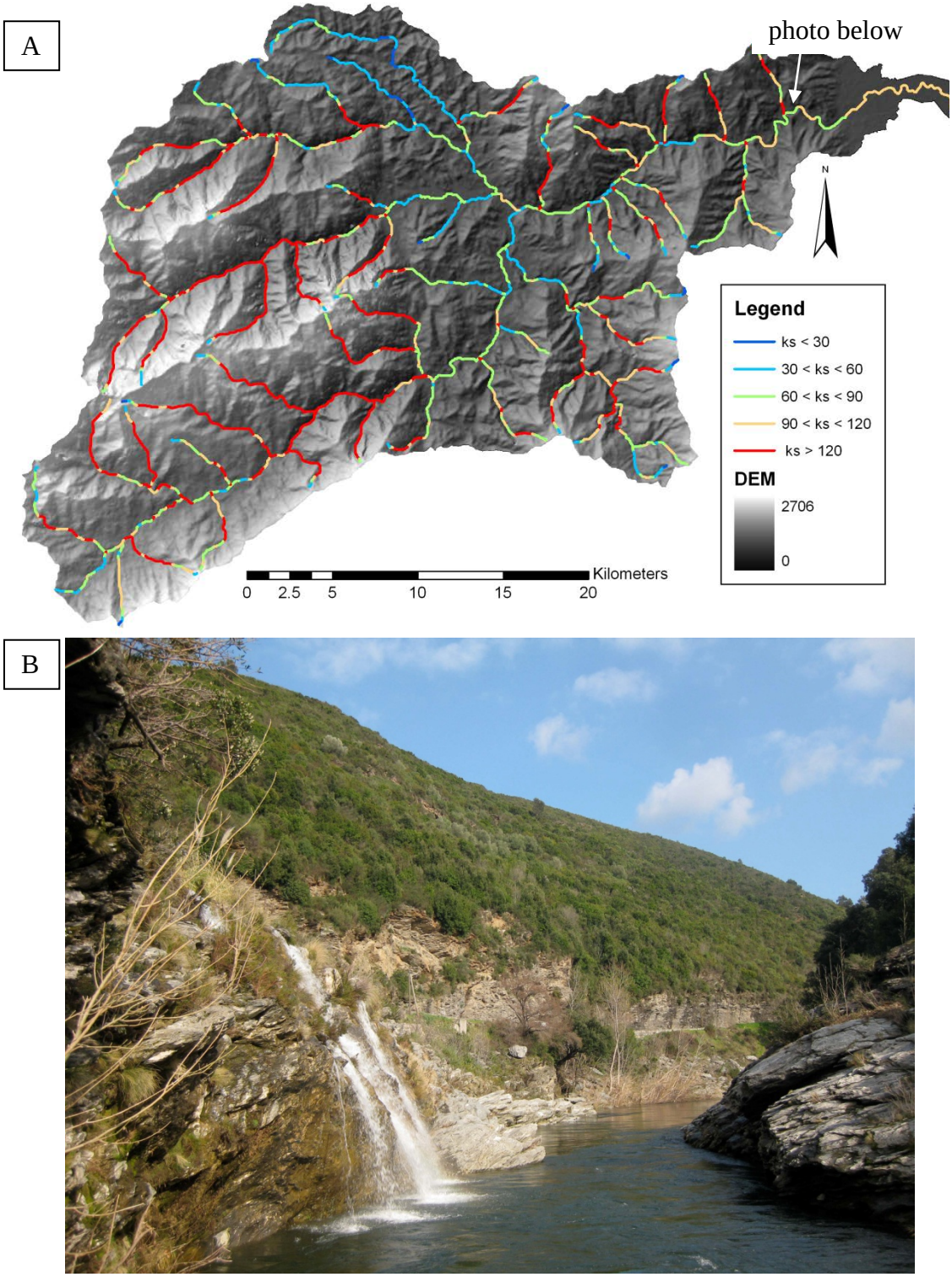

Figure 3.10 Ksn in relation to the watershed. A)DEM with steepness overlapped shows a tendency of higher steepness values where tributaries merge with the Golo River, especially in the Schistes Lustres reach (III). White arrow indicates location of waterfall in photo below. B) Example: waterfall in lower reach.

Conclusions

Within this watershed, a combination of climatic, lithologic, structural and glacio-eustatic controls factor are governing the landscape. Climate signatures and surface processes in the upper reaches of these rivers has led to oversteepened reaches and knickpoints while lithologic variation has influenced the overall variability of the longitudinal profile. Longitudinal profile analysis shows broad convexities in the schist and granitic-rhyolitic units that do not significantly correlate with any major changes in lithology. These convexities most likely reflect the contrast in dominant controls between the two distinct geologic reaches. In the upper reaches of the granitic-rhyolitic Golo and Asco Rivers, less pronounced concavities seem to be correlated to mapped glacial extents while a broad convexity, in tandem with knickpoints in the Asco and Tartagine, are caught up on Mt. Cinto caldera margin. Knickzones with high steepness values and deeply incised canyons above the Alpine contact are suggestive that there is movement on the fault with base-level lowering driving incision. Although Corsica is commonly considered tectonically quiescent, thermochronologic studies in conjunction with evidence presented here suggest deformation is taking place.

Minor changes in lithology and/or foliation orientation may be influencing small-scale, stair-stepping knickpoints, as seen in Reach III of the Golo River; however, these are more likely a result of oscillating sea-level propagating up through system.

CHAPTER 4

LOOKING FORWARD

Corsica is an ideal location for investigating fluvial and landscape responses to climate, sea-level and tectonics due its small size and direct influence of base-level changes, tectonic activity and Quaternary climate record. Earlier use of U-series dating and ^{14}C has been troublesome (Conchon, 1986) as well as most attempts at OSL (Krumrie, 2009; Sømme et al., 2011). Due to limited material suitable for ^{14}C dating, OSL is the best tool to use for age determination. Sample selection is of vital importance and could prove challenging due to limited outcrop exposure and reworked alluvium overlying bedrock straths. It is possible that the quartz sediment from this system is not suitable for OSL dating due to poor luminescence properties of the quartz grains and dominant intermediate to slow components of the signal that can lead to an age underestimation (Jain et al., 2003). New advancements in infrared stimulated luminescence (IRSL) may be more applicable for this system. Potassium feldspar has a much brighter luminescence signal than that of quartz and can measure higher dose equivalents because it does not saturate as quickly as quartz (Buylaert et al., 2009.) IRSL ages may resolve the true depositional age of the Torra Terrace and corroborate the quartz-OSL EBG ages determined for the OIS 3 and younger samples. In order to build a comprehensive framework of fluvial response to climate and sea-level in this area, future work could also extend to correlate onshore fluvial deposits to

offshore deposits using sequence stratigraphy and OSL ages from cores taken by IFREMER/Exxon Mobile (in progress).

The Golo River was a gravel-bedded river choked with coarse sediment during glacial periods. Exposure, accessibility and availability of outcrops in addition to the scarcity of sand lenses are the two limiting factors for OSL sample collection. It would be useful to employ the services of a backhoe in order to dig large trenches into fluvial terrace deposits on the coastal plain and within the river valley to create better exposures and allow for better descriptions of the internal architecture of these deposits. Creating new exposures may reveal structural and stratigraphic relationships between the various fluvial terraces and strath terraces within the river valley that are not currently understood.

Kuhlemann et al. (2008) present a good baseline for upland erosion rates based on ^{10}Be inventories, but age control in the lower reaches of the catchment need improvement. A study of erosion rates within the entire Golo River catchment using cosmogenic nuclides (CRN) would be a good method for understanding erosion rates and sediment supply in northeastern Corsica. CRN derived sediment yield can be used as an indicator of major changes in sediment production and transport. Evaluation of erosion rates can help estimate changes in overall sediment contribution throughout the watershed. Because erosion rates can vary based on elevation, hillslopes, uplift, etc., (Burbank, 2002) erosion rates from individual catchments as well as the entire watershed may help delineate the variable contributions at different locations throughout the watershed. Collecting a sample of fine-grained sediment at a downstream point

above major confluences in each catchment would be useful for capturing the individual rates of erosion in addition to a sample from the mouth of the Golo River to represent the watershed as a whole. CRN determined rates could also be compared to incision rates based on updated luminescence geochronology to further assess landscape evolution.

REFERENCES

Aitken, M.J., 1998, An introduction to optical dating: Oxford, Oxford University Press, 267 p.

Andreucci, S., Pascucci, V., Murray, A.S., and Clemmensen, L.B., 2009, Late Pleistocene coastal evolution of San Giovanni di Sinis, west Sardinia (Western Mediterranean): Sedimentary Geology, v. 216, p. 104-116.

Bailey, R.M., 2000, The interpretation of quartz optically stimulated luminescence equivalent dose versus time plots: Radiation Measurements, v. 32, p. 129-140.

Bailey, R.M., 2010, Direct measurement of the fast component of quartz optically stimulated luminescence and implications for the accuracy of optical dating: Quaternary Geochronology, v. 5, p. 559-568, doi: 10.1016/j.quageo.2009.10.003.

Blum, M., and Törnqvist, T., 2000, Fluvial responses to climate and sea-level change: a review and look forward: Sedimentology, v. 47 (Suppl. 1), p. 2-48.

Brunet, C., Monié, P., Jolivet, L., and Cadet, J.P., 2000, Migration of compression and extension in the Tyrrhenian Sea from $^{49}Ar/^{39}Ar$ ages on micas along a transect from Corsica to Tuscany: Tectonophysics, v. 321, p. 127-155.

Brocklehurst, S.H., and Whipple, K.X., 2004, Hypsometry of glaciated landscapes: Earth Surface Processes and Landforms, v. 29, p. 907-926.

Bruno, C., Dupré, G., Giorgetti, G., Giorgetti, J.P., and Alesandri, J., 2001, Chí tempu face? Météorologie, climat et microclimats de la Corse, CNDP-CRDP de Corse/Météo France, Ajaccio, France.

Bull, W.B., 1991, Geomorphic responses to climate change: New York, Oxford University Press, 326 p.

Burbank, D.W., 2002, Rates of erosion and their implications for exhumation: Mineralogical Magazine, v. 66, p. 25-52.

Burbank, D.W., and Anderson, R.S., 2001, Tectonic Geomorphology: Massachusetts, Blackwell Science Ltd, 274 p.

Buylaert, J.P., Murray, A.S., Thomsen, K.J. and Jain, M., 2009, Testing the potential of an elevated temperature IRSL signal from K-feldspar: Radiation Measurements, v. 44, p. 560-565, doi:10.1016/j.radmeas.2009.02.007.

Cacho, I., Grimalt, J.O., Pelejero, C., Canals, M., Sierro, F.J., Flores, J.A., and Shackelton, N., 1999, Dansgaard-Oeschger and Heinrich event imprints in Alboran Sea paleotemperatures: Paleoceanography, v. 14, p. 698-705.

Cavazza, W., Zattin, M., Ventura, B., and Zuffa, G., 2001, Apatite fission-track analysis of Neogene exhumation in northern Corsica (France): Terra Nova, v. 13, p. 51-57.

Cavazza, W., DeCelles, P.G., Fellin, M.G., and Paganelli, L., 2007, The Miocene Saint-Florent Basin in northern Corsica: Stratigraphy, sedimentology and tectonic implications: Basin Research v. 19, p. 507-527, doi: 10.1111/j.1365-2117.00334.x

Conchon, O., 1972, Caracteres generaux et chronologie relative des alluvions fluviatiles rubefiees de quelques vallees de Corse Orientale: Bulletin de l’Association Francaise pour l’Etude du Quaternaire, v. 3, p. 171-184.

Conchon, O., 1975, The human settlement of Corsica: Palaeogeographic and tectonic considerations: Journal of Human Evolution, v. 5, p. 241-248.

Conchon, O., 1977, Néotectonique en Corse orientale d'après l'étude des formations quaternaires, comparaison entre la Marana et la plaine d'Aleria: Bulletin de la Société Géologique de France, (7), XIX, 3, p. 631-639.

Conchon, O., 1978, Quaternary studies in Corsica (France): Quaternary Research, v. 9, p. 41-53.

Conchon, O., 1979, Maximum extension of Wuermian glaciation around the western Mediterranean, *in* Sibrava, V., and Shotton, F. (eds.): Quaternary glaciations in the Northern Hemisphere, IGCP Project v. 24, no. 5, p. 77-88.

Conchon, O., 1984, Corrélations entre la sédimentation fluviatile et la sédimentation marine littorale en Corse: Bulletin de l’Association française pour l’étude du quaternaire, v. 21, pg. 151-156.

Conchon, O., 1985a, Le Quaternaire littoral de Corse: nouvelles données: Bulletin de l'Association française pour l'étude du quaternaire, v. 22, pg. 13-20.

Conchon, O., 1985b, Nouvelle observations sur les formations glaciaires quaternaires en Corse: Bulletin de l'Association française pour l'étude du quaternaire, v. 22, p. 5-11.

Conchon, O., 1986, Corrélation entre les formations glaciaires, fluviatiles et marines de Corse et les sédiments sousmarins de Méditerranée occidentale au Pléistocène supérieur: Revue de géologie dynamique et de géographie physique, v. 27, p. 85-93.

Conchon, O., 1987, Hydrodynamic variations and correlations with Quaternary sea-level change on a rocky coast in Corsica, Western Mediterranean: Progress in Oceanography, v. 18, p. 103-117.

Conchon, O., 1988a, Paléogeographie et paléoclimatologie de la Corse au Quaternaire; chronologie des événements: Bulletin Societé Géologique de France, Huitieme Serie, v. 4, p. 587-594.

Conchon, O., 1988b, Manifestations et Chronologie de la Déglaciation Fini-Würmienne en Corse: Bulletin de l'Association française pour l'étude du quaternaire,v. 2, p. 91-96.

Conchon, O., 1999, Le littoral de Corse (France) au Quaternaire: Quaternaire, v. 10, p. 95-105.

Conchon, O., Loÿe-Pilot, M., Paskoff, R., Sanlaville, P., 1986, Quaternary marine and lagoonal deposits in the Vadina-Urbino Area (Aleria Region, Eastern Corsica): Radiometri dating and field evidence: Zeitschrift fur Geomorphologie, v. 62, p. 103-108.

Crosby, B. T., Whipple, K.X., Gasparini, N.M., and Wobus, C.W., 2005, Knickpoint generation and persistence following base-level fall: an examination of erosional thresholds in sediment flux dependent erosion models, AGU, Fall Meeting, San Francisco, CA, abstract #H34A-05.

Crosby, B.T., and Whipple, K.X., 2006, Knickpoint initiation and distribution within fluvial networks: 236 waterfalls in the Waipaoa River, North Island, New Zealand: Geomorphology, v. 82, p. 16-38.

Cunningham, A.C., and Wallinga, J., 2010, Selection of integration time intervals for quartz OSL decay curves: Quaternary Geochronology, v. 5, p. 657-666.

Danišík, M., Kuhlemann, J., Dunkl., I., Székely, B., and Frisch, W., 2007, Burial and exhumation of Corsica (France) in the light of fission track data: Tectonics, v. 26, TC1001, doi:10.1029/2005TC001938.

Durand-Delga, M., 1984, Principaux trait de la Corse Alpine et corrélation avec les Alpes ligures: Mémoire la Société Geologique Italienne, v. 28, p. 285-329.

Durcan, J.A., and Duller, G.A.T., 2011, The fast ratio: A rapid measure for testing the dominance of the fast component in the initial OSL signal from quartz: Radiation Measurements, v. 46, p. 1065-1072, doi:10.1016/j.radmeas.2011.07.016.

Fellin, M. G., Zattin, M., and Picotti, V., 2005a, Relief evolution in northern Corsica (western Mediterranean): Constraints on uplift and erosion on long-term and short-term timescales: Journal of Geophysical Research, v. 110, F01016, doi:10.1029/2004JF000167.

Fellin, M. G., Picotti, V. and Zattin, M., 2005b, Neogene to Quaternary rifting and inversion in Corsica: Retreat and collision in the western Mediterranean: Tectonics, v. 24, TC1011, doi:10.1029/2003TC001613.

Frankel, K.L, Pazzaglia, F.J., and Vaughn, J.D., 2007, Knickpoint evolution in a vertically bedded substrate, upsteam-dipping terraces, and Atlantic slope bedrock channels: GSA Bulletin, v. 119, no. 3/4, p. 476-486.

Galbraith, R.F., Roberts, R.G., Laslett, G.M., Yoshida, H., Olley, J.M., 1999, Optical dating of single and multiple grains of quartz from Jinmium Rock Shelter, Northern Australia: Part 1, experimental design and statistical models: Archaeometry, v. 41, p. 339-364.

Guérin, G., Mercier, N., Adamiec, G., 2011, Dose-rate conversion factors: update: Ancient TL, v. 29, 231-238.

Hack, J.T., 1973, Stream profile analysis and stream-gradient index: U.S. Geological Survey Journal of Research, v. 1, p. 421-429.

Hancock, G.S., Anderson, R.S., 2002, Numerical modeling of fluvial strath-terrace formation in response to oscillating climate: GSA Bulletin, v. 144, p. 1131-1142.

Hayakawa, Y. S., and Oguchi, T., 2009, GIS analysis of fluvial knickzone distribution in Japanese mountain watersheds: Geomorphology, v. 111, p. 27-37, doi:10.1016/j.geomorph.2007.11.016

Hayes, A., Kucera, M., Kallel, N., Sbaffi, L., and Rohling, E.J., 2005, Glacial Mediterranean sea surface temperatures based on planktonic foraminiferal assemblages: Quaternary Science Review, v. 24, p. 999-1016.

Holbrook, J., and Schumm, S.A., 1999, Geomorphic and sedimentary response of rivers to tectonic deformation: a brief review and critique of a tool for recognizing subtle epeirogenic deformation in modern and ancient settings: Tectonophysics, v. 305, p. 287–306.

Huntley, D.J., Godfrey-Smith, D.I., and Thewalt, M.L.W., 1985, Optical dating of sediments: Nature, v. 313, p. 105–107.

Hurrell, J.W., 1995, Decadal trends in the North Atlantic Oscillation: Regional temperatures and precipitation: Science, v. 269, p. 676-679.

Hurtrez, J.E., Sol, C., and Lucazeau, F., 1999, Effect of drainage area on hypsometry from an analysis of small-scale drainage basins in the Siwalik Hills (central Nepal): Earth Surface Processes and Landforms, v. 24, p. 799–808.

Jain, M., Choi, J.H., Thomas, P.J., 2003, The ultrafast OSL component in quartz: Origins and implications: Radiation Measurements, v. 43, p. 709-714.

Jeong, G.Y., Cheong, C., and Choi, J., 2007, The effect of weathering on optically stimulated luminescence: Quaternary Geochronology, v. 2, p. 117-122.

Jolivet, L., Daniel, J.-M., Fournier, M., 1991, Geometry and kinematics of extension in Alpine Corsica: Earth and Planetary Science Letters, v. 104, p. 278-291.

Jolivet, L., Faccenna, C., Goffé, B., Mattei, M., Rossetti, F., Brunet, C., Storti, F., Funiciello, R., Cadet, J.P., d'Agostino, N., and Parra, T., 1998, Midcrustal shear zones in postorogenic extension: Examples from the Tyrrhenian Sea: Journal of Geophysical Research, v. 103, p. 12,123-12,160.

Johnston, J. W., Thompson, T. A., and Baedke, S J., 2007, Systematic pattern of beach-ridge development and preservation: Conceptual model and evidence from ground penetrating radar: Geological Society of America Special Papers, v. 432, p. 47-58, doi:10.1130/2007.2432(04).

Kirby, E., and Whipple, K.X., 2001, Quantifying differential rock-uplift rates via stream profile analysis: Geology, v. 29, p. 415-418.

Kirby, E., and Whipple, K.X., 2012, Expression of active tectonics in erosional landscapes: Journal of Structural Geology, v. 44, p. 54-75.

Knighton, D., 1998, Fluvial forms and processes: A new perspective: London, Arnold, 383 p.

Koss, J.E., Ethridge, F.G., Schumm, S.A., 1994, An experimental study of the effects of base-level change on fluvial, coastal plain and shelf systems: Journal of Sedimentary Research, v. B64, no. 2, p. 90-98.

Krumrie, I., 2009, Wuermian glaciation and climate in the western Mediterranean based on investigations in the mountain chain of Corsica [Ph.D. thesis], Eberhard-Karls-Universität Tübingen, 143 p.

Kuhlemann, J., Frisch, W., Székely, B., Dunkl., I., Danišík, M., and Krumrie, I., 2005, Würmian maximum glaciation in Corsica: Austrian Journal of Earth Sciences, v. 97, p. 68-81.

Kuhlemann, J., van der Borg, K., Bons, P.D., Danišík, M., and Frisch, W., 2008, Erosion rates on subalpine paleosurfaces in the western Mediterranean by in-situ 10Be concentrations in granites: implications for surface processes and long-term landscape evolution in Corsica (France): International Journal of Earth Science (Geol Rundsch), v. 97, p. 549-564.

Lahondére, J.-C., Conchon, O., Lahondére, D., 1994, Vescovato, in Carte Géologique de la France, BRGM, Map 1107, scale 1:50,000, Orleans, France.

Larroque, C., Delouis, B., Godel, B., and Nocquet, J.,2009, Active deformation at the southwestern Alps–Ligurian basin junction (France–Italy boundary): Evidence for recent change from compression to extension in the Argentera massif: Tectonophysics, v. 467, p. 22–34.

Malavieille J, Chemenda A, and Larroque C., 1998, Evolutionary model for Alpine Corsica: mechanism for ophiolite emplacement and exhumation of high-pressure rocks: Terra Nova, v. 10, p. 317–322.

Mather, A.E., 2009, Tectonic setting and landscape development, *in* Woodward. J.C., ed., The Physical Geography of the Mediterranean: Oxford, Oxford University Press, p. 5-32.

Mauffret, A., Contrucci, I., and Brunet, C., 1999, Structural evolution of the Northern Tyrrhenian Sea from new seismic data: Marine and Petroleum Geology, v. 16, p. 381-407.

Mazzoli, S., and M. Helman, 1994, Neogene patterns of relative motion for Africa-Europe: Some implications for recent central Mediterranean tectonics: Geol Rundsch, v. 83, p. 464-468.

Merrits, D.J., Vincent, K.R., Wohl, E.E., 1994, Long river profiles, tectonism, and eustacy: A guide to interpreting fluvial terraces: Journal of Geophysical Research, v. 99, p. 14,031-14,050.

MeteoFrance (http//climat.meteofrance.com/jsp/site/Portal.jsp?page_id=14289&CLIMAT_PORTLET.path=climateNormales/REG17)

Michard A, and Martinotti G., 2002, The Eocene unconformity of the Brianconnais domain in the French-Italian Alps, revisited (Marguareis massif, Cuneo); a hint for a Late Cretaceous–Middle Eocene frontal bulge setting: Geodinamica Acta, v. 15, p. 289–301.

Murray, A.S., and Wintle, S.G., 2000, Luminescence dating of quartz dating using an improved regenerative-dose protocol: Radiation Measurements, v. 32, p. 57-73.

Olley, J.M., Caitcheon, G., Murray, A.S., 1998, The distribution of apparent dose as determined by optically stimulated luminescence in small aliquots of fluvial quartz: Implications for dating young sediments: Quaternary Science Review, v. 17, p. 1033-1040.

Olley, J.M., Caitcheon, G.G., Roberts, R.G., 1999, The origin of dose distributions in fluvial sediments, and the prospect of dating single grains from fluvial deposits using optically stimulated luminescence: Radiation Measurements, v. 30, p. 207-217.

Pazzaglia, F. J., 2003, Landscape evolution models, *in* Gillespie, A. R., Porter, S. C., and Atwater, B. F., eds., The Quaternary Period in the United States: Amsterdam, Elsevier, p. 247-274, doi:10.1016/S1571-0866(03)01012-1.

Penck, A., and Brückner, E., 1909, Die alpen im Eiszeitalter: Tauchnitz, Leipzig, 1199p.

Pérez-Peña, J.V., Azañón, J.M., and A. Azor, 2009, CalHypso: An ArcGIS extension to calculate hypsometric curves and their statistical moments. Applications to drainage basin analysis in SE Spain: Computers and Geosciences, v. 35, p. 1214-1223, doi:10.1016/j.cageo.2008.06.006.

Prescott, J.R. and Hutton, J.T.,1988, Cosmic ray and gamma ray dosimetry for TL and ESR: Nuclear Tracks, v. 14, p. 223 227.

Prescott, J.R., and Hutton, J.T., 1995, Environmental dose rates and radioactive disequilibrium from some Australian luminescence dating sites: Quaternary Science Review, v. 14, p. 439-448.

Reille, R., Gamisans, J., deBeaulieu, J.-L., and Andrieu, V., 1997, The late-glacial at Lac de Creno (Corsica, France): a key site in the western Mediterranean basin: New Phytologist, v. 135, p. 547-559.

Rittenour, T. M. 2008, Luminescence dating of fluvial deposits: applications to geomorphic, paleoseismic and archaeological research: Boreas, v.37, p. 613–635.

Rohling, E.J., Abu-Zied, R.H., Casford, J.S.L., Hayes, A., and Hoogakker, B.A.A., 2009, The marine environment: present and past, *in* J.C. Woodward (ed.) The Physical Geography of the Mediterranean, Oxford University Press, Oxford, p. 33-67.

Schumm, S.A., 1993, River response to baselevel change: Implications for sequence stratigraphy: Journal of Geology, v. 101, p. 279-294.

Seidl, M.A., and Dietrich, W.E., 1992, The problem of channel erosion into bedrock, Functional geomorphology, landform analysis and models: Cantena Supplement, v. 23, p. 101-124.

Snyder, N.P., Whipple, K.X., Tucker, G.E., and Merritts, D.J., 2000, Landscape response to tectonic forcing: digital elevation model analysis of stream profiles in the Mendocino triple junction region: northern California Geological Society of America Bulletin, v. 112, p. 1250–1263.

Snyder, N.P., Whipple, K.X., Tucker, G.E., Merritts, D.J., 2003, Channel response to tectonic forcing: field analysis of stream morphology and hydrology in the Mendocino triple junction region, northern California: Geomorphology, v. 53, p. 97-127.

Sømme, T. O., Piper, D. J.W., Deptuck, M.E., and Helland-Hansen, W., 2011, Linking onshore-offshore sediment dispersal in the Golo source-to-sink system (Corsica, France) during the Late Quaternary: Journal of Sedimentary Research, v. 81, p. 118-137.

Strahler, A.N., 1952, Hypsometric (area–altitude) analysis of erosional topography: Geological Society of America Bulletin, v. 63, p. 1117–1142.

Stewart, I.S. and Morhange, C. 2009, Coastal geomorphology and sea-level change, *in* J.C. Woodward (ed.) The Physical Geography of the Mediterranean, Oxford University Press, Oxford, p. 385-413.

Tommasini, S., Poli, G., Halliday, A., 1995, The role of sediment subduction and crustal growth in Hercynian plutonism: Isotopic and trace element evidence from the Sardinia-Corsica batholith: Journal of Petrology, v. 35, p. 1305-1332.

Waelbroeck, C., Labeyrie, L., Michel, E., Duplessy, J.C., McManus, J.F., Lambeck, K., Balbon, E., and Labracherie, M., 2002, Sea-level and deep water temperature changes derived from benthic foraminifera isotope records: Quaternary Science Reviews, v. 21, p. 295-305, doi:10.10106/S0277-3791(01)00101-9.

Whipple, K.X., and Tucker, G.E., 1999, Dynamics of the stream-power river incision model: Implications for height limits of mountain ranges, landscape response timescales, and research needs: Journal of Geophysical Research, v. 104, p. 17 661–17 674.

Whipple, K., Wobus, C., Crosby, B., Kirby, E., and Sheehan, D., 2007, New Tools for Quantitative Geomorphology: Extraction and Interpretation of Stream Profiles from Digital Topographic Data, GSA Annual Meeting.

Wintle, A.G., 2010, Future directions of luminescence dating of quartz: Geochronometria, v. 37, p. 1-7, doi: 10.2478/v10003-010-0023-3.

Wintle, S.G., and Murray, A.S., 2006, A review of quartz optically stimulated luminescence characteristics and their relevance in single-aliquot regeneration dating protocols: Radiation Measurements, v. 41, p. 369-391.

Wobus, C., Whipple, K., Kirby, E., Snyder, N., Johnson, J., Spyropolou, K., Crosby, B., and Sheehan, D., 2006, Tectonics from topography: Procedures, promise and pitfalls, *in* Willett, S.D., Hovius, N., Brandon, M.T., and Fisher, D.M., eds., Tectonics, Climate, and Landscape Evolution: Geological Society of America Special Paper 398, Penrose Conference Series, p. 55074, doi:10.1130/2006.2398(04).

Wolinsky, M. A., and Pratson, L.F., 2005, Constraints on landscape evolution from slope histograms: Geology, v. 33, p. 477-480, doi: 10.1130/G21296.1.

Zaprowski, B.J., F. J. Pazzaglia, and Evenson, E.B., 2005, Climatic influences on profile concavity and river incision: Journal of Geophysical Research, v. 110, F03004, doi:10.1029/2004JF000138.

Zarki-Jakni, B., van der Beek, P., Poupeau, G., Sosson, M., Labrin, E., Rossi, P., Ferrandini, J., 2004, Cenozoic denudation of Corsica in response to Ligurian and Tyrrhenian extension: Results from apatite fission-track thermochronology: Tectonics, v. 23, TC1003, doi:10.1029/2003TC001535.

APPENDICES

Appendix A. Weathering Rinds and Soil Color

Traditionally, Corsican deposits are correlated based on the intensity of weathering within the matrix and the clasts. This study made of broad sweep of the N2 terrace to determine the usefulness of this method of comparison and concluded that it was unnecessary to continue with the other terraces on the coastal plain.

Previous mapping used the degree of weathering of ophiolite clasts (metabasalts, serpentinites, eclogites and metagabbros) in which thicker weathering rinds (1-4 mm) represent older deposits and thinner to absent weathering rinds represent younger deposits (Conchon 1978). The intensity of weathering of the matrix and clasts has served as the criteria for mapping and correlation of all the Quaternary deposits of Corsica, with the N1-N6/7 regional sequence first established in the Bravona valley (Conchon, 1972). This was also used to correlate deposits and assign a relative age. Rubified deposits represent the older units while grey, weakly developed soils represent younger units. Conchon (1978) noted a matrix resemblance (both with 7.5 YR 6/6) between the two oldest terraces (N2 and N3) with a slight difference in the abundance of rhyolite and the intensity of the weathering rind.

Five sites, two within the river valley and three on the Marana Plain, were chosen to distinguish the differences between deposits (Figure A.1). Four sites occur at elevations ranging from 50-25 m above the modern river channel and are mapped as the Fw (N2). The last site is 5 m above the modern river and mapped as the Fy1 (N4) geologic unit (Lahondére, et al 1994). This method of comparing Munsel color and weathering is the common way in Corsica to determine which terrace/age deposit one is looking at.

Two-meter horizontal clast-count transects at varying depths were used to compare the four highest study sites (Figure A.2). These transect's determine the relative percentage of weathered clasts within each in order to compare deposits mapped as the same unit.

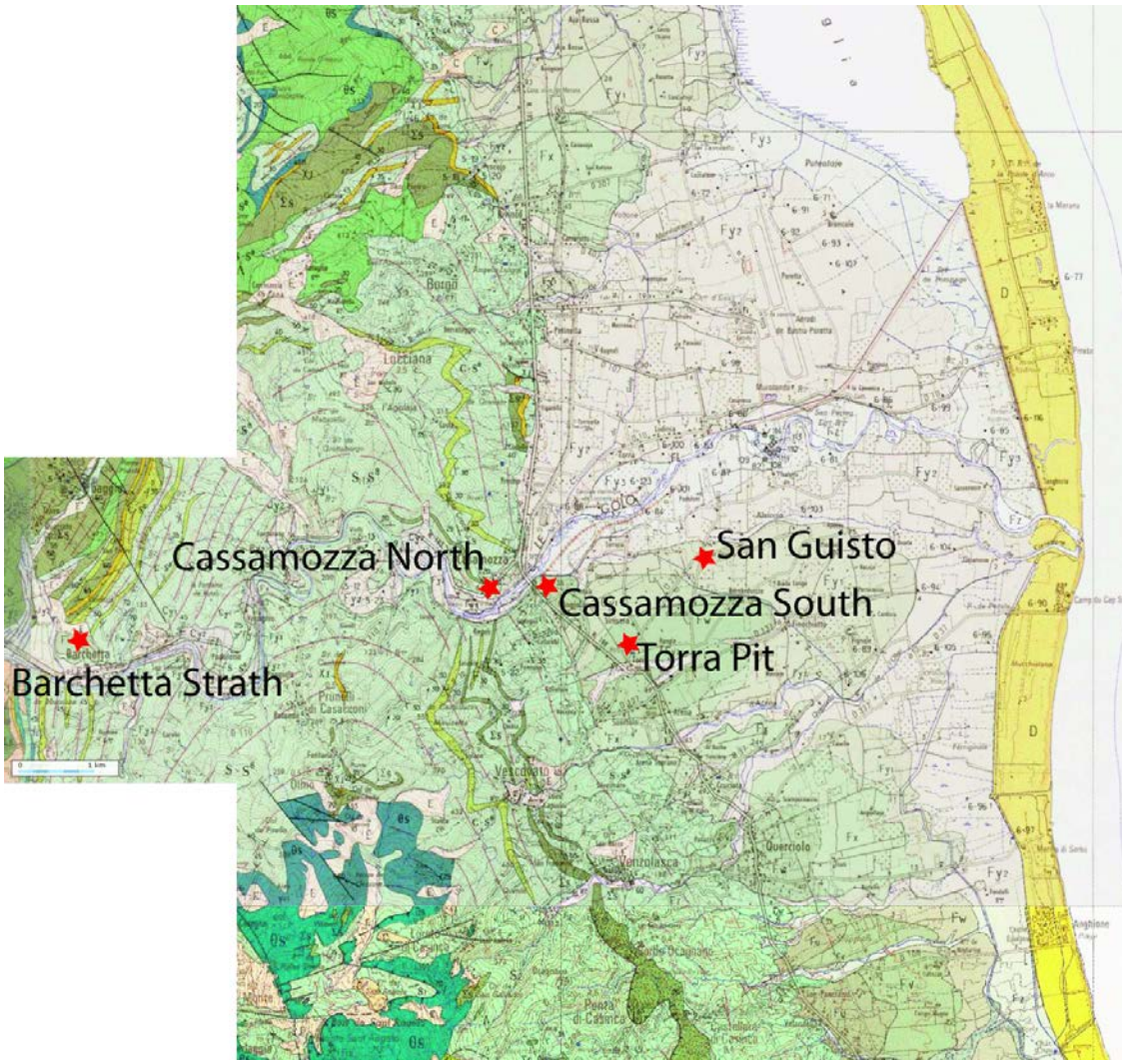

Figure A.1 Geologic map and site locations for weathering and transect studies.

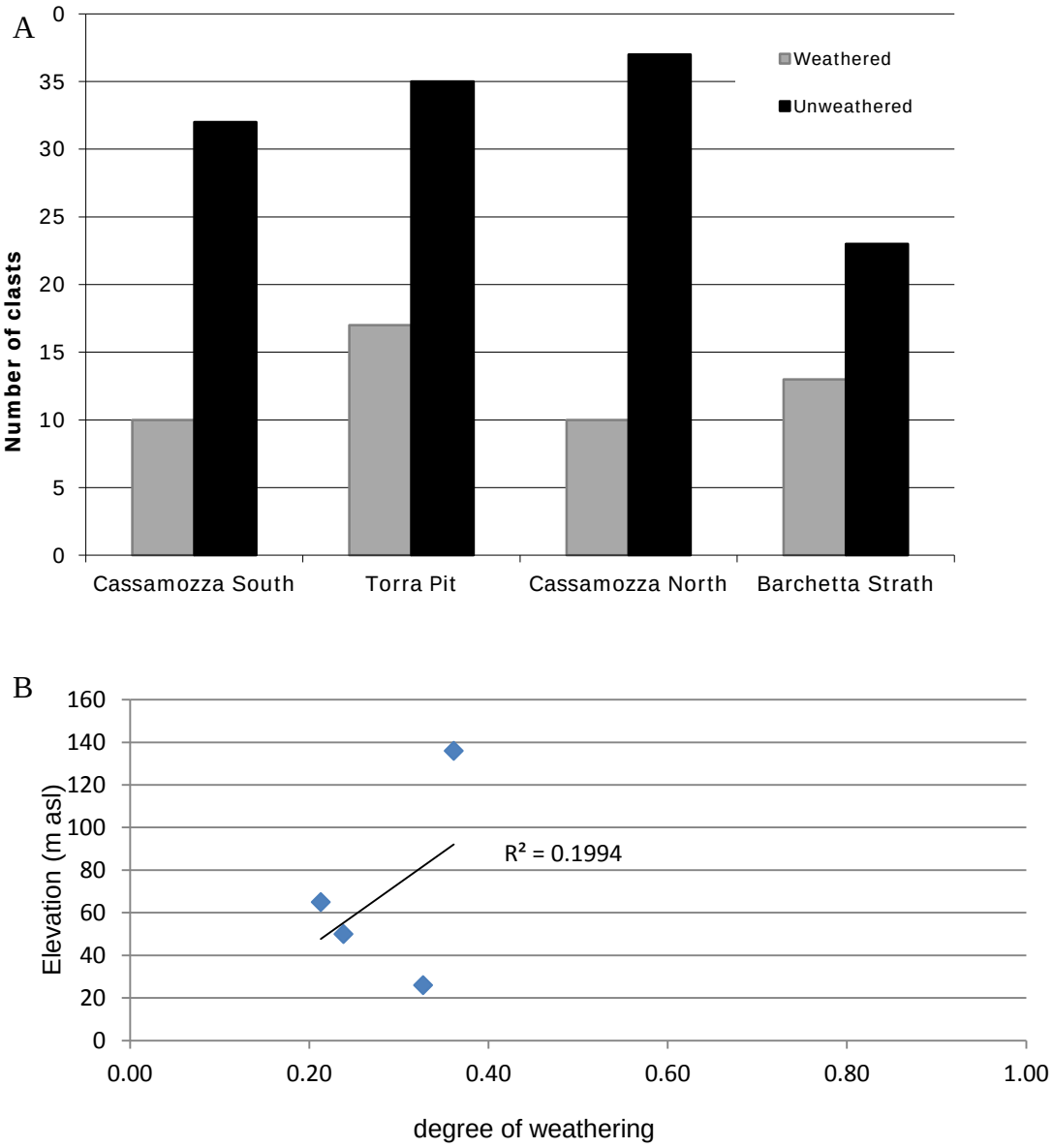

Figure A.2 Two-meter horizontal transects for the N2/Fw deposit. A) The overall weathering shows no systematic distribution for the same deposit. B) Variation has a low R^2 value and is not a function of elevation.

Table A. 1 Geographic Coordinates and metrics for study sites.

Lahondère et al., 1994	N#	Conchon Soil Color	Site Name	Soil Color (this study)	Location	Elevation (m)
Fw	N2	7.5 YR 6/6	Torra Pit	5YR 5/8	N 42.51554 E 9.46299	26
			Cassamozza South	5YR 5/8	N 42.51615 E 9.44472	40
			Cassamozza North	7.5 YR 5/8	N 42.51658 E 9.43173	65
			Barchetta Strath	7.5 YR 5/6-5/8	N 42.50903 E 9.36713	137
Fy1	N4	10 YR 6/6	San Giusto	2.5 YR 4/4	N 42.52130 E 9.47034	15

Degree of weathering determination was based on the audible response of clasts to tapping and prodding with a metal trowel and was not delineated by lithology. Separate weathering rind measurements were conducted on randomly selected clasts. Terraces are referenced to the Conchon (1977) and Lahondère et al. (1994) nomenclature to reduce confusion. Coordinates and metrics are summarized in Table A.1.

Study Sites

Sites were chosen to assess the consistency of the degree and intensity of weathering. Sites were named in a similar fashion as sampling sites for OSL age dating and refer to nearest townships.

Torra Terrace (Fw/N2)

On the southern side of the modern river (16 m above the modern river), a large pit has exposed fluvial gravels and colluvial sediments. Fluvial gravels consist of rounded clast-supported cobbles and pebbles. These gravels contain intensely grusified granites, calcschists and micaschists with weathering rinds ranging up to 1mm while metabasalts typically had weathering rinds ranging from 1-2 mm (Figure A.3). The matrix consists of Golo pebbles and very coarse grained sand and is yellowish red (5YR 5/8). Two 2-meter transects were measured near OSL sample USU-868, one at 2 meters depth and another closer to the surface. Transects indicate that this deposit exhibits 33% weathering.

Cassamozza South Roadcut (N2/Fw)

Where the Golo River emerges from the schistic bedrock river valley onto the coastal plain, an outcrop on the south side of the Golo River, 25 m above the modern river (50 m asl), consists of rounded cobbles and pebbles with weak bedding and imbrications and is yellowish red (5 YR 5/8) (Figure A.4). This deposit is matrix supported with subrounded, fine-coarse sand with some pea gravel in a clay rich matrix. This deposit displays intense grusification of granites

and rhyolites tend to show more through-going weathering with alteration of feldspars to clay and in situ disintegration. This outcrop has many highly weathered pebbles but there is extreme variability between and within lithologies. One metabasalt exhibits the largest weathering rind observed (4 and 6 mm) while other metabasalts have no rind. Based on two transects at 1 and 1.5 m depth, 24% of the clasts in this outcrop are weathered.

Cassamozza North Roadcut (N2/Fw)

Near the crest of a hill (~10 km from the mouth) on the north side of road N193A, a limited exposure of a strath terrace is, 40 m above the modern river (65 m asl) with a strong brown (7.5 YR 5/8) matrix. The exposure is moderately covered by vegetation with approximately 2.5 m of alluvial overlying schists. Two transects 1 and 2 m below the surface show that 21% of the clasts are weathered. Weathering rind analysis was not addressed at this location.

Barchetta Strath (N2/Fw)

A southwest facing exposure of a strath terrace above the town of Barchetta consists of 1.4 m of poorly sorted, rounded granitic cobbles to boulders and subangular to angular cobbles of schists and metabasalts. The poorly sorted alluvium sits directly on top of 1.2 m of exposed micaschists and calcschists of the Schistes Lustrés that are separated by an erosional, scour contact (Figure A.5). The matrix of this deposit is strong brown (7.5 YR 5/6-5/8). Within the alluvial sediments, micaschists have the largest weathering rinds at 2mm while rhyolite and metabasalt clasts lack any rind. Based on 2 transects,

36% of the clasts at this site are weathered. This unit is 50 m above the modern river at 136m asl. This strath terrace is mapped as the same geologic unit as the Fw/N2 in the Torra Pit.

San Guisto (N4/Fy1)

A northwest facing roadcut (15m asl) exposes sediments on the Torra Terrace riser near the tread of the Poretta. This outcrop consists 1.5-2 m of rounded cobbles and pebbles with a reddish brown (2.5 YR 4/4) matrix (Figure A.6). Rhyolites and calcshists have weathering rinds ~1mm thick and granites are commonly grusified. Micaschists are heavily altered along schistose planes and metabasalts are highly weathered with alteration penetrating up to 4 mm. Weathering transects were not measured at this location.

Figure A.3 Torra pit sample location and weathering rinds. A) fluvial gravels B) rhyolite C) grusified granite D) micaschist E) metabasalt.

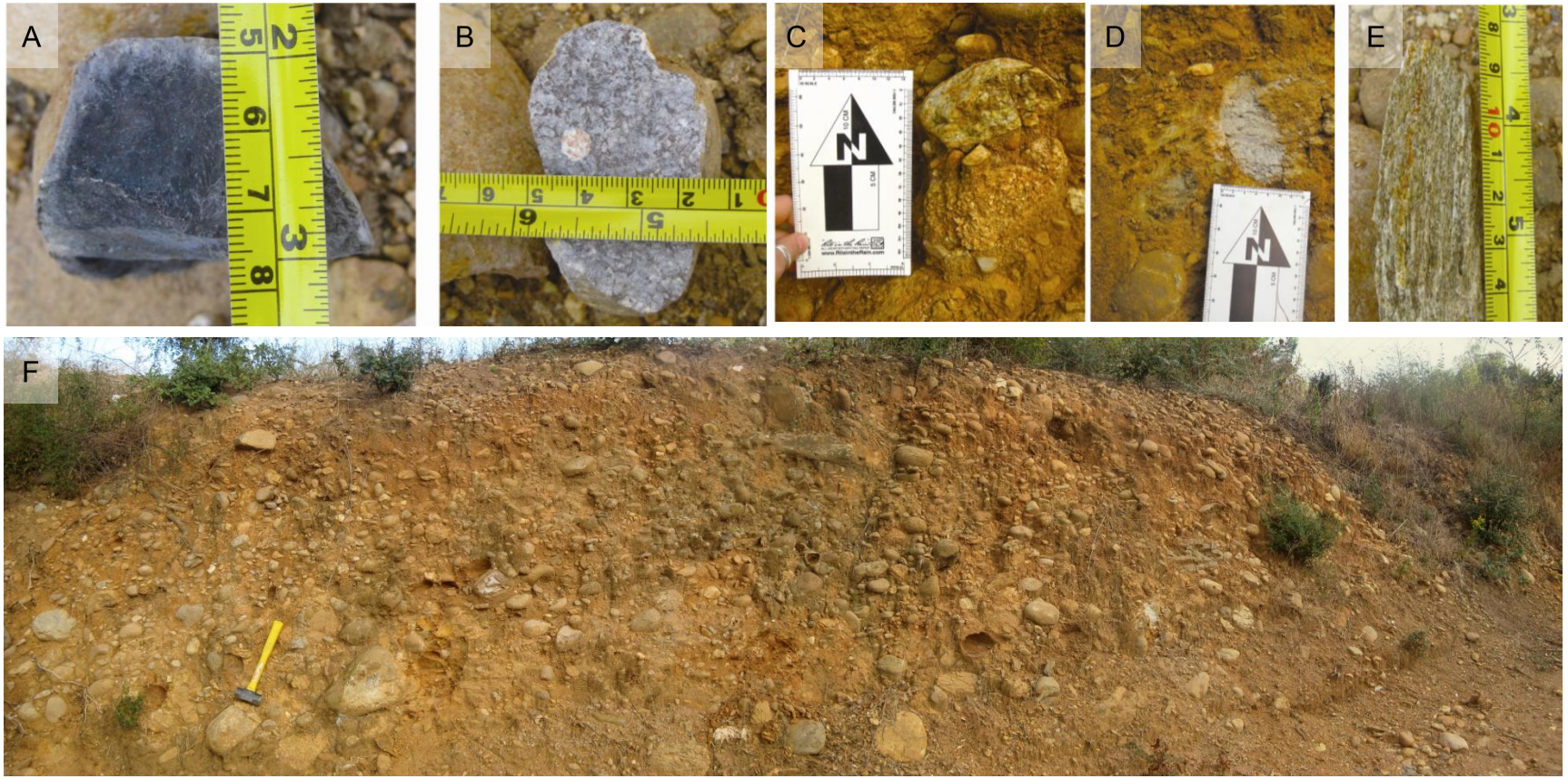

Figure A.4 Cassamozza road cut south and weathering rinds. A) metabasalt B) rhyolite C) grusified granite D) intensely weathered rhyolite E) micaschist F) fluvial gravels.

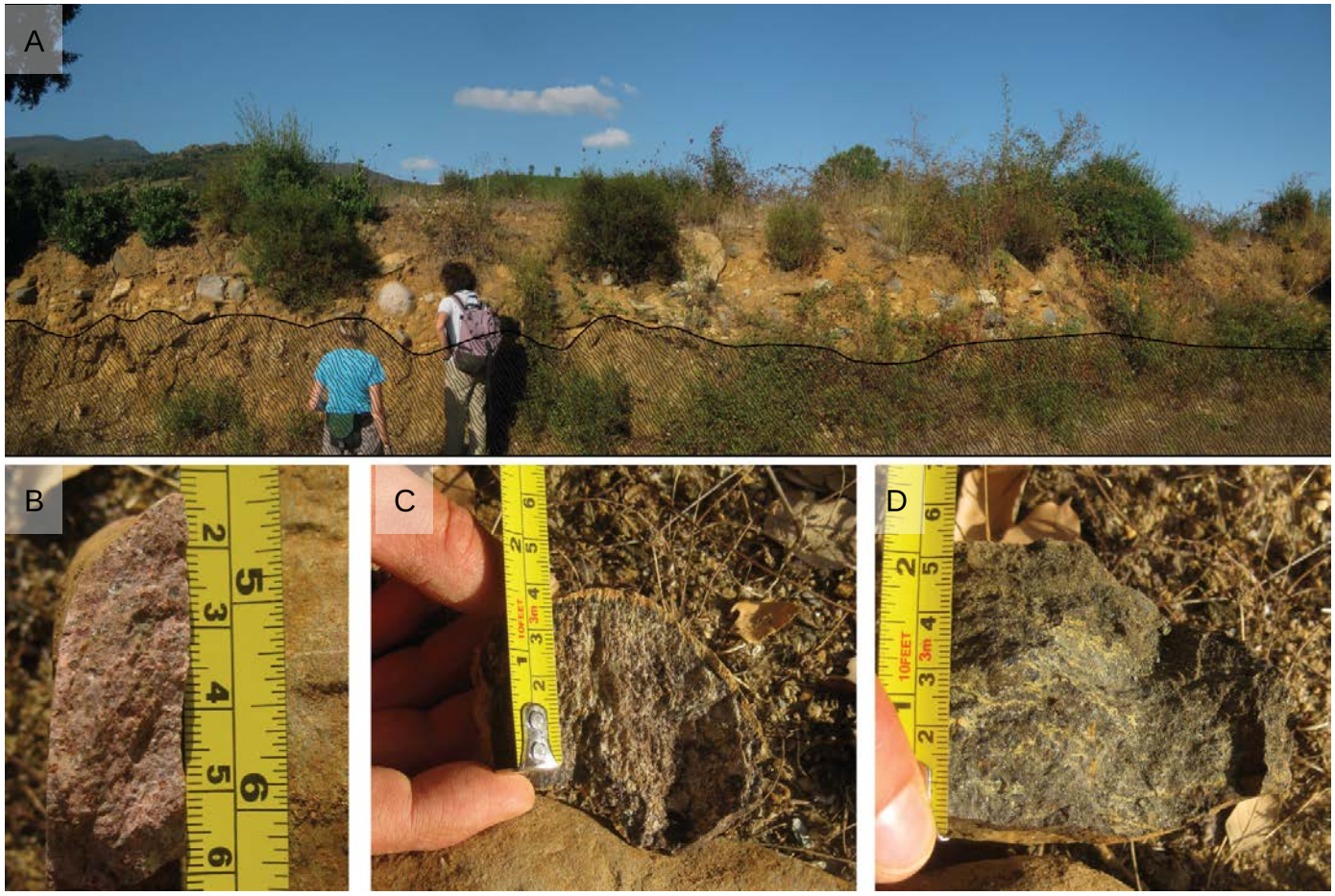

Figure A.5 Barchetta strath outcrop and weathering rinds. A) strath outcrop with gravels directly on top of Schistés Lustrés bedrock (shaded black) B) rhyolite C) calcschist D) metabasalt.

Figure A.6 San Guisto outcrop

Appendix B. OSL samples

Ages were calculated using the minimum age model (MAM) for the youngest Canonica terrace and beach deposits while the central age model (CAM) was used for all other samples following Galbraith et al. (1999). Errors on OSL ages are reported at two-sigma standard error, unless otherwise noted. Early background subtraction (EBG) was used to determine the equivalent dose on all samples except the youngest. All OSL age results and corresponding sample information can be found in Table 2.1 and 2.2.

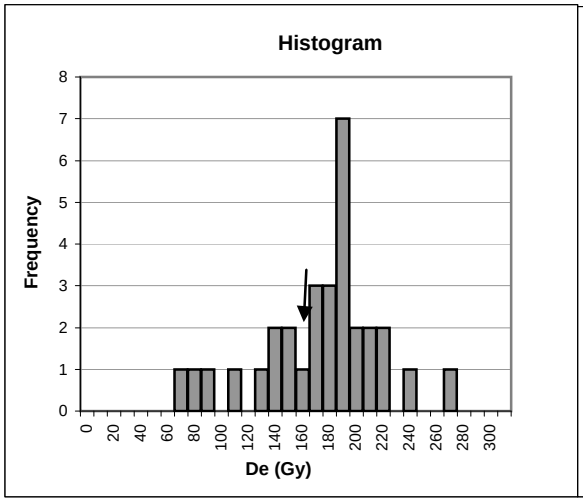

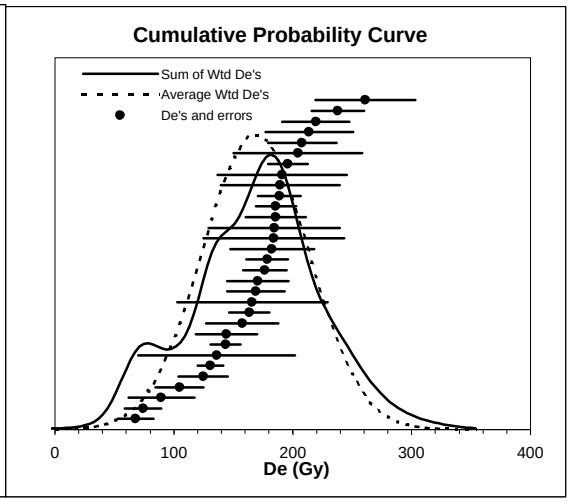

Golo-0315-1
USU-797

Poretta Terrace (Qat3)

Individual Aliquot Data

	De (Gy)	±	Age (ka)	±
CAM =	**165.90**	**8.48**	**50.18**	**6.37**
MAM =	**127.75**	**8.60**	**38.64**	**4.90**
Median =	178.47		54.0	6.8
Min =	67.83		20.5	2.6
Max =	213.98		64.7	8.2
n =	**31**	**Aliquots**		
S.D. =	44.57			
Standard error =	8.01			
Random Errors=	10.48	%		
Systematic Error=	7.15	%		
Total Error=	12.69	%		
Bin Width =	10.00	**Gy**		
Overdispersion (%) =	22.4	±	4.4	
		+/-		
dose rate=	**3.31**	**0.20**	**Gy/ka**	
U =	2.70	0.2	**ppm**	
Th =	11.70	1.1	**ppm**	
K2O =	3.01	0.08	**wt. %**	
Rb2O=	146.0	5.8	**ppm**	
H2O=	20.0	6.0	**wt. %**	
Cosmic=	0.16	**Gy/ka**		
depth =	1.9	**m**		
latitude=	42	**degrees (north positive)**		
longitude=	9	**degrees (east positive)**		
elevation=	0.01	**km asl**		

De (Gy)	±	Age (ka)	±
67.83	14.90	20.52	2.60
74.10	15.46	22.41	2.84
89.61	27.68	27.11	3.44
104.73	20.15	31.68	4.02
124.77	20.67	37.74	4.79
131.00	10.77	39.63	5.03
136.01	66.01	41.14	5.22
143.50	12.48	43.41	5.51
144.38	25.97	43.67	5.54
157.51	30.48	47.64	6.05
163.47	16.94	49.45	6.27
165.91	63.33	50.19	6.37
169.12	24.24	51.16	6.49
170.62	25.95	51.61	6.55
176.37	18.26	53.35	6.77
178.47	17.27	53.98	6.85
182.64	35.25	55.24	7.01
184.36	59.23	55.77	7.08
184.44	55.28	55.79	7.08
185.74	25.12	56.18	7.13
185.83	16.96	56.21	7.13
188.90	18.09	57.14	7.25
189.61	50.10	57.35	7.28
191.14	54.38	57.82	7.34
195.91	16.73	59.26	7.52
204.49	54.13	61.85	7.85
207.88	28.86	62.88	7.98
213.98	36.88	64.73	8.21
219.40	28.36	66.36	8.42
238.11	22.01	72.02	9.14
261.16	41.94	79.00	10.02

Notes: Quartz SAR OSL age following Murray and Wintle, 2000
CAM and MAM from Galbraith et al., 1999

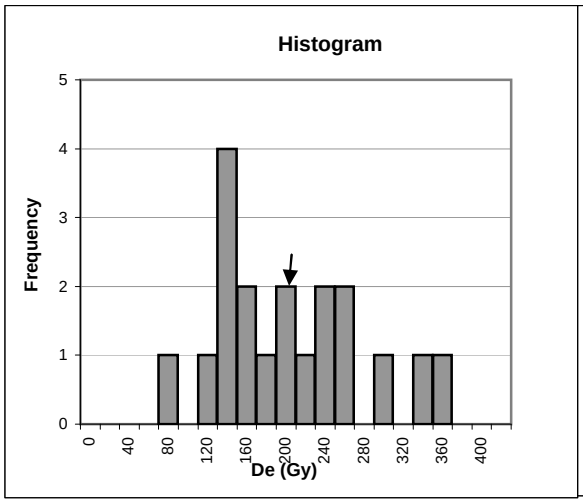

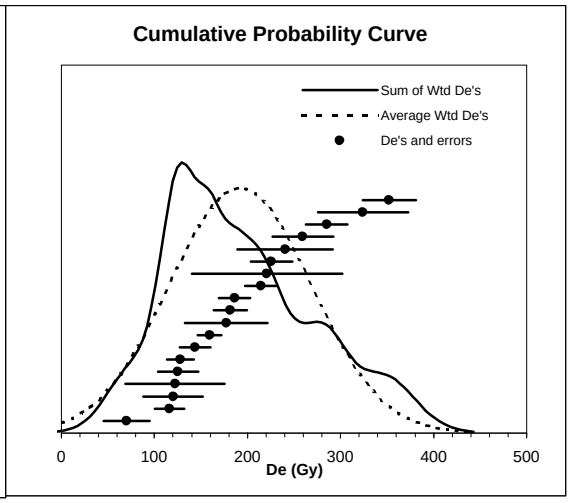

Golo-0316-2 **Poretta Terrace (Qat3)**
USU-798

	De (Gy)	±	Age (ka)	±
CAM =	**185.66**	**16.06**	**57.51**	**10.75**
MAM =	**114.02**	**17.31**	**35.32**	**6.60**
Median =	181.72		56.3	10.5
Min =	70.10		21.7	4.1
Max =	352.40		109.2	20.4
n =	**19**	**Aliquots**		
S.D. =	76.06			
Standard error =	17.45			
Random Errors=	17.29	%		
Systematic Error=	7.12	%		
Total Error=	18.69	%		
Bin Width =	20.00	**Gy**		
Overdispersion (%) =	33.5	±	6.7	

		+/-	
dose rate=	**3.23**	**0.19**	**Gy/ka**
U =	2.50	0.2	**ppm**
Th =	12.40	1.1	**ppm**
K2O =	2.89	0.07	**wt. %**
Rb2O=	146.0	5.8	**ppm**
H2O=	20.0	6.0	**wt. %**
Cosmic=	0.16	**Gy/ka**	
depth =	2.0	**m**	
latitude=	42	**degrees (north positive)**	
longitude=	9	**degrees (east positive)**	
elevation=	0.02	**km asl**	

Individual Aliquot Data

De (Gy)	±	Age (ka)	±
70.10	24.47	21.72	4.06
116.32	16.02	36.03	6.74
120.18	32.04	37.23	6.96
122.09	53.35	37.82	7.07
125.32	21.80	38.82	7.26
128.02	14.63	39.66	7.41
144.04	16.48	44.62	8.34
159.34	12.89	49.36	9.23
177.20	44.20	54.89	10.26
181.72	18.04	56.29	10.52
186.12	16.60	57.66	10.78
214.33	17.03	66.39	12.41
220.87	80.72	68.42	12.79
225.90	22.58	69.98	13.08
240.54	51.28	74.51	13.93
259.59	32.73	80.41	15.03
285.08	22.02	88.31	16.51
324.07	48.59	100.39	18.77
352.40	28.75	109.16	20.41

Notes: Quartz SAR OSL age following Murray and Wintle, 2000
CAM and MAM from Galbraith et al., 1999

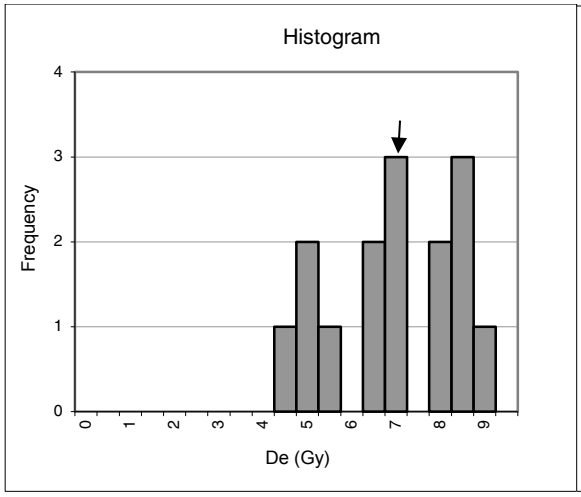

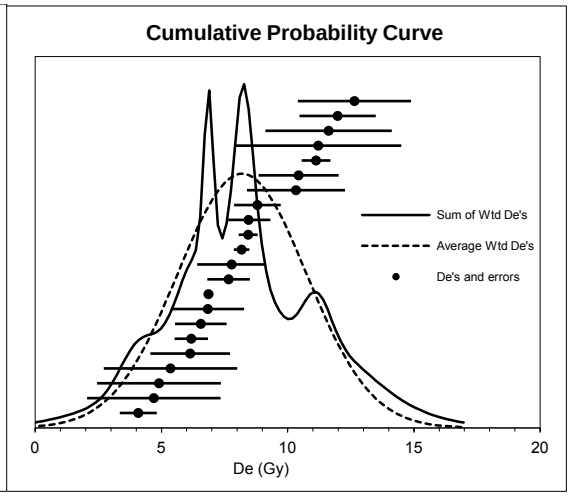

Sample # Golo 10-11-10-15 **Biguglia (Hb)**
USU-860

	De (Gy)	±	Age (ka)	±
CAM =	**8.22**	**0.48**	**3.78**	**1.19**
MAM =	**6.80**	**0.15**	**3.13**	**0.98**
Median =	7.98		3.7	1.2
Min =	4.08		1.9	0.6
Max =	12.65		5.8	1.8
n =	**22**	**Aliquots**		
S.D. =	2.55			
Standard error =	0.54			
Random Errors=	30.78	%		
Systematic Error=	6.69	%		
Total Error=	31.50	%		
Bin Width =	0.50	**Gy**		
Overdispersion (%) =	21.5	±	4.8	
		+/-		
dose rate=	**2.17**	**0.11**	**Gy/ka**	
U =	1.10	0.1	**ppm**	
Th =	5.20	0.5	**ppm**	
K2O =	2.17	0.05	**wt. %**	
Rb2O=	103.8	4.2	**ppm**	
H2O=	15.6	4.7	**wt. %**	
Cosmic=	0.17	**Gy/ka**		
depth =	1.4	**m**		
latitude=	42	**degrees (north positive)**		
longitude=	9	**degrees (east positive)**		
elevation=	0.00	**km asl**		

Individual Aliquot Data

De (Gy)	±	Age (ka)	±
4.08	0.73	1.88	0.59
4.70	2.64	2.16	0.68
4.90	2.45	2.26	0.71
5.36	2.64	2.47	0.78
6.14	1.58	2.82	0.89
6.18	0.66	2.84	0.90
6.56	1.02	3.02	0.95
6.84	1.44	3.15	0.99
6.86	0.19	3.16	0.99
7.66	0.84	3.52	1.11
7.78	1.36	3.58	1.13
8.18	0.31	3.76	1.18
8.44	0.38	3.88	1.22
8.45	0.87	3.89	1.22
8.80	0.92	4.05	1.28
10.33	1.94	4.75	1.50
10.43	1.59	4.80	1.51
11.12	0.57	5.12	1.61
11.21	3.29	5.16	1.62
11.62	2.50	5.35	1.68
11.98	1.51	5.51	1.74
12.65	2.24	5.82	1.83

Notes: Quartz SAR OSL age following Murray and Wintle, 2000
CAM and MAM from Galbraith et al., 1999

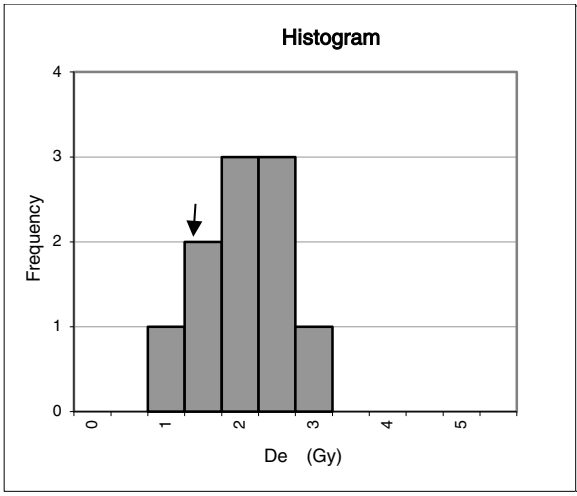

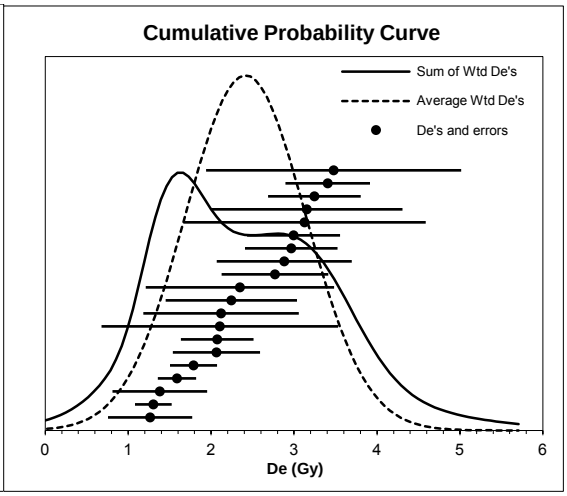

Sample # Golo 10-7-10-10 **Canonica Terrace (Qat1)** **Individual Aliquot Data**
USU-861

	De (Gy)	±	Age (ka)	±
CAM =	**2.31**	**0.19**	**0.82**	**0.22**
MAM =	**1.65**	**0.24**	**0.58**	**0.16**
Median =	2.30		0.8	0.2
Min =	1.26		0.4	0.1
Max =	3.48		1.2	0.3
n =	**20**	**Aliquots**		
S.D. =	0.66			
Standard error =	0.15			
Random Errors=	26.16	%		
Systematic Error=	6.14	%		
Total Error=	26.87	%		
Bin Width =	0.50	**Gy**		
Overdispersion (%) =	24.4	±	7.9	

		+/-	
dose rate=	**2.83**	**0.13**	**Gy/ka**
U =	1.80	0.1	**ppm**
Th =	9.70	0.9	**ppm**
K2O =	2.28	0.06	**wt. %**
Rb2O=	107.7	4.3	**ppm**
H2O=	11.6	3.5	**wt. %**
Cosmic=	0.15	**Gy/ka**	
depth =	2.3	**m**	
latitude=	42	**degrees (north positive)**	
longitude=	9	**degrees (east positive)**	
elevation=	0.01	**km asl**	

De (Gy)	±	Age (ka)	±
1.26	0.51	0.45	0.12
1.30	0.22	0.46	0.12
1.38	0.57	0.49	0.13
1.59	0.23	0.56	0.15
1.79	0.28	0.63	0.17
2.06	0.53	0.73	0.20
2.07	0.44	0.73	0.20
2.10	1.43	0.74	0.20
2.12	0.94	0.75	0.20
2.24	0.79	0.79	0.21
2.35	1.14	0.83	0.22
2.77	0.64	0.98	0.26
2.88	0.81	1.02	0.27
2.97	0.56	1.05	0.28
2.99	0.56	1.06	0.28
3.13	1.46	1.11	0.30
3.15	1.15	1.12	0.30
3.25	0.56	1.15	0.31
3.41	0.51	1.20	0.32
3.48	1.54	1.23	0.33

Notes: Quartz SAR OSL age following Murray and Wintle, 2000
CAM and MAM from Galbraith et al., 1999

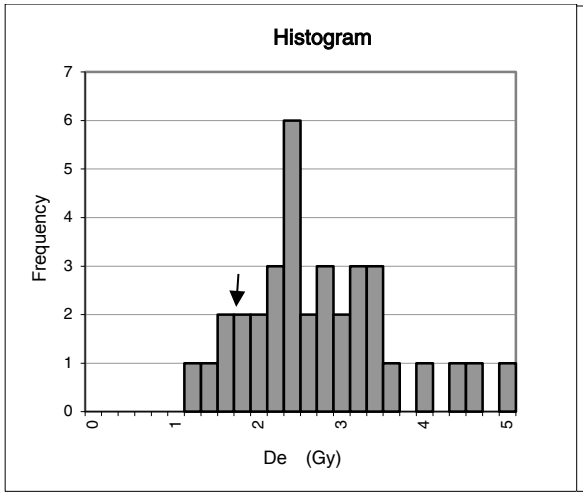

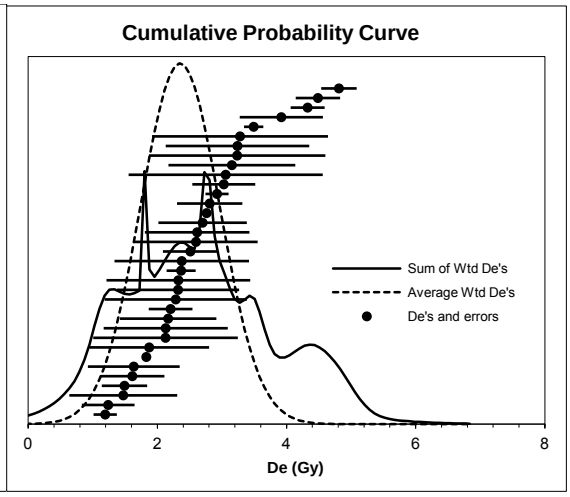

Sample # Golo10-7-10-8 **Canonica Terrace (Qat1)**
USU-862

	De (Gy)	±	Age (ka)	±
CAM =	**2.61**	**0.18**	**1.09**	**0.33**
MAM =	**1.67**	**0.23**	**0.70**	**0.21**
Median =	2.25		0.9	0.3
Min =	1.19		0.5	0.1
Max =	2.62		1.1	0.3
n =	**35**	**Aliquots**		
S.D. =	0.75			
Standard error =	0.13			
Random Errors=	28.81	%		
Systematic Error=	8.57	%		
Total Error=	30.06	%		
Bin Width =	0.20	**Gy**		
Overdispersion (%) =	31.3	±	5.8	

		+/-	
dose rate=	**2.39**	**0.18**	**Gy/ka**
U =	2.00	0.1	**ppm**
Th =	8.20	0.7	**ppm**
K2O =	2.35	0.06	**wt. %**
Rb2O=	80.3	3.2	**ppm**
H2O=	28.7	8.6	**wt. %**
Cosmic=	0.16	**Gy/ka**	
depth =	2.0	**m**	
latitude=	42	**degrees (north positive)**	
longitude=	9	**degrees (east positive)**	
elevation=	0.01	**km asl**	

Notes: Quartz SAR OSL age following Murray and Wintle, 2000
CAM and MAM from Galbraith et al., 1999

Individual Aliquot Data

De (Gy)	±	Age (ka)	±
1.19	0.18	0.50	0.15
1.24	0.41	0.52	0.16
1.47	0.84	0.62	0.18
1.49	0.35	0.62	0.19
1.61	0.50	0.67	0.20
1.63	0.71	0.68	0.21
1.83	0.02	0.76	0.23
1.87	0.93	0.78	0.24
2.13	1.12	0.89	0.27
2.13	0.96	0.89	0.27
2.17	0.75	0.91	0.27
2.21	0.34	0.92	0.28
2.29	1.10	0.95	0.29
2.32	0.95	0.97	0.29
2.33	1.11	0.97	0.29
2.37	0.23	0.99	0.30
2.38	1.04	0.99	0.30
2.51	0.43	1.05	0.32
2.60	0.95	1.09	0.33
2.62	0.81	1.09	0.33
2.70	0.68	1.13	0.34
2.76	0.07	1.15	0.35
2.81	0.51	1.17	0.35
2.92	0.18	1.22	0.37
3.03	0.49	1.27	0.38
3.06	1.50	1.28	0.38
3.15	0.98	1.32	0.40
3.24	1.37	1.35	0.41
3.24	1.11	1.35	0.41
3.28	1.36	1.37	0.41
3.49	0.15	1.46	0.44
3.92	0.64	1.64	0.49
4.33	0.26	1.81	0.54
4.49	0.34	1.87	0.56
4.81	0.27	2.01	0.60

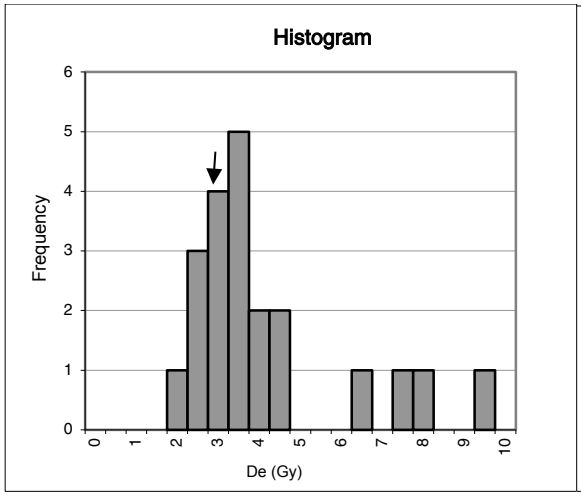

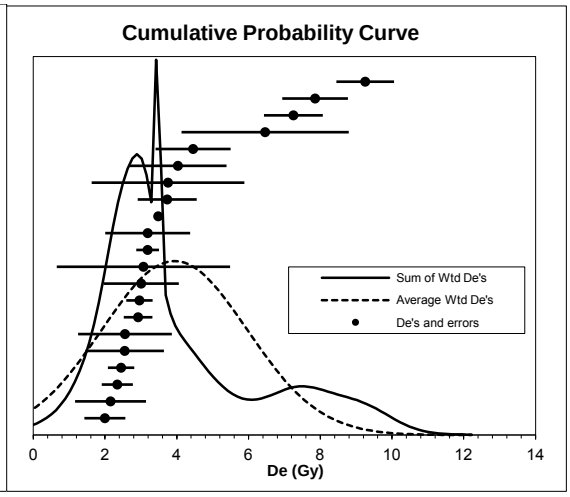

Sample # Golo 10-7-10-9 **Canonica Terrace (Qat1)** **Individual Aliquot Data**
USU-863

	De (Gy)	±	Age (ka)	±
CAM =	**3.73**	**0.40**	**1.31**	**0.29**
MAM =	**2.89**	**0.18**	**1.02**	**0.23**
Median =	3.19		1.1	0.3
Min =	1.99		0.7	0.2
Max =	9.25		3.3	0.7
n =	**21**	**Aliquots**		
S.D. =	2.13			
Standard error =	0.46			
Random Errors=	21.55	%		
Systematic Error=	6.07	%		
Total Error=	22.39	%		
Bin Width =	0.50	**Gy**		
Overdispersion (%) =	40.9	±	8.6	
		+/-		
dose rate=	**2.85**	**0.13**	**Gy/ka**	
U =	1.70	0.1	**ppm**	
Th =	7.90	0.7	**ppm**	
K2O =	2.55	0.06	**wt. %**	
Rb2O=	108.8	4.4	**ppm**	
H2O=	10.0	3.0	**wt. %**	
Cosmic=	0.14	**Gy/ka**		
depth =	3.0	**m**		
latitude=	42	**degrees (north positive)**		
longitude=	9	**degrees (east positive)**		
elevation=	0.01	**km asl**		

De (Gy)	±	Age (ka)	±
1.99	0.57	0.70	0.16
2.15	0.99	0.76	0.17
2.34	0.43	0.82	0.18
2.45	0.37	0.86	0.19
2.55	1.09	0.89	0.20
2.55	1.31	0.90	0.20
2.92	0.40	1.03	0.23
2.96	0.37	1.04	0.23
3.01	1.05	1.06	0.24
3.07	2.42	1.08	0.24
3.19	0.32	1.12	0.25
3.19	1.18	1.12	0.25
3.48	0.05	1.22	0.27
3.73	0.82	1.31	0.29
3.75	2.13	1.32	0.30
4.03	1.36	1.42	0.32
4.45	1.05	1.56	0.35
6.46	2.33	2.27	0.51
7.25	0.82	2.55	0.57
7.86	0.92	2.76	0.62
9.25	0.80	3.25	0.73

Notes: Quartz SAR OSL age following Murray and Wintle, 2000
CAM and MAM from Galbraith et al., 1999

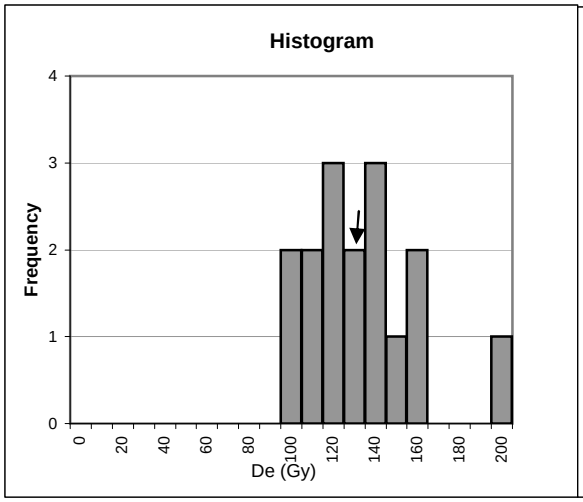

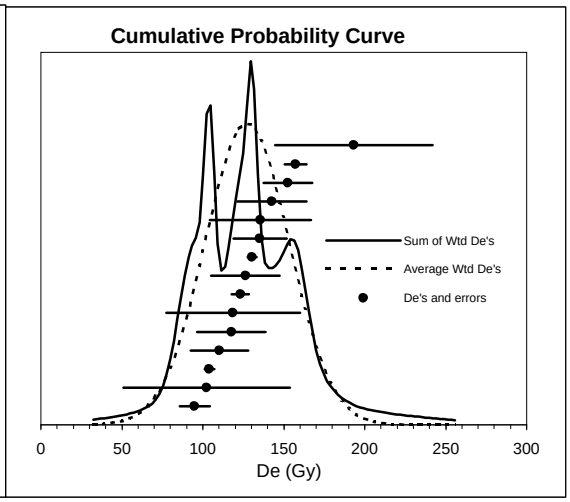

Golo 10-11-10-13 **Torra alluvium-colluvium (Qac)**
USU-864

Individual Aliquot Data

	De (Gy)	±	Age (ka)	±
CAM =	**124.22**	**6.17**	**32.64**	**3.93**
MAM =	**98.03**	**5.70**	**25.76**	**3.10**
Median =	126.32		33.2	4.0
Min =	93.06		24.4	2.9
Max =	193.26		50.8	6.1
n =	**16**	**Aliquots**		
S.D. =	26.01			
Standard error =	6.50			
Random Errors=	10.28	%		
Systematic Error=	6.25	%		
Total Error=	12.04	%		
Bin Width =	10.00	**Gy**		
Overdispersion (%) =	15.0	±	4.2	

De (Gy)	±	Age (ka)	±
93.06	8.28	24.45	2.94
94.99	9.27	24.96	3.00
102.27	51.40	26.87	3.23
103.99	2.96	27.32	3.29
110.12	17.76	28.93	3.48
117.75	21.11	30.94	3.72
118.68	41.22	31.18	3.75
123.29	5.32	32.39	3.90
126.32	20.99	33.19	3.99
130.42	2.94	34.27	4.12
135.33	16.48	35.56	4.28
135.51	31.18	35.60	4.29
142.78	21.26	37.51	4.52
152.68	15.08	40.12	4.83
157.37	6.71	41.35	4.98
193.26	48.62	50.78	6.11

dose rate=	**3.81**	**+/- 0.19**	**Gy/ka**
U =	2.70	0.2	**ppm**
Th =	15.60	1.4	**ppm**
K2O =	2.92	0.07	**wt. %**
Rb2O=	139.7	5.6	**ppm**
H2O=	13.1	3.9	**wt. %**
Cosmic=	0.16	**Gy/ka**	
depth =	1.9	**m**	
latitude=	42	**degrees (north positive)**	
longitude=	9	**degrees (east positive)**	
elevation=	0.02	**km asl**	

Notes: Quartz SAR OSL age following Murray and Wintle, 2000
CAM and MAM from Galbraith et al., 1999

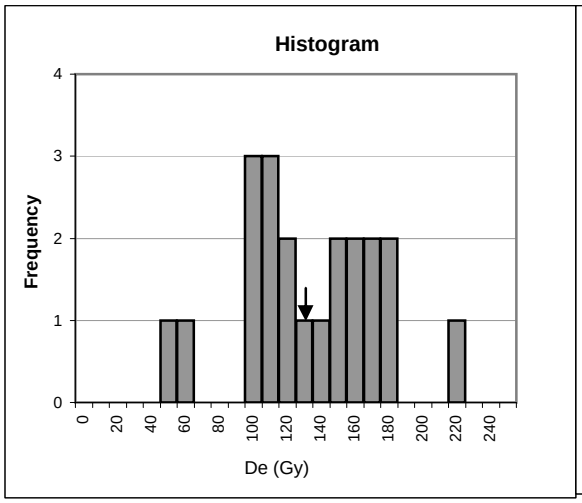

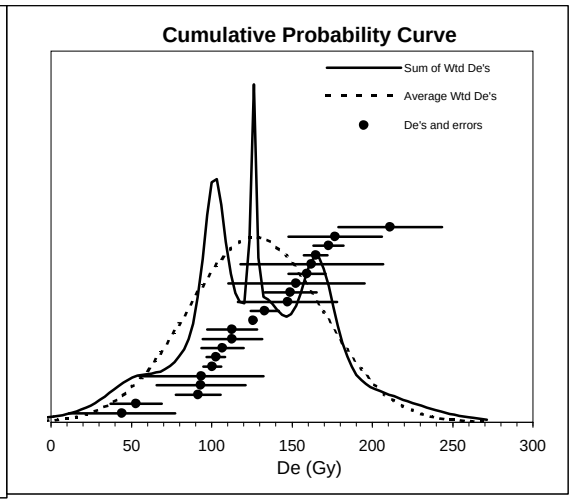

Golo 10-4-10-6 **Torra alluvium-colluvium (Qac)**
USU-865

	De (Gy)	±	Age (ka)	±
CAM =	**128.97**	**7.62**	**41.07**	**3.65**
MAM =	**96.52**	**8.83**	**30.74**	**2.73**
Median =	126.05		40.1	3.6
Min =	44.19		14.1	1.3
Max =	211.26		67.3	6.0
n =	**21**	**Aliquots**		
S.D. =	36.45			
Standard error =	7.95			
Random Errors=	6.48	%		
Systematic Error=	6.08	%		
Total Error=	8.89	%		
Bin Width =	10.00	**Gy**		
Overdispersion (%) =	22.0	±	4.8	

dose rate=	**3.14**	**+/- 0.14**	**Gy/ka**
U =	1.80	0.1	**ppm**
Th =	10.35	0.9	**ppm**
K2O =	2.77	0.07	**wt. %**
Rb2O=	136.4	5.5	**ppm**
H2O=	10.0	3.0	**wt. %**
Cosmic=	0.16	**Gy/ka**	
depth =	2.0	**m**	
latitude=	42	**degrees (north positive)**	
longitude=	9	**degrees (east positive)**	
elevation=	0.02	**km asl**	

Individual Aliquot Data

De (Gy)	±	Age (ka)	±
44.19	33.05	14.07	1.25
53.11	15.86	16.91	1.50
91.56	13.91	29.16	2.59
93.39	27.77	29.74	2.64
93.50	38.58	29.78	2.65
100.45	5.70	31.99	2.84
102.67	5.77	32.70	2.91
106.75	13.11	34.00	3.02
112.87	18.42	35.95	3.19
112.90	15.49	35.95	3.19
126.05	1.70	40.14	3.57
133.16	8.76	42.41	3.77
147.38	30.86	46.94	4.17
149.16	16.14	47.50	4.22
152.68	42.36	48.62	4.32
159.36	11.41	50.75	4.51
162.30	44.45	51.69	4.59
164.88	7.38	52.51	4.67
172.80	9.41	55.03	4.89
176.92	29.20	56.35	5.01
211.26	32.19	67.28	5.98

Notes: Quartz SAR OSL age following Murray and Wintle, 2000
CAM and MAM from Galbraith et al., 1999

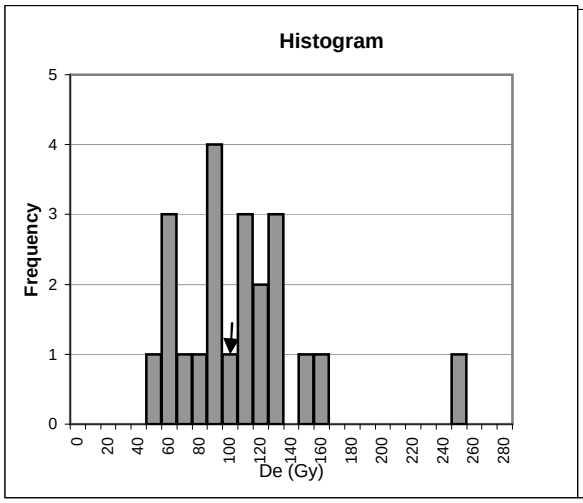

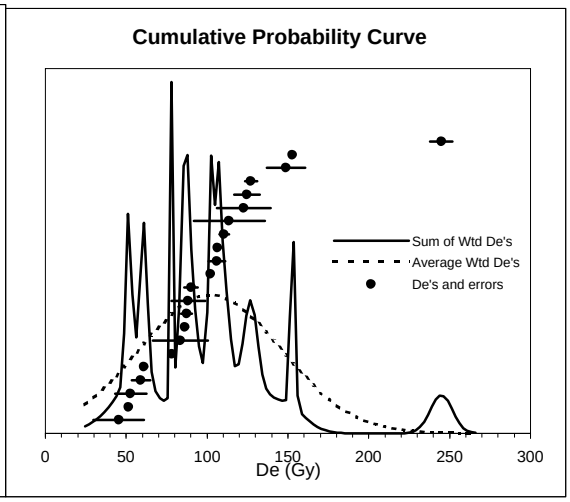

Golo10-11-10-11 **Revinco Alluvial Fan (Qaf_3)**
USU-866

	De (Gy)	±	Age (ka)	±
CAM =	**96.21**	**7.84**	**43.22**	**7.51**
MAM =	**51.71**	**1.92**	**23.23**	**4.04**
Median =	96.15		43.2	7.5
Min =	45.41		20.4	3.5
Max =	244.82		110.0	19.1
n =	**22**	**Aliquots**		
S.D. =	43.87			
Standard error =	9.35			
Random Errors=	16.31	%		
Systematic Error=	6.00	%		
Total Error=	17.38	%		
Bin Width =	10.00	**Gy**		
Overdispersion (%) =	36.8	±	5.9	

		+/-	
dose rate=	**2.23**	**0.10**	**Gy/ka**
U =	1.50	0.1	**ppm**
Th =	7.10	0.6	**ppm**
K2O =	1.75	0.04	**wt. %**
Rb2O=	72.8	2.9	**ppm**
H2O=	10.4	3.1	**wt. %**
Cosmic=	0.15	**Gy/ka**	
depth =	2.3	**m**	
latitude=	42	**degrees (north positive)**	
longitude=	9	**degrees (east positive)**	
elevation=	0.05	**km asl**	

Individual Aliquot Data

De (Gy)	±	Age (ka)	±
45.41	15.61	20.40	3.54
51.37	1.69	23.08	4.01
52.76	9.60	23.70	4.12
59.12	5.71	26.56	4.61
60.87	2.05	27.34	4.75
78.30	0.80	35.17	6.11
83.48	16.88	37.50	6.52
86.23	2.00	38.73	6.73
87.27	3.35	39.20	6.81
88.45	10.64	39.73	6.90
90.05	4.18	40.45	7.03
102.25	1.40	45.93	7.98
106.10	5.30	47.66	8.28
106.55	1.78	47.86	8.32
110.49	3.01	49.63	8.62
113.68	21.94	51.06	8.87
122.72	16.75	55.13	9.58
124.60	7.88	55.97	9.73
127.13	3.73	57.10	9.92
148.82	11.78	66.85	11.62
152.94	1.41	68.70	11.94
244.82	6.91	109.97	19.11

Notes: Quartz SAR OSL age following Murray and Wintle, 2000
CAM and MAM from Galbraith et al., 1999

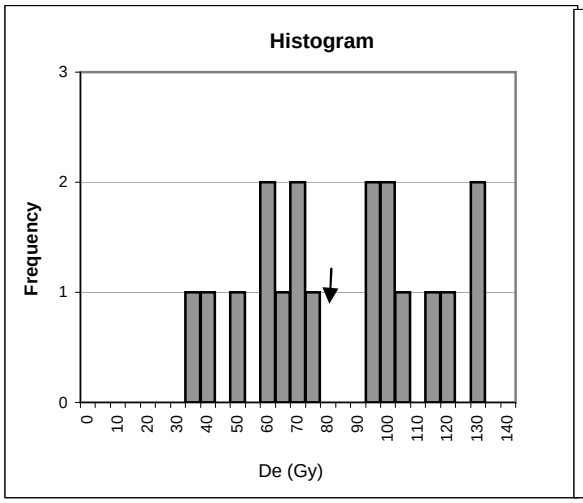

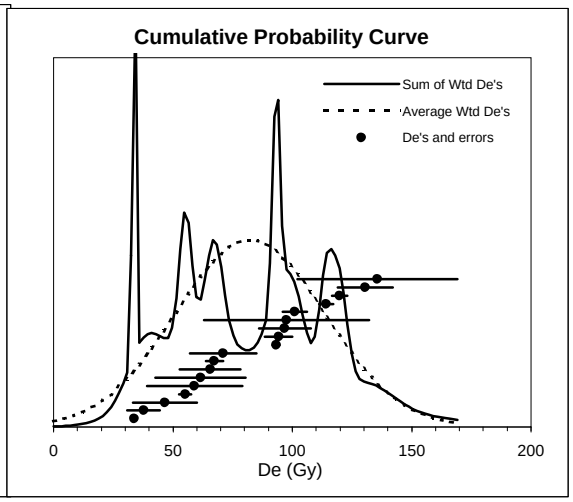

Golo 10-3-10-3 **Revinco Alluvial Fan (Qaf_3)** **Individual Aliquot Data**

USU-867

	De (Gy)	±	Age (ka)	±
CAM =	**77.33**	**7.64**	**52.19**	**10.86**
MAM =	**33.72**	**0.66**	**22.76**	**4.73**
Median =	82.17		55.5	11.5
Min =	33.67		22.7	4.7
Max =	135.69		91.6	19.1
n =	**18**	**Aliquots**		
S.D. =	31.26			
Standard error =	7.37			
Random Errors=	19.74	%		
Systematic Error=	6.56	%		
Total Error=	20.80	%		
Bin Width =	5.00	**Gy**		
Overdispersion (%) =	38.6	±	7.5	

De (Gy)	±	Age (ka)	±
33.67	0.63	22.72	4.73
37.71	6.89	25.45	5.29
46.69	13.48	31.51	6.56
55.18	2.59	37.24	7.75
59.11	19.90	39.90	8.30
61.63	18.92	41.60	8.65
65.56	12.66	44.25	9.20
67.36	3.56	45.46	9.46
71.08	13.88	47.97	9.98
93.26	1.50	62.94	13.09
94.27	5.86	63.63	13.24
96.88	10.82	65.38	13.60
97.61	34.64	65.88	13.71
101.16	5.06	68.27	14.20
114.15	3.00	77.04	16.03
119.81	3.25	80.86	16.82
130.48	11.50	88.06	18.32
135.69	33.49	91.58	19.05

dose rate=	**1.48**	**+/- 0.08**	**Gy/ka**
U =	0.70	0.1	**ppm**
Th =	3.80	0.3	**ppm**
K2O =	1.42	0.04	**wt. %**
Rb2O=	34.3	1.4	**ppm**
H2O=	14.5	4.4	**wt. %**
Cosmic=	0.11	**Gy/ka**	
depth =	5.0	**m**	
latitude=	42	**degrees (north positive)**	
longitude=	9	**degrees (east positive)**	
elevation=	0.06	**km asl**	

Notes: Quartz SAR OSL age following Murray and Wintle, 2000
CAM and MAM from Galbraith et al., 1999

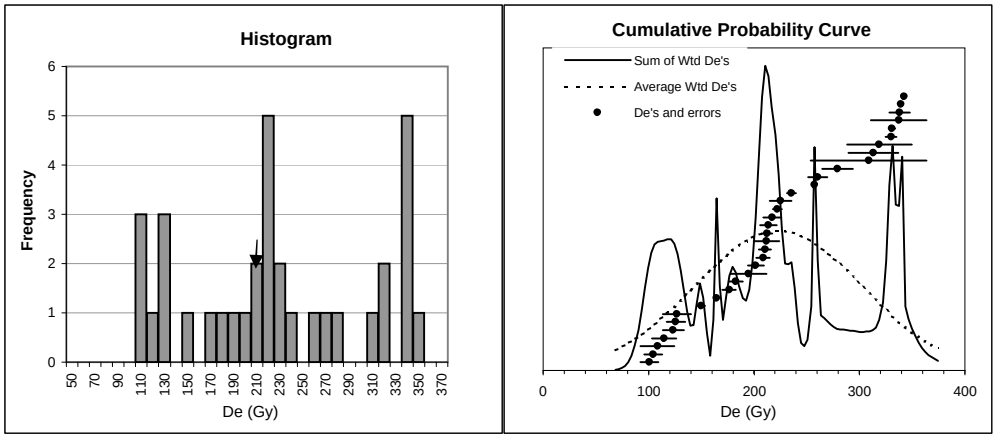

Golo10-4-10-4 **Torra Terrace (Qat4)**
USU-868

	De (Gy)	±	Age (ka)	±
CAM =	**209.57**	**13.34**	**51.82**	**6.01**
MAM =	**5.23**	**0.00**	**1.29**	**0.15**
Median =	201.66		49.9	5.8
Min =	100.81		24.9	2.9
Max =	342.34		84.7	9.8
n =	**34**	**Aliquots**		
S.D. =	74.37			
Standard error =	12.75			
Random Errors=	7.16	%		
Systematic Error=	9.13	%		
Total Error=	11.60	%		
Bin Width =	10.00	**Gy**		
Overdispersion (%) =	36.6	±	4.6	

		+/-	
dose rate=	**4.04**	**0.34**	**Gy/ka**
U =	3.30	0.2	**ppm**
Th =	17.10	1.5	**ppm**
K2O =	2.90	0.07	**wt. %**
Rb2O=	165.7	6.6	**ppm**
H2O=	10.0	10.0	**wt. %**
Cosmic=	0.12	**Gy/ka**	
depth =	4.5	**m**	
latitude=	42	**degrees (north positive)**	
longitude=	9	**degrees (east positive)**	
elevation=	0.03	**km asl**	

Notes: Quartz SAR OSL age following Murray and Wintle, 2000
CAM and MAM from Galbraith et al., 1999

Individual Aliquot Data

De (Gy)	±	Age (ka)	±
100.81	8.65	24.93	2.89
104.41	8.44	25.82	3.00
108.57	16.04	26.85	3.11
114.81	11.37	28.39	3.29
123.32	10.11	30.49	3.54
125.94	8.84	31.14	3.61
126.71	13.39	31.33	3.64
149.65	4.13	37.00	4.29
164.59	2.02	40.70	4.72
176.55	6.31	43.66	5.07
182.73	6.60	45.18	5.24
195.05	17.02	48.23	5.60
201.66	7.67	49.86	5.79
208.53	6.24	51.57	5.98
210.52	5.72	52.06	6.04
211.90	11.99	52.40	6.08
212.24	5.21	52.48	6.09
213.46	7.86	52.78	6.12
217.23	8.72	53.72	6.23
222.11	4.11	54.92	6.37
225.41	10.34	55.74	6.47
235.55	4.32	58.25	6.76
257.56	1.77	63.69	7.39
260.47	9.05	64.41	7.47
279.35	14.66	69.08	8.01
308.84	54.84	76.37	8.86
313.25	23.80	77.46	8.99
318.93	30.59	78.86	9.15
330.14	5.19	81.63	9.47
330.96	3.14	81.84	9.49
337.39	26.44	83.43	9.68
338.36	9.73	83.67	9.71
339.32	1.00	83.90	9.73
342.34	0.41	84.65	9.82

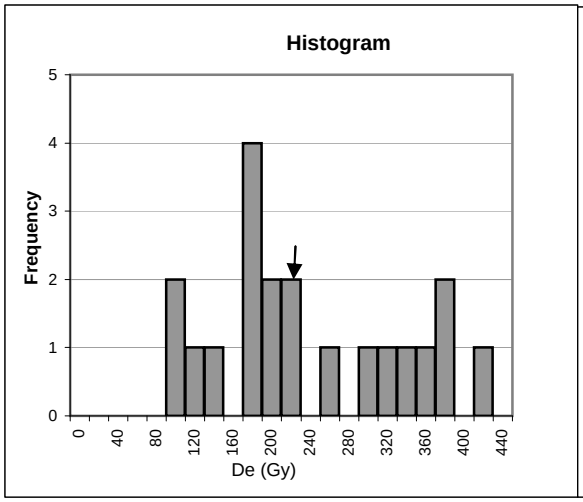

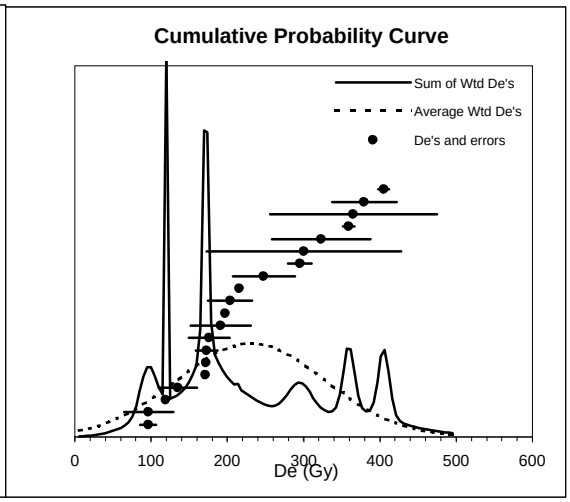

Golo10-11-10-14 **Torra Terrace (Qat4)**
USU-869

	De (Gy)	±	Age (ka)	±
CAM =	**211.11**	**20.03**	**62.53**	**12.44**
Median =	200.48		59.4	11.8
Min =	96.22		28.5	5.7
Max =	405.21		120.0	23.9
n =	**20**	**Aliquots**		
S.D. =	97.26			
Standard error =	21.75			
Random Errors=	18.90	%		
Systematic Error=	6.22	%		
Total Error=	19.90	%		
Bin Width =	20.00	**Gy**		
Overdispersion (%) =	39.7	±	7.1	

		+/-	
dose rate=	**3.38**	**0.16**	**Gy/ka**
U =	2.50	0.2	**ppm**
Th =	10.90	1.0	**ppm**
K2O =	2.88	0.07	**wt. %**
Rb2O=	148.7	5.9	**ppm**
H2O=	12.1	3.6	**wt. %**
Cosmic=	0.12	**Gy/ka**	
depth =	4.0	**m**	
latitude=	42	**degrees (north positive)**	
longitude=	9	**degrees (east positive)**	
elevation=	0.03	**km asl**	

Individual Aliquot Data

De (Gy)	±	Age (ka)	±
96.22	10.42	28.50	5.67
96.89	32.62	28.70	5.71
119.03	1.22	35.26	7.01
134.95	25.07	39.97	7.95
171.54	2.81	50.81	10.11
171.69	4.11	50.86	10.12
172.71	14.32	51.16	10.18
176.37	26.68	52.24	10.39
191.21	39.17	56.64	11.27
197.27	0.04	58.43	11.63
203.70	29.06	60.34	12.00
215.39	0.53	63.80	12.69
247.73	40.62	73.38	14.60
295.12	15.63	87.42	17.39
300.54	127.76	89.02	17.71
323.36	64.58	95.78	19.06
359.30	7.44	106.43	21.17
365.44	109.87	108.24	21.54
379.45	42.29	112.40	22.36
405.21	7.22	120.02	23.88

Notes: Quartz SAR OSL age following Murray and Wintle, 2000
CAM and MAM from Galbraith et al., 1999

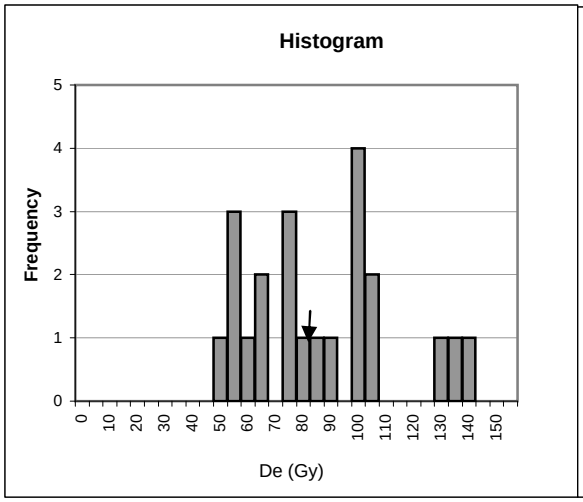

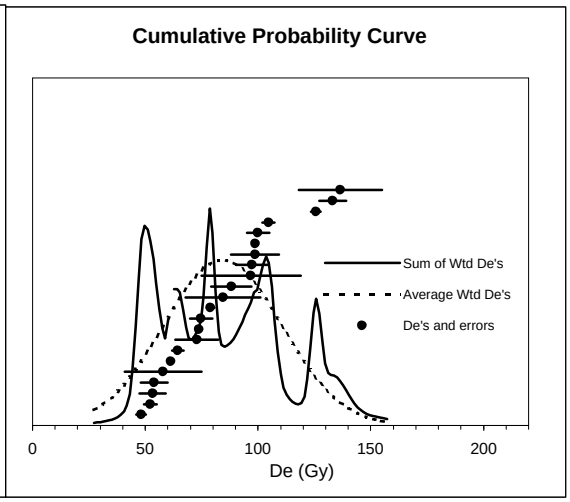

Golo 10-5-10-7 **Sant Antone (Qaf_3)** **Individual Aliquot Data**
USU-870

	De (Gy)	±	Age (ka)	±
CAM =	**80.86**	**5.36**	**29.38**	**4.31**
MAM =	**48.67**	**0.41**	**17.68**	**2.59**
Median =	81.65		29.7	4.4
Min =	48.16		17.5	2.6
Max =	136.52		49.6	7.3
n =	**22**	**Aliquots**		
S.D. =	26.22			
Standard error =	5.59			
Random Errors=	13.36	%		
Systematic Error=	6.07	%		
Total Error=	14.67	%		
Bin Width =	5.00	**Gy**		
Overdispersion (%) =	29.5	±	4.9	

		+/-	
dose rate=	**2.75**	**0.12**	**Gy/ka**
U =	1.40	0.1	**ppm**
Th =	8.70	0.8	**ppm**
K2O =	2.39	0.06	**wt. %**
Rb2O=	106.5	4.3	**ppm**
H2O=	10.0	3.0	**wt. %**
Cosmic=	0.11	**Gy/ka**	
depth =	5.0	**m**	
latitude=	42	**degrees (north positive)**	
longitude=	9	**degrees (east positive)**	
elevation=	0.03	**km asl**	

De (Gy)	±	Age (ka)	±
48.16	2.22	17.50	2.57
52.26	2.73	18.99	2.79
53.24	5.69	19.34	2.84
53.94	5.85	19.60	2.88
57.86	16.99	21.02	3.09
61.45	0.51	22.33	3.28
64.53	2.59	23.45	3.44
72.90	9.53	26.49	3.89
73.90	0.08	26.85	3.94
74.73	4.99	27.15	3.98
78.83	1.70	28.64	4.20
84.46	16.51	30.69	4.50
88.23	8.96	32.06	4.70
96.87	21.99	35.20	5.16
97.44	7.30	35.40	5.19
98.67	10.59	35.85	5.26
98.71	0.13	35.86	5.26
100.03	4.99	36.35	5.33
104.62	2.71	38.01	5.58
125.61	2.24	45.64	6.70
133.19	5.98	48.39	7.10
136.52	18.42	49.60	7.28

Notes: Quartz SAR OSL age following Murray and Wintle, 2000
CAM and MAM from Galbraith et al., 1999

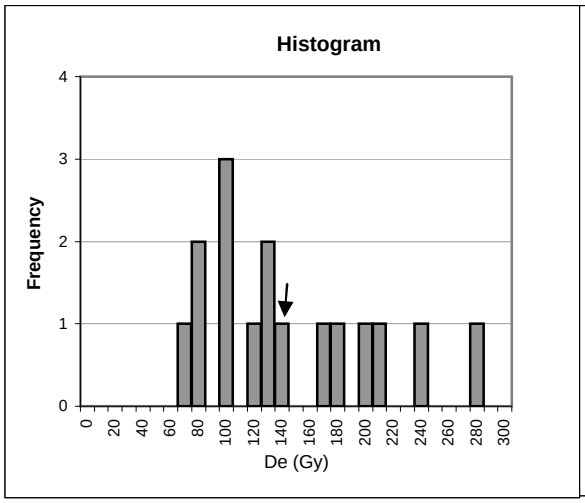

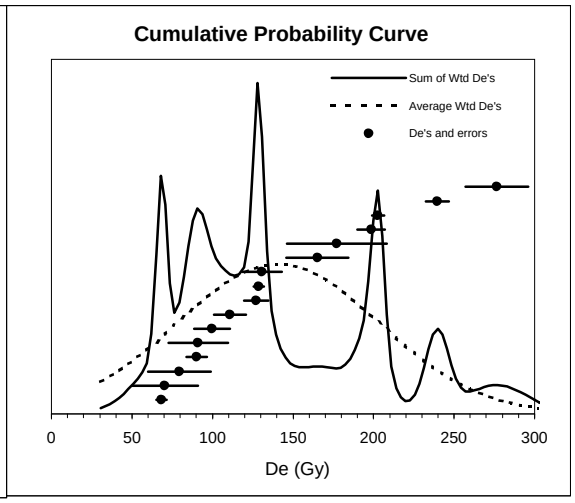

Golo10-11-10-12 **Sant Antone (Qaf_3)** **Individual Aliquot Data**

USU-871

	De (Gy)	±	Age (ka)	±
CAM =	**132.04**	**13.85**	**55.08**	**12.30**
MAM=	**67.27**	**4.20**	**28.06**	**6.26**
Median =	127.86		53.3	11.9
Min =	68.45		28.6	6.4
Max =	276.52		115.3	25.7
n =	**16**	**Aliquots**		
S.D. =	62.86			
Standard error =	15.71			
Random Errors=	20.90	%		
Systematic Error=	7.85	%		
Total Error=	22.32	%		
Bin Width =	10.00	**Gy**		

De (Gy)	±	Age (ka)	±
68.45	3.25	28.55	6.37
70.52	20.63	29.42	6.57
79.45	19.49	33.14	7.40
90.00	6.36	37.54	8.38
91.11	18.49	38.00	8.48
99.66	11.14	41.57	9.28
110.97	9.92	46.29	10.33
127.06	7.63	53.00	11.83
128.67	3.06	53.67	11.98
130.86	12.27	54.59	12.19
165.13	19.30	68.88	15.38
177.11	30.99	73.88	16.49
198.52	8.58	82.81	18.49
202.75	3.84	84.57	18.88
239.62	7.28	99.95	22.31
276.52	19.62	115.34	25.75

Overdispersion (%) = 40.2 ± 7.7

dose rate=	2.40	+/- 0.16	Gy/ka
U =	1.10	0.1	**ppm**
Th =	7.10	0.6	**ppm**
K2O =	2.59	0.06	**wt. %**
Rb2O=	78.8	3.2	**ppm**
H2O=	22.7	6.8	**wt. %**
Cosmic=	0.10	**Gy/ka**	
depth =	5.4	**m**	
latitude=	42	**degrees (north positive)**	
longitude=	9	**degrees (east positive)**	
elevation=	0.03	**km asl**	

Notes: Quartz SAR OSL age following Murray and Wintle, 2000
CAM and MAM from Galbraith et al., 1999

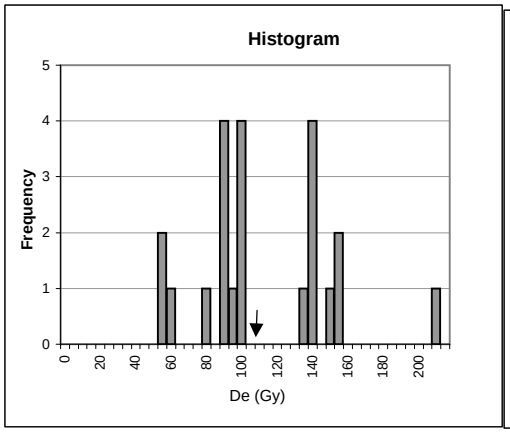

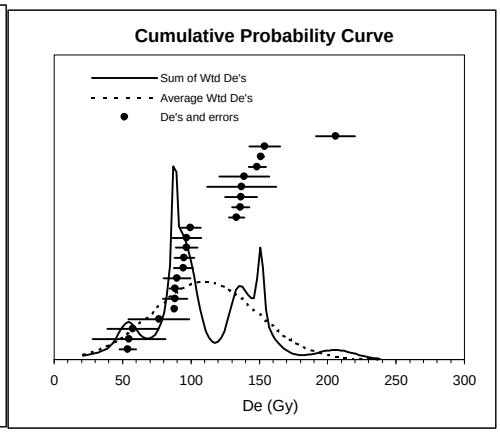

Golo 10-4-10-5 **Torra alluvium-colluvium (Qac)**
USU-872

	De (Gy)	±	Age (ka)	±
CAM =	**108.77**	**7.35**	**28.60**	**4.27**
MAM =	**72.71**	**16.35**	**19.12**	**2.85**
Median =	96.98		25.5	3.8
Min =	53.75		14.1	2.1
Max =	205.76		54.1	8.1
n =	**22**	**Aliquots**		
S.D. =	38.18			
Standard error =	8.14			
Random Errors=	13.68	%		
Systematic Error=	5.95	%		
Total Error=	14.92	%		
Bin Width =	5.00	**Gy**		
Overdispersion (%) =	29.2	±	5.0	

		+/-	
dose rate=	**3.80**	**0.18**	**Gy/ka**
U =	2.45	0.2	**ppm**
Th =	16.40	1.5	**ppm**
K2O =	2.72	0.07	**wt. %**
Rb2O=	148.2	5.9	**ppm**
H2O=	10.0	3.0	**wt. %**
Cosmic=	0.16	**Gy/ka**	
depth =	2.0	**m**	
latitude=	42	**degrees (north positive)**	
longitude=	9	**degrees (east positive)**	
elevation=	0.03	**km asl**	

Individual Aliquot Data

De (Gy)	±	Age (ka)	±
53.75	6.20	14.13	2.11
54.84	26.71	14.42	2.15
57.62	18.56	15.15	2.26
76.65	22.18	20.16	3.01
87.84	1.31	23.10	3.45
88.40	8.94	23.25	3.47
88.45	4.00	23.26	3.47
89.90	9.91	23.64	3.53
94.47	7.03	24.84	3.71
95.19	7.25	25.03	3.73
96.96	8.01	25.50	3.80
97.00	10.52	25.51	3.80
99.91	7.16	26.27	3.92
133.36	5.58	35.07	5.23
136.39	6.40	35.86	5.35
136.71	11.58	35.95	5.36
137.26	25.26	36.09	5.38
139.11	18.28	36.58	5.46
148.45	6.35	39.04	5.82
151.21	2.08	39.76	5.93
153.95	11.27	40.48	6.04
205.76	14.30	54.11	8.07

Notes: Quartz SAR OSL age following Murray and Wintle, 2000
CAM and MAM from Galbraith et al., 1999